博士論文

Study of Electromagnetic Vibration Energy Harvesting Based on Combined Free / Impact Motion for Low Frequency Operation

(低周波数で駆動するフリー・インパクトモーション混合型電磁気振動環境発電に関する研究)

ハローン　アハメッド　フォエド

Table of Contents

Chapter 1 Introduction

1.1 Introduction

This chapter gives an introduction to low frequency electromagnetic vibration energy harvesting based on combined free / impact motion with a literature survey on low frequency energy harvesting and other harvesters utilizing impact. First, the importance of vibration energy harvesting and how it is deemed by important kinds of applications are introduced. Then, some common associated problems are stated with a focus on the problem of low frequency energy harvesting using conventional spring – mass systems. Previously researches have been conducted to improve the harvesting performance at low frequencies. One of the proposed successful techniques is based on up converting the input frequency. Many harvesting architectures are presented in literature based on the principle of frequency – up conversion, where some of them have been mentioned in this chapter. A vibration transmission mechanism or oscillator based on combined free / impact motion is proposed in this work. Impact was previously introduced in vibration energy harvesting by different ways and for different purposes. However, free / impact motion mechanism is proposed for low frequency energy harvesting. The combined free / impact oscillator is described in this chapter. The oscillator dynamic behavior is largely depends on the way of impact. Two ways of impact are introduced in this work which are impact with soft stops and impact with hard stops resulting in two kinds of harvesting architectures. The working principle of each is explained as well as the preferable working conditions. Finally the layout of the dissertation is stated.

1.2 The importance of vibration energy harvesting (VEH)

Self-powering of wireless sensors and wireless micro-devices attract the attention of many researchers nowadays. Problems associated with chemical batteries such as limited

life time and minimization restrictions can be solved by using the approach of energy harvesting. Various ambient energy sources such as vibration, thermal, light, wind, etc. could be harvested and converted into electrical energy. However, vibration energy harvesting is more convenient for important kinds of applications such as machine condition monitoring, where sensors are placed in a deep dark or dirty environment, and Human body-powered devices, whether they are implantable or wearable devices.

1.3 Problems associated with VEH

Typical vibrational energy harvester is composed of a mass attached to vibrating cantilever or spring with base excitation. The ambient vibration acts as an input, which results the mass to oscillate. These mechanical oscillations are converted into electrical energy through electromagnetic [1, 2, 3], electrostatic [4, 5, 6], or piezoelectric [7, 8, 9] transductions. Regardless the technique exploited in the energy harvesting, the current configuration of vibration energy harvesters depends on designing a linear vibration resonator, in which the optimal harvester performance is obtained when the exciting frequency matches its resonant frequency. If the surrounding exciting frequency deviates from the resonance condition, the output power decreases drastically.

One of the problems associated with VEH is that increasing frequency bandwidth usually accompanies with a decrease in the Q-factor and vice versa. Many researchers tried to increase the bandwidth while maintaining high Q-factor by different ways. Tang et al [10] make a review of the recent advances in broadband vibration-based energy harvesting. A way of introduce nonlinear stiffness [11, 12], bistable spring [13, 14, 15], active and autonomous tuning [16, 17, 18] in vibration energy harvesting are proposed to deal with such problem.

Magnetoelectric laminated structure is utilized in vibration energy harvesting [19, 20, 21]. An improvement in the energy harvesting performance is shown [22, 23], where the nonlinear motion not only leads to a broadband energy harvesting but also resulted in a double power peak, as well as the ability of bi-directional energy harvesting. Multiple power peaks which can widen the operational frequency can be achieved by utilizing spiral cantilever [24] or folded cantilever [25].

Another problem that arises in VEH is matching low frequencies. Usually frequency matching is done by controlling the utilized mass and/or spring stiffness. Using large oscillating mass to match low frequencies associates with larger system weight and size, which sometimes limited by the application restrictions. However, low frequency matching using low spring stiffness associates with a decrease in the Q-factor and consequently degradation in harvesting performance.

1.4 Low frequency energy harvesting

Few techniques are introduced to improve energy harvesting at low frequencies. One of the most successful is the frequency-up conversion. It depends on generating internal oscillations with a frequency higher than the input vibration frequency. Many Frequency–up converting architectures are introduced. Kulah and Najafi [26] achieve frequency-up conversion in an electromagnetic harvester by magnetic interaction between a compliant driving beam and high resonant generating beam. Lee et al [27] up converted the input frequency through a sharp probe attached to a piezoelectric bimorph cantilever and contact with ridges attached to micro slider mechanism. Results show that it generates an output power larger than similar conventional resonant harvester. Galchev et al [28] present an electromagnetic harvester for low frequency non-periodic vibrations. The

proposed harvester is non-resonant and has more advantages with amplitudes larger than the harvester internal displacement. Pillatsch et al [29] up-converted the input frequency in a piezoelectric electric harvester, in which a piezoelectric beam is plucked by a magnetic coupling with free oscillating mass. Gu and Livermore [30] utilize frequency-up conversion with impact energy harvesting in a non-resonant harvester in which a low frequency beam drive a high frequency generating beam by impact.

Other ways of improving low frequency energy harvesting is presented. Naruse et al [31] propose a micro-electrostatic generator based on new electret structure, which can deliver 40μW at 2 Hz and 0.4g acceleration. Jo et al [32] utilize the magnetic spring and planner coil structure to fabricate a low frequency electromagnetic energy harvester to be used for human body vibrations. A prototype of approximately 25×25×16 mm size is able to generate a maximum power of 430μW at 8 Hz resonant frequency.

1.5 Free / impact oscillator

In this work a vibration transmission mechanism or oscillator associated with electromagnetic transduction is introduced for low frequency energy harvesting. It depends on generating combined free / impact motion between a permanent magnet mass and a frame–carrying coil. The frame is directly connected to the vibrating source, and the magnet can move freely within a certain distance inside the frame and make impacts with two side end stops. The magnet/frame relative oscillation generates an electrical voltage by induction.

Previously impact is introduced and modelled in vibration energy harvesting in different ways and for different purposes. Impact with end stops that limit the internal mass displacement is introduced in beam-based harvesters where the impact nonlinearity

resulted in broadening frequency bandwidth [33, 34, 35]. Impact is modelled in electrostatic energy harvesters with rigid stops [36], and with slave transducer stops [37] for large acceleration amplitudes. Impact energy harvesting associated with piezoelectric transduction is presented to increase the deformation of piezoelectric material and consequently the generated current [38, 39, 40, 41]. Renaud et al [42] achieve non-resonant impact energy harvesting from the repeated impacts of a free ball on two piezoelectric plates. The obtained harvester utilizes harvesting via impact, however, it losses the power enhancement from resonance operation.

Vibro-impact mechanism with end stops is introduced in vibration energy harvesting with either piezoelectric [43, 44] or electromagnetic [45] transductions, where a broadband energy harvesting and increase in the total output power could be obtained. However, Vanderwater and Moss [46] recently carried out a theoretical modelling with experimental validation of a vibro-impact energy harvester implemented as ball-bearing/permanent magnet arrangement. The study shows there is a trade-off between the operating bandwidth and output power.

Although impact has been extensively modelled before with vibration energy harvesting, the mechanism which involves combined free / impact motion associated with electromagnetic transduction have not been discussed. The free motion can allow higher relative oscillations at low frequencies. The performance of the presented oscillator largely depends on the way of mass / frame impact. Two ways of impact are introduced in this work, which are impact with elastic end stops and impact with hard end stops resulted in two different kinds of harvesting systems. The dynamic behavior and harvesting performance of each is studied, analyzed and tested in this work.

The harvester involves free motion with elastic stops impact (FEH) shows a resonant behavior, in which its resonant frequency could be shifted to lower range with the same mass and spring stiffness as similar conventional spring – mass oscillator (CH) without a decrease in the resonant relative amplitude. Hence, improvement in the harvesting performance could be achieved at low frequencies.

The harvester involves free motion with hard stops impact (FHH) shows a non-resonant behavior, in which the output power increases by input amplitude and /or frequency. The harvester shows an effective performance with large amplitude - low frequency vibrations. In addition, it has a simple construction which allows fabrication with small sizes. Thus, this harvester could be well suited for human body associated applications.

In general, human body induced vibration is unsteady and large amplitude – low frequency in natural, which considered as a problem when matching by linear spring – mass harvesters. Non-resonant harvesters can propose a solution for such problem. One of the earlier works in this way is the electrostatic Coulomb-force parametric generator (CFPG) [47, 48]. The relative displacement in CFPG is allowed only at the maximum input acceleration. This can be achieved by adjusting a holding electrostatic force to an optimum value, which is slightly below the maximum inertia force. Exciting CFPG with a high acceleration allow a higher holding force to be adjusted and consequently higher power harvesting. In fact, holding force can be easily adjusted by setting the prime voltage to an optimal value for a given source of acceleration. However, for a variable acceleration source such as human body motion, optimization should be carried out dynamically, which required an optimization power supply module [49]. MEMS-CFPG is studied, and analyzed in [48], fabricated and tested by a low frequency shaker in the range of 10-100 Hz [49] as well as by actual human walking motion [50]. However, some

problems are observed in the experiment such tilting of the proof mass, late landing of the moving plate due to air damping, etc, which need further improvements [49].

Bowers and Arnold [51] utilize the free oscillation to achieve low frequency energy harvesting. They construct an electromagnetic non-resonant architecture which consists of a ball magnet allowed to move freely within a spherical cavity wrapped with copper coil windings. Rao et al [52] integrate the same harvester [51] with a power management circuit and test a prototype of 100 cm^3 with the actual body motion during different activities. The harvester shows an average power of 300 μW when attached to human ankle during walking. The harvester output power is quite large, however its large size remains an obstacle for the usage with human body applications.

Lee and Chung [53] present an electromagnetic harvester of 21cm^3 and 30g mass which consists of planner spring, NdFeB permanent magnets, and a copper coil. The proposed harvester is able to generate a maximum power of 65.33 μW at a resonance frequency of 8 Hz and 1.96 ms^{-2}.

FHH was tested with steady harmonic vibrations. Since human body powered – devices are considered one of its important applications, energy harvesting by FHH from human body locomotion is investigated in this work. The harvester performance is tested at three different body locations during three common activities. Two harvester prototypes are considered. FHH generally shows significant output power from human induced vibration during the considered activities. Further, parameters selection guidelines or optimization procedure of FHH for a specified body application is discussed.

1.6 Structure of the dissertation

The dissertation is organized as follows; Chapter 1 gives an introduction to vibration energy harvesting and its associated problems with a focus on low frequency energy harvesting. It ends with a brief description of the presented work. Chapter 2 briefly explains the concept of free motion for low frequency energy harvesting upon which the presenting harvesting systems are based. Chapter 3 gives a detailed study and analysis of electromagnetic vibration energy harvesting based on free motion with elastic stops impact. The study includes proposing an architecture based on this vibrating mechanism. Analysis of its dynamic behavior and investigation of harvesting performance, followed by a simulation and experimental comparison with a similar harvester based on linear spring – mass. Oscillator. Chapter 4 presents vibration energy harvesting based on free motion with hard stops impact. The study also covers analysis of the dynamic behavior of a proposed architecture and investigation of the harvesting performance. Experimental study also conducted on different harvester prototypes, followed by a comparison between the proposed harvester and previously fabricated low frequency energy harvesters. In Chapter 5, investigation of free / hard stops impact harvester with human body motion is carried out, where it shows a significant output power from the motion of body limbs during different activities. Further, a parameter selection procedure for optimizing the harvester to a certain body application is discussed. Chapter 6 finally gives the conclusions of this work and future prospective of this research.

1.7 Summary

Vibration energy harvesting (VEH) is an important technique for self-powering of wireless sensors and wireless devices associated with some important applications such as machine condition monitoring, industrial health monitoring, and human body – powered devices. It is basically rely on generating mechanical relative oscillation through spring – mass suspension, which then converted to electrical energy by three transduction mechanisms. Some problems are associated with VEH such as low Q-factor and consequently degradation of the harvesting performance upon widening bandwidth or matching low frequencies. Many researches have been conducted to deal with those problems, which resulted in many different harvesting architectures. In this work electromagnetic harvesting architectures based on generating combined free / impact motion for low frequency operation is proposed and studied. The way of impact involved largely affects the system behavior, and consequently harvesting performance. Two ways of impact are presented which are impact with elastic stops and impact with hard stops leading to two different harvesting systems.

Chapter 2 The concept of free motion

2.1 Introduction

This chapter begins by briefly explaining the concept of electromagnetic vibration energy harvesting, and the factors that affect the harvesting performance. Spring – mass system is the common vibrating system employed for vibration energy harvesting. However, it becomes inappropriate when utilized for low frequency energy harvesting in its conventional form. An idea of employing free motion oscillation for low frequency operation is proposed. The concept of utilizing free oscillations for low frequency energy harvesting is illustrated. Practically, pure free motion cannot be guaranteed unless larger harvester sizes (compare to the relative oscillation amplitudes) are considered. Thus, combined free motion with end stops impact becomes the more general case, which have been focused in this study. In addition, impact can improve the harvesting performance in some cases. Finally, the concept of two harvesting architectures based on combined free/impact motion is illustrated

2.2 Electromagnetic vibration energy harvesting

Electromagnetic kinetic energy harvesting mainly depends on generating variable magnetic flux across an electrical coil, which causes an induced voltage across the coil turns. The variable magnetic flux is usually achieved from the relative oscillation between a permanent magnet and a coil. The magnet/coil relative motion is transmitted from an external source through a vibration transmission mechanism or a vibrating system.

Increasing the induced voltage and consequently improving power harvesting can be achieved by increasing either the flux rate of change with respect to the coil displacement, or the magnet/coil relative velocity. The flux rate of change depends on the magnet position within the coil, coil number of turns, magnetic strength, etc. as discussed in

Chapter 3. However, the magnet/coil relative velocity depends on the external vibration and the vibrating system configuration.

2.3 Linear spring – mass oscillator

The common vibrating system utilized for vibration energy harvesting basically relies on linear spring – mass suspension. The relative motion is generated between a proof mass and a frame connected to each other by spring or a spring – damper element, while the frame is directly connected to the vibration source as shown in Fig. 2-1

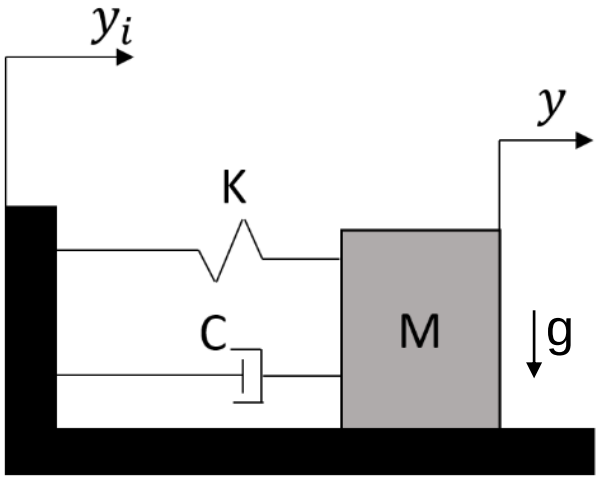

Fig. 2-1. Spring-mass suspending system or linear spring-mass oscillator, which is basically used for kinetic energy harvesting.

Increasing the relative velocity to improve power harvesting could be achieved from high Q-factor or high resonant relative amplitude. However, matching low frequencies using low spring stiffness usually associated with an increase in the damping ratio (Fig. 2-2, Eq. 2-1) [54], consequently degradation of the harvesting performance (sometimes there are restrictions in utilized mass and involved damping coefficient) which is considered as the drawback of linear resonator for low frequency applications.

$$\Lambda = \frac{\left(\frac{\omega}{\omega_n}\right)^2}{\sqrt{\left(1-\left(\frac{\omega}{\omega_n}\right)^2\right)^2 + \left(2\zeta\frac{\omega}{\omega_n}\right)^2}} \qquad (2-1)$$

Where ω, ω_n , and ζ are the input angular frequency, angler natural frequency and damping ratio respectively.

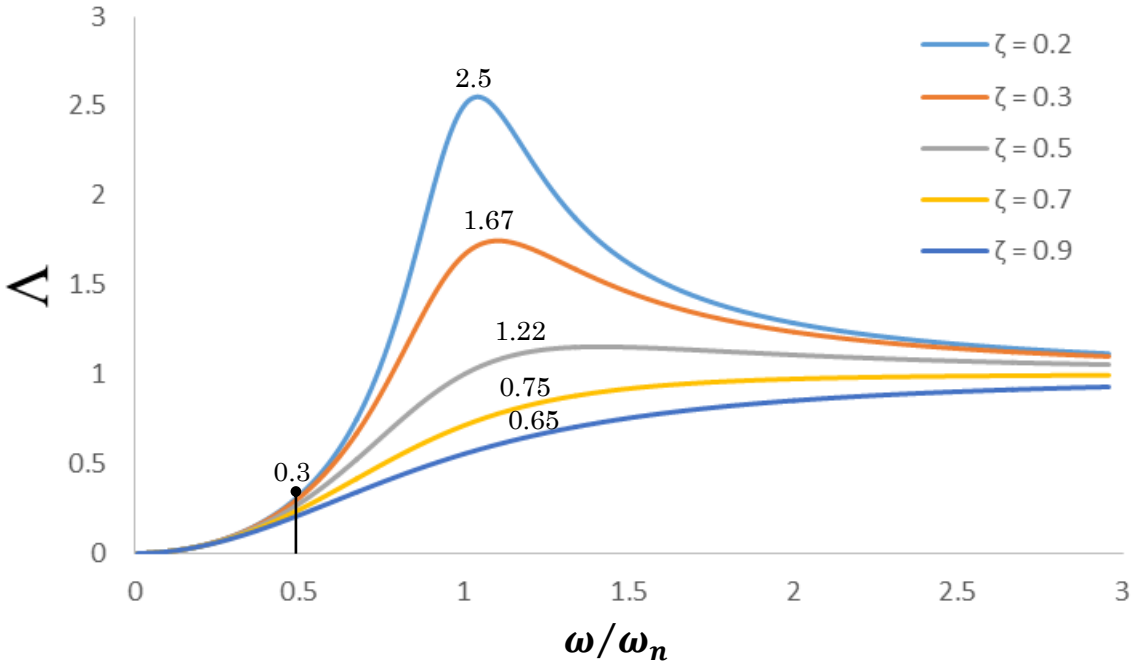

Fig. 2-2. Variation of the amplitude ratio Λ with the frequency ratio for different values of damping ratio (Eq. 2-1)

2.4 Free motion oscillation

Suppose that the mass is allowed to move freely inside the coil without spring connection as shown in Fig. 2-3. In that case, the mass should be supported by the frame, which represents a guide for the mass motion.

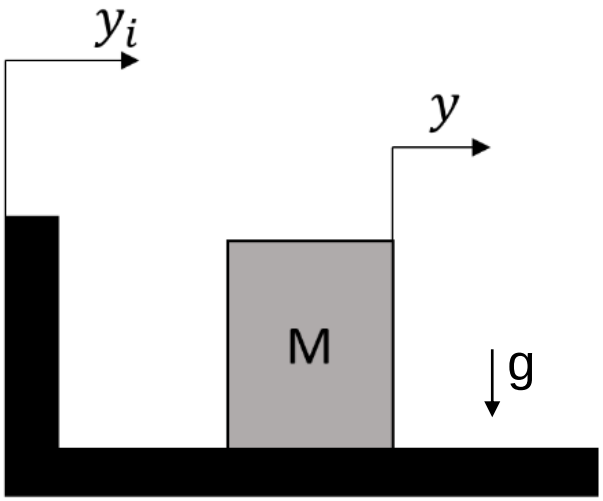

Fig. 2-3 the mass is allowed to vibrate freely while supported by the vibrating frame

If we consider a zero friction or damping in this system, the relative vibration amplitude and velocity would be exactly equal to the input amplitude and velocity in magnitude respectively at any input frequency. This could be a kind of improvement over the linear spring-mass system at low frequencies (linear spring – mass system does not show a resonant magnification over a damping ratio of around 0.7). However, when allowing such kind of free motion, the frame support becomes mandatory, which adds a kind of coulomb's friction to the relative oscillation. The coulomb's damping due to sliding will overwhelm the total damping in the system in contrast with spring-mass oscillator, in which the viscous damping of the utilized spring overwhelms whether it is in the form of cantilever, simply supported beam, or even helical spring.

If we consider the coulomb's friction due to sliding, the relative velocity could be obtained from the dynamic model of the system as follows:

The mass equation of motion due to an input vibration (y_i) could be expressed as:

$$-\frac{\dot{z}}{|\dot{z}|}\,\mu M g = M\ddot{y} \qquad (2-2)$$

$$\ddot{y} = -\frac{\dot{z}}{|\dot{z}|}\mu g \qquad (2-3)$$

where z is the relative displacement, and μ is the coulomb's friction coefficient

which means, the mass can move with a constant acceleration in a direction opposite to the relative velocity. Thus, for harmonic input vibration the input and mass velocities can be represented as shown in Fig. 2-4.

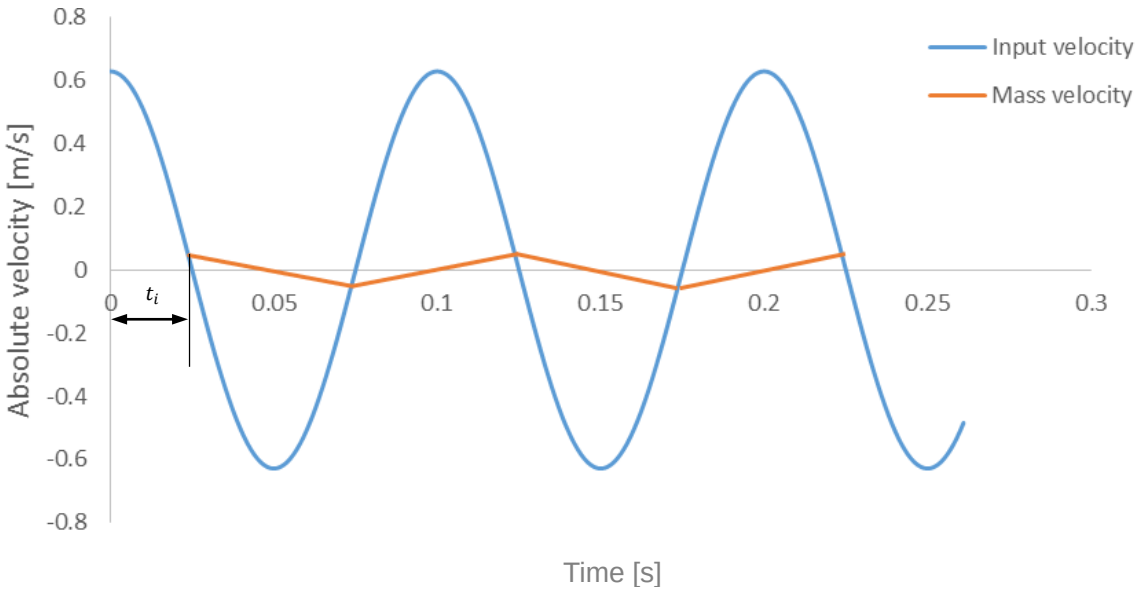

Fig. 2-4. The absolute velocities for a harmonic input vibration of ($Amp. = 10mm, and\ freq. = 10Hz$) to the free oscillator of ($\mu = 0.2$) coulomb's friction coefficient.

The mass velocity amplitude can be expressed as:

$$V = \mu g \frac{\pi}{2\omega} \qquad (2-4)$$

Then, the mass/frame relative velocity in the first half cycle (of $(-\mu g)$ mass acceleration) as indicated by Fig. 2-4 can be expressed as:

$$\dot{z} = \mu g \left(\frac{\pi}{2\omega} - t\right) - Y_i \omega \cos \omega(t + t_i) \qquad (2-5)$$

Where Y_i is the input vibration amplitude, and t_i is given by:

$$t_i = \frac{1}{\omega}\cos^{-1}\frac{\mu g \pi}{2Y_i\omega^2} \qquad (2-6)$$

The relative velocity for one complete cycle of a harmonic input vibration is depicted by Fig. 2-5. The case simulated in Fig. 2-5 is for an input vibration of 10 mm amplitude and 10 Hz frequency with 0.2 coulomb's friction coefficient. The resulted relative velocity amplitude is 0.626 m/s while the input velocity amplitude is 0.628 m/s, which are so close to each other. The deviation between the relative and input velocity amplitudes increases for lower input frequencies and higher friction coefficients. Table 2-1 shows the values of relative and input velocity amplitudes at different input frequencies for 0.2 friction coefficient.

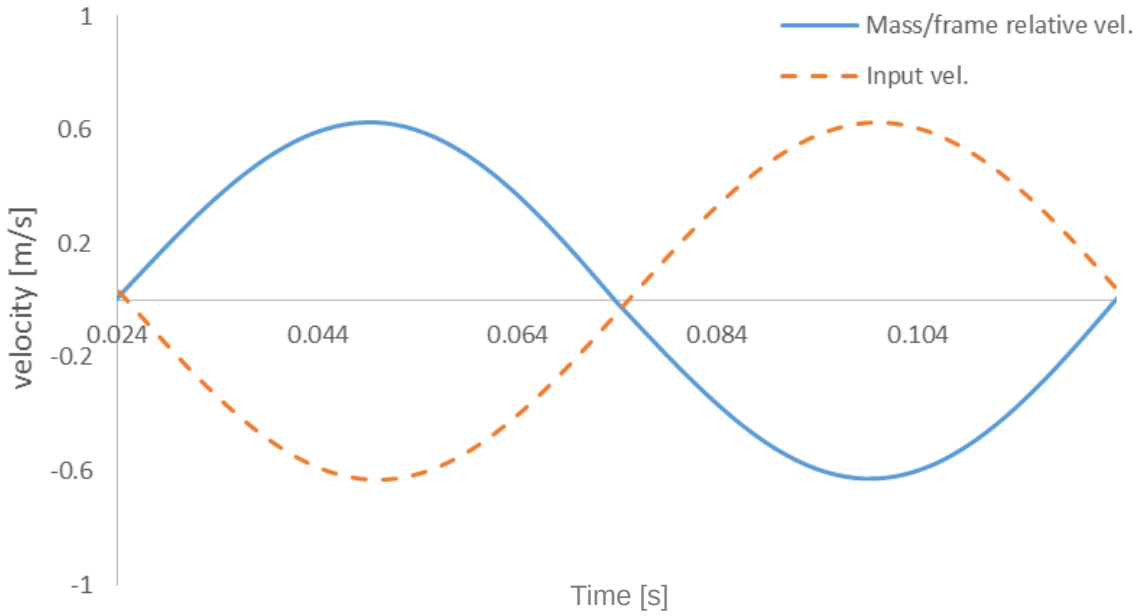

Fig. 2-5. Input and relative velocities by the free oscillator for an input vibration of ($Y_i = 10\,mm, f = 10\,Hz$) and coulomb's friction coefficient of ($\mu = 0.2$)

Table 2-1

The relative and input vibration velocities to the free oscillator at different input frequencies in case of 0.2 coulomb's friction coefficient

F(Hz)	Input velocity amp. ($Y_i\omega$)	Relative Velocity amp. (V_{rel})	Amplitude ratio
3	0.189	0.15	0.79
4	0.251	0.224	0.89
5	0.314	0.301	0.96
6	0.376	0.369	0.98

The values listed in Table 2-1 show that the free oscillator has a superior performance over spring – mass oscillator at low frequencies (lower than the resonant frequency) even at a low damping ratio. The amplitude ratio of the free oscillator increases over that of spring – mass oscillator (Fig. 2-2) as the frequency decreases.

It is worth mentioning that in the above example, the coulomb's friction coefficient is taken 0.2. If the involved coulomb's friction increases, the amplitude ratio provided by the free oscillator will decrease. Hence, coulomb's friction becomes an important issue in the free oscillator performance. In addition, there is a minimum limit of the frequency that the free oscillator can work with, which is also determined by the existing coulomb's friction in the system. The input acceleration should exceed the frictional acceleration (μg) so that the relative motion could appear.

2.5 Free / impact motion oscillation

Most energy harvesting systems have size boundaries, which are determined by the harvester frame size. As in some spring – mass based harvesters, stops are used to limit the internal mass displacement [33, 34, 35], and bound the harvester size to the application size constraints. The same situation appears in case of free motion oscillation. The harvester frame puts a limit to the allowed free motion distance. Thus, impacts with frame

end stops would appear when the mass approaches the frame boundaries. Practically, pure free motion cannot be guaranteed unless large frame sizes relative to the internal oscillation amplitudes are utilized. Hence, the combined free / impact motion would be the general case of oscillation. In addition to that, impact with end stops improves the harvesting performance in some cases as discussed in later chapters.

The way of the impact with frame end stops largely affects the oscillator dynamic behavior and consequently the harvesting performance. Two ways of impacts are possible; impact with soft or elastic stops, and impact with hard stops. Those two ways of impacts lead to two kinds of harvesting systems.

In this work we study two harvesting architectures based on free / impact motion. The first is the free / elastic stops impact harvester (FEH), and the second is free / hard stops impact harvester (FHH). In both cases we study in details the oscillator dynamic behavior, and analysis the system performance, followed by discussion of the advantages and limitations of utilizing each for practical applications.

2.5.1 Free / elastic stops impact harvester (FEH)

In this harvesting architecture, a permanent magnet mass is allowed to move freely inside a frame – carrying an electrical coil. The frame has two side soft stops which are in the form of two short compliant helical springs. The mass can move freely within a certain distance inside the frame and make impacts with the frame end stops upon reach to its boundaries. This kind of harvester is comparable to linear spring – mass harvester with compliant spring to match low frequencies. The harvester shows a resonant behavior in which the output power is magnified at a certain frequency and decreases away from it. However, the resonant frequency of FEH is affected by the allowed free motion

distance as well as the utilized mass and spring stiffness. The allowed free motion distance allows matching lower frequencies with an increase in the resonant relative amplitude. Thus, significant improvement over conventional spring – mass harvester could be obtained at low frequencies. In addition, the nonlinearity provided by impact broaden the frequency bandwidth.

2.5.2 Free / hard stops impact harvester (FHH)

This harvester simply consists of a hollow tube – carrying an electrical coil with a permanent magnet inside. The tube is closed at both ends with two hard end stops. Due to impact with hard stops the harvester shows a non-resonant behavior in which the output power increases with input amplitude and / or frequency. Owing to the simple construction of FHH, it could be fabricated with small sizes. Therefore, FHH can be well suited for micro device applications associated with unsteady large amplitude vibrations such as human body associated electronics. The simple construction of FHH also allows utilizing different shape magnets. Hence, in this work the harvester performance is investigated and tested experimentally with different magnet shapes.

2.6 Summary

Electromagnetic vibration energy harvesting basically depends on generating mechanical relative oscillations between permanent magnet and a coil from external vibration source through a vibrating system. The common vibrating systems rely on linear spring – mass suspension. Matching low frequencies by linear spring – mass oscillator usually associated with a decrease in the Q-factor and consequently degradation of the system performance. A free motion oscillator is proposed in this work which can guarantee a relative oscillation amplitude nearly equal to the input vibration amplitude.

Thus, the free oscillator can have a better performance over linear spring – mass oscillator at low frequencies. Pure free oscillation cannot be guaranteed unless larger size systems are utilized compare to the free oscillation amplitudes. Thus, combined free motion with end stops impact can be considered as the general case. In addition, impact with end stops can improve the harvesting performance in some cases. Just free oscillator or even free/impact oscillator could also have a simple construction which can give flexibility in fabrication according to the application constrains as well as increase the minimization ability.

Chapter 3 Study of free / elastic stops impact harvester (FEH)

3.1 Introduction

In this chapter a study of electromagnetic vibration energy harvesting based on free motion with elastic stops impact is presented. In the free / elastic stops harvester (FEH), a permanent magnet mass is allowed to move freely within a certain distance (stroke) inside a frame-carrying an electrical coil and makes impacts with spring end stops. The resulted harvester shows a resonant behavior over the range of exciting frequencies. The resonant frequency shows a dependency on the allowed free motion distance by which it could be shifted to lower frequency ranges with an increase in the resonant relative amplitude. Hence, significant power could be harvested at low frequencies. In addition, the impact nonlinearity broadens the frequency bandwidth [33, 36].

A nonlinear mathematical model including impact and electromagnetic induction is derived which can be solved by time domain simulation. Impact with elastic end stops is modeled through spring-damper element. Analysis of the dynamic behavior and investigation of the system performance is carried out with the aid of case study simulation. FEH shows a unique way of oscillation in which four different ways of response or response types of the magnet/frame relative motion appear over the range of exciting frequencies. The relative displacement amplitude increases within one response type and decreases within others. Hence, an approximate mathematical condition for this response type is derived. A relation for the resonant frequency of FEH is derived which reveals a resonant frequency dependency on the allowed free motion distance as well as the utilized mass and spring stiffness. Simulation and experimental comparisons between FEH and conventional energy harvester (CH) tuned to resonate at the same frequency are carried out which show the superior performance of FEH at low frequencies.

3.2 Structure and working principle

Electromagnetic vibration energy harvesting mainly based on generating relative oscillation between an electrical coil and magnetic flux. The relative oscillation could be achieved from a permanent magnet mass attached by a spring or spring-damper element to a frame-carrying coil, while the frame is directly connected to the vibration source as shown in Fig. 3-1a. Whether the utilized spring is mechanical or magnetic, it always remains in contact with the oscillating mass. However, in the electromagnetic energy harvester based on free motion with soft impacts (FEH), the mass is allowed to move freely within a certain distance (stroke) inside the frame and make impacts with spring end stops as shown in Fig. 3-1b. Whether the mass is allowed to move freely within a certain distance in FEH or directly attached to a compliant spring for low frequency energy harvesting in the proposed design of CH, it should to be supported by a guide in order to guarantee the right oscillation direction within the frame.

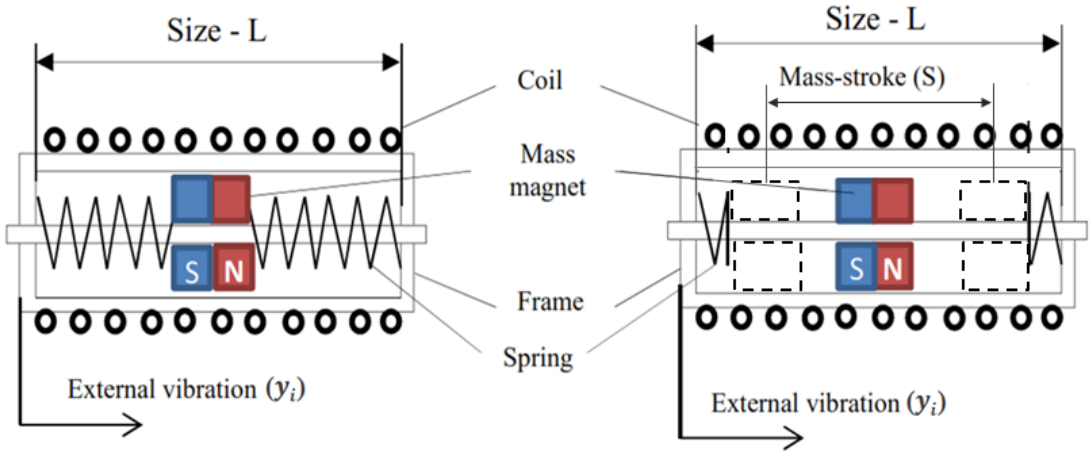

(a) (b)

Fig. 3-1. (a) Conventional electromagnetic energy harvester (CH), (b) free/ elastic stops impact electromagnetic energy harvester (FEH)

The relative motion between the magnet and the frame causes a magnetic flux variation through the coil turns and consequently generates an induced electromotive force (emf).

3.3 Mathematical modelling

Electromagnetic energy harvester is a coupled electro-mechanical system, which includes mechanical system and electrical circuit. Mechanical system provides relative motion between a permanent magnet and a coil, while the induced electricity puts an electrical damping on the mass motion. Modelling of FEH includes some nonlinear terms, which significantly affect the system performance such coulomb's friction force and impact force with stops. Thus, the obtained mathematical model is nonlinear which can be solved by time domain simulation.

3.3.1 Mechanical system

When an external vibration applies to the harvester frame, three type of force are transmitted to the mass magnet; the viscous friction force, coulomb's friction force, and impact force during the moments of impact. According to Newton 2nd law of motion, the mass equation of motion is given by:

$$M\ddot{y} + (C_a + C_i + C_e)\dot{z} + k_e\left[|z| - \frac{S}{2}\right] + \frac{\dot{z}}{|\dot{z}|}\mu Mg = 0 \qquad (3-1)$$

where,

$$k_e = \begin{cases} k & z > S/2 \\ 0 & S/2 > z > -S/2 \\ -k & z < -S/2 \end{cases} \qquad (3-2)$$

$$C_i = \begin{cases} C_s & z > S/2 \\ 0 & S/2 > z > -S/2 \\ C_s & z < -S/2 \end{cases} \qquad (3-3)$$

C_a is the air damping coefficient, C_i is an additional damping when mass and spring are in contact which takes the value of C_s during contact and zero at any other position, C_e is the electrical damping coefficient which depends on electromagnetic parameters

(as described later), k_e is the effective spring stiffness which takes the value of spring stiffness (k)during impact and zero elsewhere, M is the mass of the permanent magnet, and μ is the dry coefficient of friction.

z is the relative displacement ($z = y - y_i$) , where y is the absolute mass displacement, y_i is the input vibration to the frame, and S is the mass stroke or the allowed free motion distance (Fig. 3-1).

3.3.2 Electromagnetic induction

According to Faraday's law, the electrical voltage generated by induction due to the frame /magnet relative motion is given by

$$emf = -\frac{d\varphi}{dt} = -\frac{d\varphi}{dz}\frac{dz}{dt} \qquad (3-4)$$

where φ is the total magnetic flux going through the coil turns.

In case of an electrical coil of length - l consists of number of coil layers - N_l, and each coil layer has number of turns - N_t , (the total number of turns – $N = N_l \times N_t$), the total magnetic flux rate of change ($d\varphi/dz$) through the coil can be approximated to the magnetic flux rate of change through the mean coil layer multiplied by the number of layers, which is calculated as follows:

First, the magnetic flux through one turn of the mean coil layer (φ_t) located at a distance z from the magnet dipole center is obtained by integrating the equation of the magnetic flux density or magnetic field ($B - in\ tesla$) through the turn [55] over the area bounded by the turn as expressed by

$$\varphi_t = \frac{\mu_o m}{2}\left[\frac{1}{\sqrt{(r^2 + z^2)}} - \frac{z^2}{(r^2 + z^2)^{3/2}}\right] \qquad (3-5)$$

where m is the magnetic moment, μ_o is the permeability of the free space, and r is the coil mean radius.

Differentiate Eq. 3-5 with respect to z

$$\frac{d\varphi_t}{dz} = \frac{\mu_o m}{2}\left[\frac{3z^3}{(r^2+z^2)^{5/2}} - \frac{3z}{(r^2+z^2)^{3/2}}\right] \qquad (3-6)$$

Since each individual turn of the mean layer is located at different distance from the magnet dipole center during the magnet oscillation, the total flux rate of change through the whole coil will be the sum of magnetic flux rate of change through each turn ($d\varphi_t/dz$) multiplied by the number of layers as expressed by:

$$\frac{d\varphi}{dz} = N_l \frac{\mu_o m}{2} \sum_{n=-N_t/2}^{n=N_t/2} z_n \left[\frac{3z_n^2}{(r^2+z_n^2)^{5/2}} - \frac{3}{(r^2+z_n^2)^{3/2}}\right] \qquad (3-7)$$

$$z_n = z + n\left(\frac{l}{N_t - 1}\right) \qquad (3-8)$$

The induced emf or the generated voltage by induction in an electrical coil included in a closed loop circuit can be expressed as:

$$emf - L\frac{di}{dt} = iR \qquad (3-9)$$

where L, R are the coil inductance, and the total circuit resistance respectively. Since the voltage drop across the coil inductance is very small compare to emf [56], the electrical power generated by induction can be expressed by:

$$P = \frac{emf^2}{R} \qquad (3-10)$$

If the maximum ideal power needs to be calculated, only coil resistance should be considered.

The electrical damping coefficient (C_e) can be calculated from the mechanical to electrical energy conversion. Assuming no losses occur due to energy conversion hence,

$$f \cdot \dot{z} = \frac{emf^2}{R} = \frac{((d\varphi/dz)\,\dot{z})^2}{R} \qquad (3-11)$$

$$f = \frac{(d\varphi/dz)^2}{R}\,\dot{z} \qquad (3-12)$$

where f represents the electrical damping force, hence

$$C_e = \frac{|f|}{|\dot{z}|} = \frac{(d\varphi/dz)^2}{R} \qquad (3-13)$$

3.4 Response types

In typical conventional energy harvesters, the relative displacement amplitude is maximized at the resonant frequency and decreases away from it. However, FEH shows an uncommon behavior in which four different ways of response of mass/frame relative motion appear over the range of input frequencies. The relative amplitude significantly increases during one response type over others. The different response types are explained here with the aid of a case study simulation with parameters listed in Tables 3-1, and 3-2.

Table 3-1

Mechanical System Parameters

Fiction coefficient – μ	0.2	Air viscous damping coef – C_a (Ns/m)	0.02
Mass – M (kg)	0.03	Spring viscous damping coef– C_s (Ns/m)	1
Stiffness – k (N/m)	196		

Table 3-2

Magnetic and Electrical Circuit Parameters

Coil mean diameter – D (m)	0.021	Coil resistance (R)	0.948Ω
Magnetic moment – m (A. m^2)	25	Coil length – l (m)	0.05
Number of coil turns (N)	75	Number of coil layers (N_l)	1

At a very low input vibration frequency (acceleration) where the inertia force cannot exceed the friction forces, the mass/frame sticky contact cannot be broken. Hence, no relative motion appears and consequently no energy harvesting. This type of response is called “sticking motion” response.

Increasing the input acceleration above the frictional acceleration threshold allows the relative motion to appear. However, at relatively low input acceleration, small relative displacement occurs. Then, the mass will vibrate freely within the frame boundaries and unable to reach both stops periodically, which is called “free motion” response. One side impact may appear in the free motion response, if the mass tilts to vibrate near to one stop.

The relative displacement amplitude increases by further increase of the input frequency for a given input amplitude. If the stroke is not quite large relative to twice the input amplitude, the mass can reach both stops periodically. It can make one impact with one side stop followed by another impact with the other stop, which is called “Impact-impact motion” response. During this response type, the relative amplitude is magnified. The travelling distance of the mass exceeds the mass stroke (S), and the relative vibration frequency is equal to the input frequency (Fig. 3-2).

If the stroke is less than twice the input amplitude, the impact-impact motion can remain the existing relative motion response by further increase of the input frequency. However, in case of stroke larger than twice input amplitude, there is an upper frequency limit after which the impact-impact motion could not exist. In such case, the energy gain by the mass due to impact with one stop cannot be balanced with the energy loss due to friction to reach and impact the other stop in the half periodic time. A form of a chaotic motion appears which involves combination between impacts and free motions. This response type is called “chaotic motion” response. Fig. 3-3 shows the existence frequency range of FEH response types with different stroke values. The frequency range of impact-impact motion response shrinks by increasing the stroke value above twice the input amplitude, while it is unbounded by an upper limit when the stroke is less than twice the input amplitude.

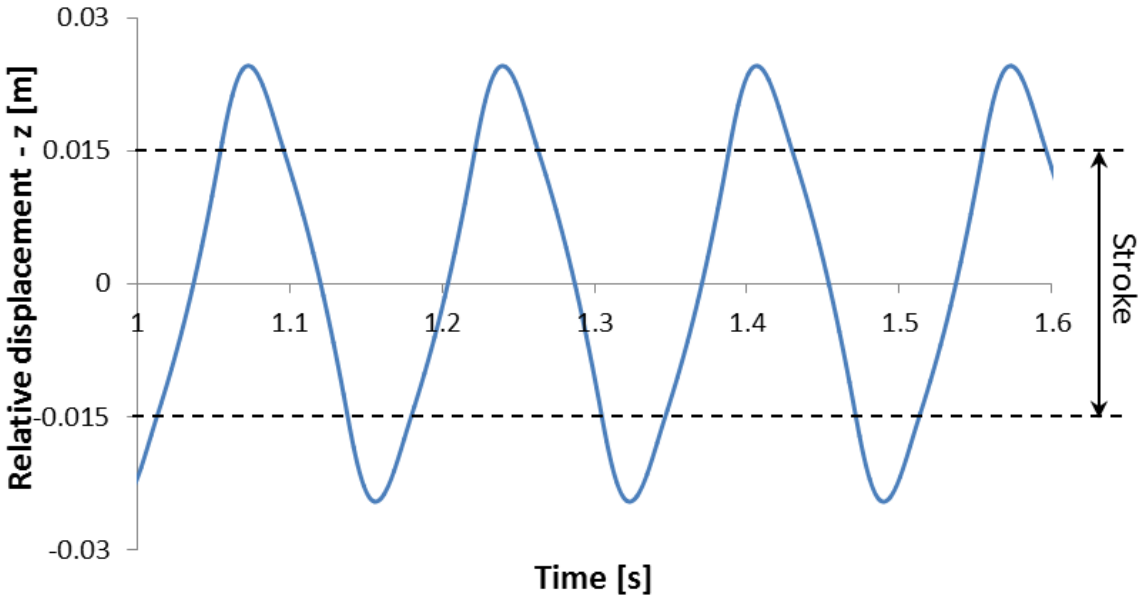

Fig. 3-2. The relative displacement (z) of FEH with 0.03m stroke, for an input vibration of 0.01m amplitude and 6 Hz frequency shows the "impact-impact motion" response

Since higher relative amplitude occurs within the impact-impact motion and consequently significant power harvesting compare to other response types, this response should be guaranteed as the exist relative motion response during harvesting operation. Hence, in this chapter a mathematical condition that determines the existence frequency range of this response type is derived.

Unlike CH, the mathematical model of FEH is nonlinear which can only be solved by time domain simulation. However, in order to derive a mathematical condition to show the effect of different parameters in the frequency range of the impact-impact motion response, the air viscous damping is excluded in analysis for simplicity. This is a valid assumption, since the air damping is small compare to coulomb's damping. However, simulation of Eq. (3-1) could be used further, for more accurate frequency range.

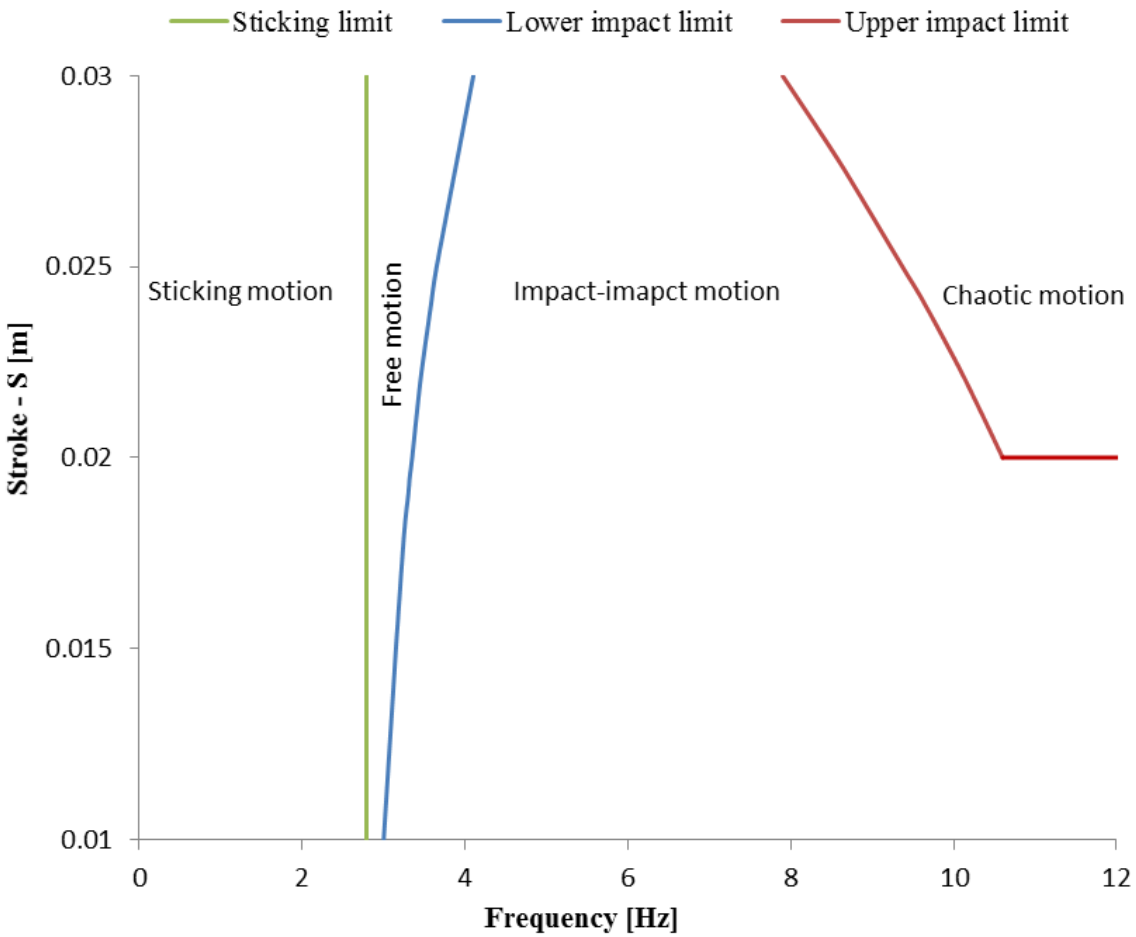

Fig. 3-3. The existence frequency range of different motion responses, which are obtained from simulation of Eq. (3-1) for different stroke values (S) at 0.01 m input vibration amplitude.

The mass can make fully consecutive impacts and the motion becomes periodic in natural (Figs. 3-2, 3-4), when the mass velocities just before and after impact at one side are equal and in opposite direction to its velocities just before and after impact at the other side respectively. In that case, there will be a balance between the energy gain due to impact, and the energy loss due to friction.

At the extreme positions near the stops, the mass velocities just before and after impact are taken u_1, and v_1 respectively (Fig. 3-4). The relation between u_1 and v_1 can take the following form:

$$u_1 = -v_1 + \mu g t_f \qquad (3-14)$$

For a periodic motion,

$$t_i + t_f = \frac{\pi}{\omega} \qquad (3-15)$$

where t_f is the time elapsed between just leaving one stop till just reaching the other, which is called the friction time, t_i is the impact time or the time taken to make one stop impact (Fig. 4), and ω is the input vibration angular frequency.

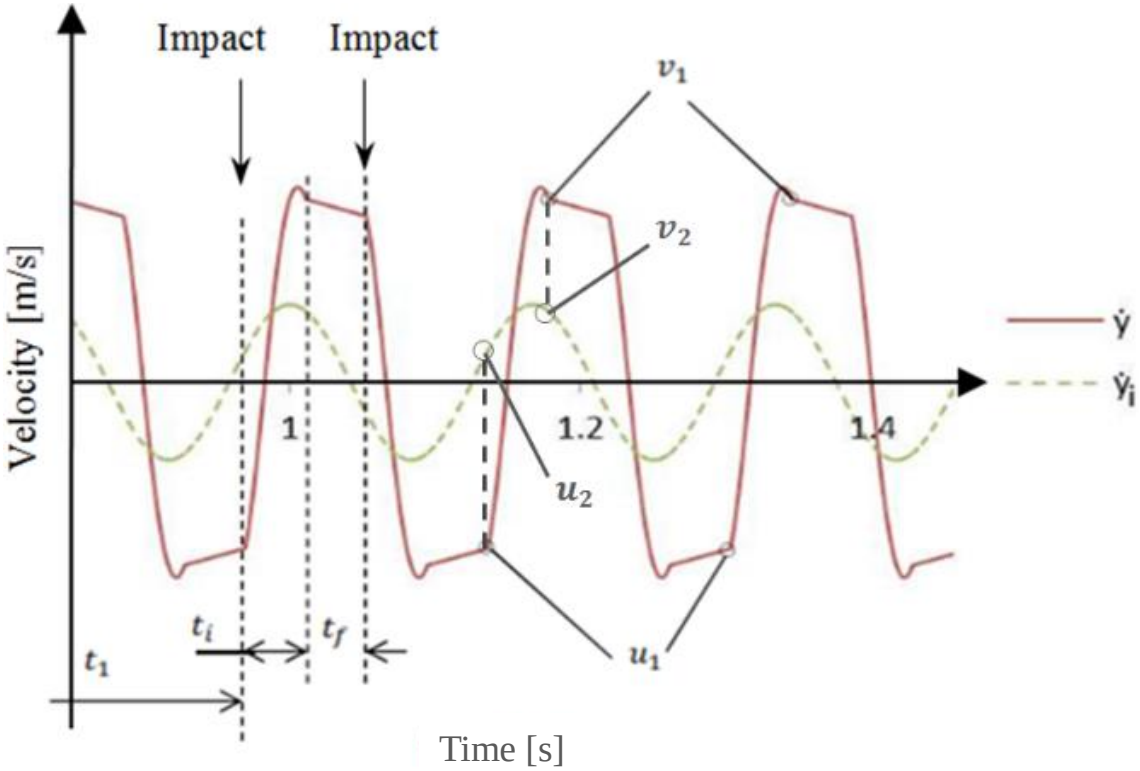

Fig. 3-4. Mass and input vibration velocities during impact-impact motion response at 0.03 m stroke and input vibration of 0.01m amplitude and 6 Hz frequency

The stroke (S) is the distance taken by the mass from just leaving one stop until reaching the other, hence the stroke could be calculated by the integration of the relative velocity over the friction time t_f as expressed by

$$S = \int_{t_1+t_i}^{t_1+t_i+t_f} \dot{z}\, dt \qquad (3-16)$$

where t_1 is any instant at which an impact starts.

Then,

$$\dot{z} = \dot{y} - \dot{y}_i \qquad (3-17)$$

For harmonic input vibration,

$$\dot{z} = [v_1 - \mu g(t - t_1 - t_i)] - [Y_i \omega \cos \omega t] \qquad (3-18)$$

After the integration (Eq.3-16), the stroke can be expressed by

$$S = v_1 t_f - \frac{\mu g}{2} t_f^2 + Y_i[(1 + \cos(\omega t_i))\sin\omega t_1 + \sin(\omega t_i)\cos\omega t_1] \qquad (3-19)$$

By applying Newton's law for collision, we can get a relation between velocities just after impact (v_1& $v_2 = Y_i \omega \cos \omega(t_1 + t_i)$), and velocities just before impacts (u_1& $u_2 = Y_i \omega \cos \omega t_1$)

$$-r = \frac{v_2 - v_1}{u_2 - u_1} \qquad (3-20)$$

where r is the restitution coefficient, u_2, and v_2 are input vibration velocities just before and after impact respectively.

By substituting with Eq. (3-14) into Eq. (3-20), we can get a relation for the velocity just after impact (v_1) as expressed by

$$v_1 = \frac{-r}{1-r}\mu g t_f + \frac{Y_i \omega}{1-r}(r \cos \omega t_1 + \cos(\omega t_1 + \omega t_i)) \qquad (3-21)$$

By substituting Eq. (3-21) into Eq. (3-19), the stroke (S) could be expressed as:

$$S = -\left(\frac{1}{2} + \frac{r}{1-r}\right)\mu g {t_f}^2 + Y_i\sqrt{A^2 + B^2}\sin(\omega t_1 + \gamma)$$

Or,

$$\sin(\omega t_1 + \gamma) = \frac{S + \left(\frac{1}{2} + \frac{r}{1-r}\right)\mu g {t_f}^2}{Y_i\sqrt{A^2 + B^2}} \qquad (3-22)$$

where $A, B, and\ \gamma$ are expressed as below:

$$A = 1 + \cos(\omega t_i) - \frac{\omega t_f}{1-r}\sin(\omega t_i) \qquad (3-23)$$

$$B = \sin(\omega t_i) + \frac{r\omega t_f}{1-r} + \frac{\omega t_f}{1-r}\cos(\omega t_i) \qquad (3-24)$$

$$\gamma = \tan^{-1}\frac{B}{A} \qquad (3-25)$$

We can get the value of impact time (t_i) and restitution coefficient by approximating the mass /stop impact to the case of under-damped free oscillation of spring-mass-damper element similar the case stated by [34] (Fig. 3-5).

Hence, the impact time and restitution coefficient could be expressed respectively by

$$t_i = \frac{\pi}{\omega_n\sqrt{1-\zeta^2}} \qquad (3-26)$$

$$r = e^{-\frac{\zeta}{\sqrt{1-\zeta^2}}} \qquad (3-27)$$

where $\zeta = \frac{C}{2\sqrt{kM}}$, $\omega_n = \sqrt{\frac{k}{M}}$

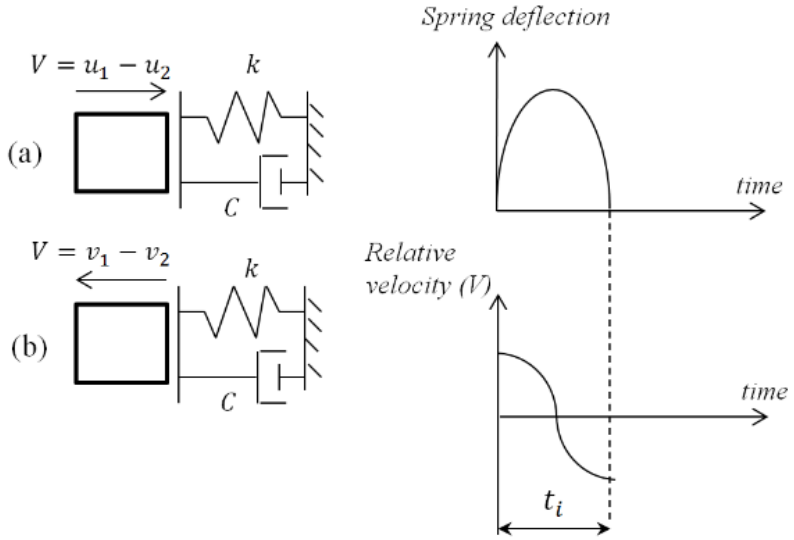

Fig. 3-5 Mass relative motion during impact can be approximated to the case of under-damped free oscillation with an initial velocity of $(u_1 - u_2)$

Equation 3-22 should be satisfied, in order to guarantee the occurrence of the impact-impact motion response. This equation contains a sine-term ($must\ be \leq 1$). Hence, the impact-impact motion response is expected to occur at a specific range of exciting frequencies. Eq. (3-22) simply shows that this range can be widened by decreasing the stroke value relative to input amplitude, as well as reducing coulomb's friction.

3.5 System performance

The mathematical model of FEH is nonlinear. Hence, the performance of FEH is studied in this section with the aid of a case study simulation. In some cases, simulation of similar CH is carried out as well for the sake of evaluation and identifying the effect of mass – spring separation. The common parameters used for FEH and CH simulations are listed in Tables 3-1 and 3-2. However, in some cases there are some parameter changes which is stated in the nearby (M=0.03 Kg does not change in all simulation cases).

3.5.1 Resonant frequency and relative amplitude

Simulation of FEH shows a peak in the relative displacement amplitude over the range of input frequencies. This peak is expected to appear within the impact-impact response, where the relative amplitude is maximized. In case of CH the peak relative amplitude appears near the natural frequency of the system ($\omega_n = \sqrt{k/M}$). However, the relative amplitude peak in case of FEH appears at an angular frequency less than ($\sqrt{k/M}$), which means that the resonant frequency of FEH becomes less due to the mass-spring separation (Fig. 3-7).

In order to show how the resonant frequency of FEH affected by the system parameters due to the mass-spring separation, a mathematical relation of its natural frequency should be derived. Natural frequency is mainly the free oscillation frequency of the undamped system. Hence, the nonlinear coulomb's friction term as well as other damping terms will be excluded in the derivation.

Consider FEH with an initial displacement (Z_o) on one spring while neglecting all frictions and damping in the system (Fig. 3-6).

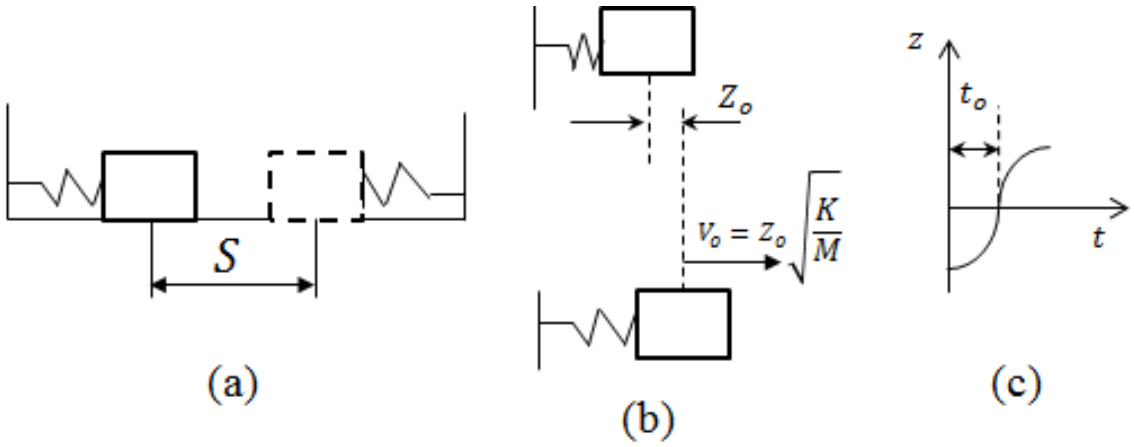

Fig. 3-6. (a) The mass position from just leaving one stop until reach the other, (b) one side spring is compressed with initial displacement (Z_o), (c) spring deflection with time after releasing the mass.

The time taken between initially releasing the mass and just after mass-spring separation is given by

$$t_o = \frac{\pi}{2\omega_n} \qquad (3-28)$$

And the mass velocity just after separation is stated by

$$V_o = Z_o\omega_n \qquad (3-29)$$

Both relations can be obtained easily by applying Newton's law or energy equation, where $\omega_n = \sqrt{k/M}$

The time taken by the mass from just leaving one spring until reach the other (t_f) which is the time taken by the mass to move the stroke distance will be

$$t_f = \frac{S}{V_o} = \frac{S}{Z_o\omega_n} \qquad (3-30)$$

Hence, the time taken to make one period of natural oscillation (T_s) will be

$$T_s = 2(2t_o + t_f) \qquad (3-31)$$

By substituting with the natural frequency of the FEH (ω_{ns}) and the time values Eq. (3-32) will be

$$\frac{2\pi}{\omega_{ns}} = 2\left(\frac{\pi}{\omega_n} + \frac{S}{Z_o\omega_n}\right) \qquad (3-32)$$

Then,

$$\omega_{ns} = \left(\frac{\omega_n}{1 + \frac{S}{Z_o}\pi}\right) \qquad (3-33)$$

Equation 3-33 shows that, the natural frequency of FEH similar to CH depends on the term ($\sqrt{k/M}$), in addition it is affected by a new term which is the stroke relative to the initial displacement (S/Z_o). The existence of this term in the natural frequency relation is a result of the free sliding period. The appearance of the initial displacement in the relation means that the resonant frequency of FEH may be affected by the input vibration amplitude or with the other meaning by the stroke relative to the input amplitude. Coulomb's fiction and other damping terms are excluded in the natural frequency derivation. However, they may have even a small effect on the resonant frequency.

The effect of stroke and input vibration amplitude on the resonant frequency can be truly investigated by simulating FEH with different values of stroke and input amplitudes over the range of input frequencies as shown in Figs. 3-7 and 3-8. Simulation results show that increasing the stroke of FEH can shift the resonant frequency to lower range for the same input amplitude. Unlike CH, this shift is not associated with a decrease in the resonant relative amplitude (Fig. 3-7). In case of CH, shifting resonant frequency to lower range with a given mass accompanied with a decrease in the Q-factor (1/ (2×damping ratio)) which leads to a decrease in the relative amplitude at resonance (Fig. 2-2). However, increasing the stroke of FEH can shift the resonant frequency to lower range with an increase in the internal mass displacement. Hence, higher resonant relative amplitude could be obtained.

Decreasing the input vibration amplitude or increasing stroke relative to the input amplitude can shift the resonant frequency to lower frequency range as expected from Eq. 3-33. This conclusion could also be observed from Fig. 3-8

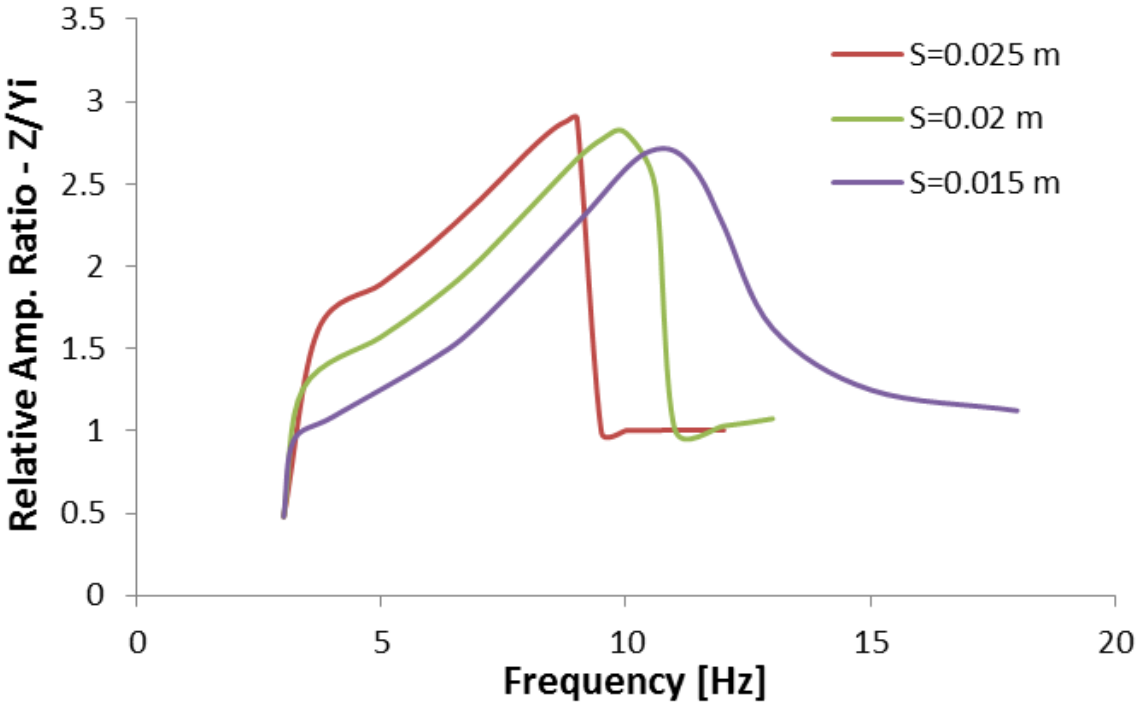

Fig. 3-7. Relative amplitude ratio of FEH with different stroke values at an input vibration amplitude of 0.01m.

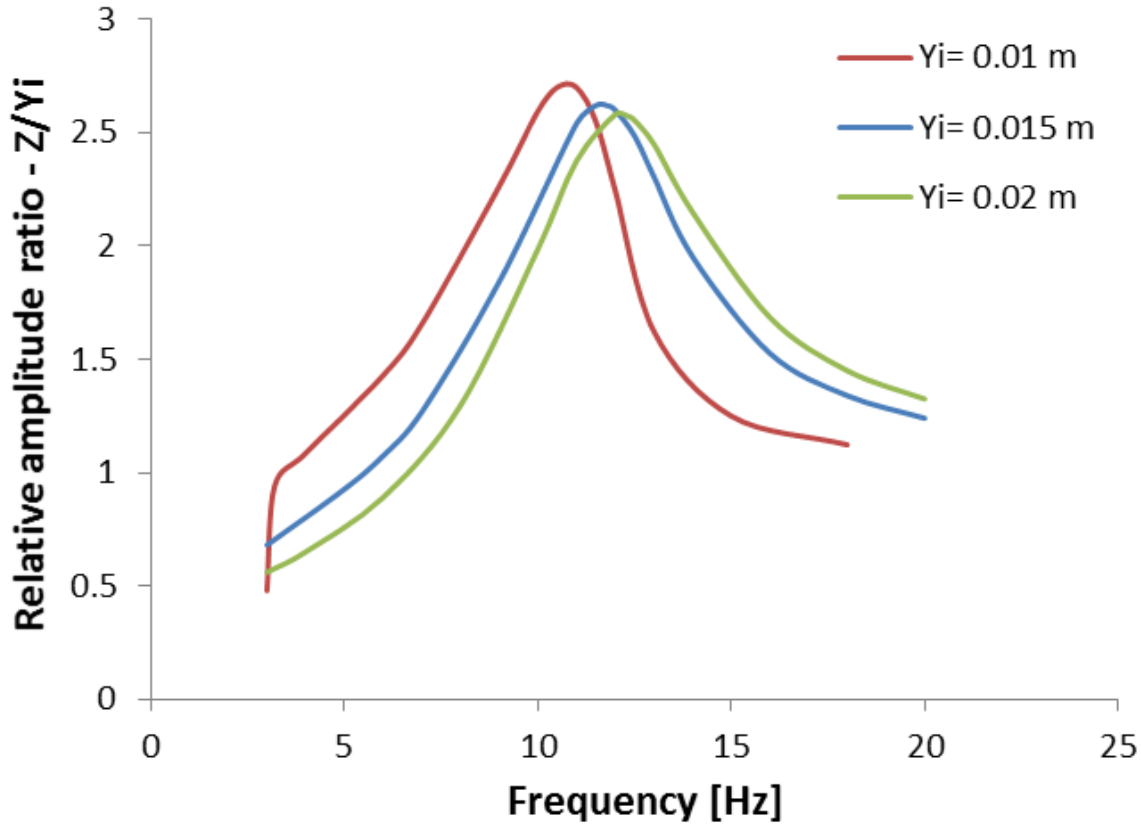

Fig. 3-8. Relative amplitude ratio of the FEH with 0.015m stroke at different input vibration amplitudes over the range of input frequencies.

3.5.2 Comparison with CH

Simulation results of FEH show that its resonant frequency can be shifted to lower ranges (using larger strokes) with an increase in the resonant relative amplitude. Thus, it can give a higher resonant amplification and consequently have a superior performance at lower frequencies. A way to evaluate the performance of FEH is to compare it with the performance of a CH tuned to have same resonant frequency. One comparison is carried out with similar CH (with the same frictional parameters) to identify the effect of mass – spring separation. Another is carried out with an optimum CH (free of coulomb's friction) at a given frequency which is better to evaluate the general performance of FEH and determine its preferable working conditions.

3.5.2.1 Comparison with similar CH

The effect of mass – spring separation can be truly investigated by comparing the performance of FEH with similar CH. One comparison is carried out between FEH with 15 mm stroke and similar CH with the same mass and frictional parameters (Tables 3-1 and 3-2). Both are tuned to have the peak relative amplitude at a frequency of 14 Hz. Tuning of both harvesters is done by altering the utilized spring stiffness, in which 196 Nm^{-1}, and 294 Nm^{-1} are used for CH and FEH respectively.

Figure 3-9 shows the relative amplitude of both harvesters over the range of input frequencies. The relative amplitude can be magnified by the mass – spring separation with the stroke value. The amplitude magnification at resonance can reach one and half at the tuned frequency. The reason of this amplitude magnification is that the resonant relative amplitude of FEH can be increased by matching lower frequency (using larger strokes) (Fig. 3-7), while the resonant relative amplitude of CH with the same mass

decreases by matching the same frequency as a result of the Q-factor decline.

Although, larger stroke can shift the resonant frequency to lower range with an increase in the resonant relative amplitude, we have to keep in mind that increasing the stroke value over twice the input amplitude reduces the frequency range of the impact-impact motion response (Eq. 3-22, Fig. 3-3) and consequently affect the frequency bandwidth (Fig. 3-7).

In case of stroke larger than twice the input amplitude, the relative amplitude is sharply dropped by increasing the input frequency after resonance; since the impact-impact response can be no longer exist after a certain frequency (Fig. 3-7). However, in case of stroke less than twice the input amplitude, the impact-impact response can continue as the system motion response by increasing the input frequency, where the relative amplitude decreases smoothly.

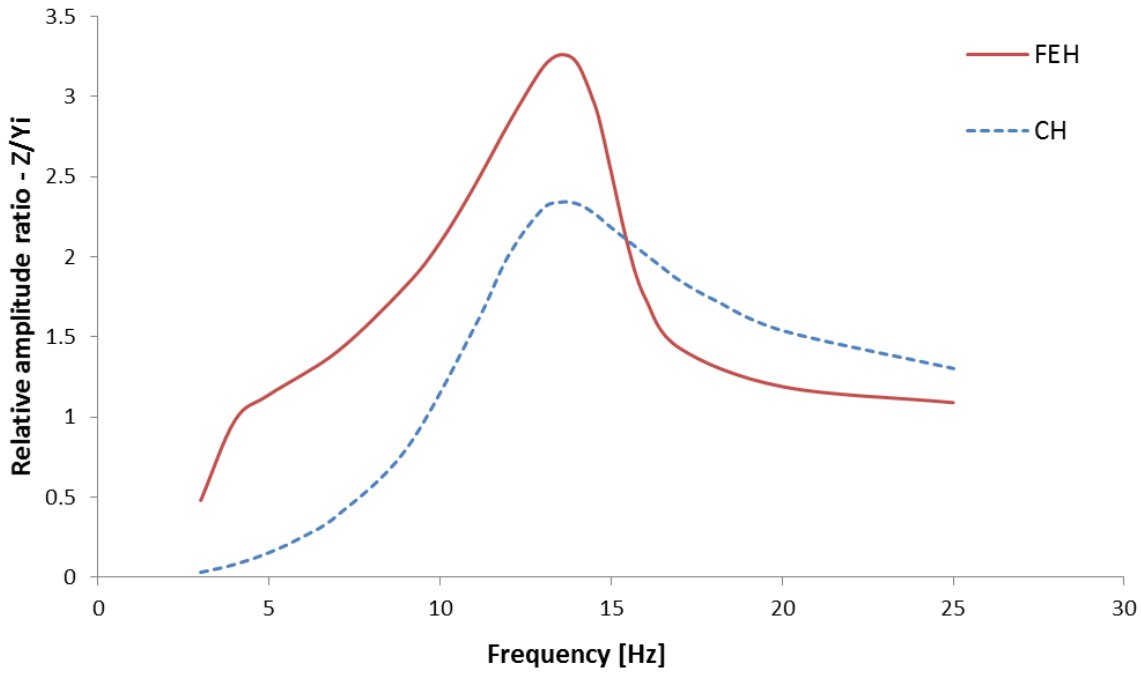

Fig. 3-9. Relative amplitude ratio of FEH-0.015m stroke and CH tuned to have a resonant frequency of 14 Hz using 294 Nm^{-1} and 196 Nm^{-1}spring stiffness respectively and input amplitude of 0.01 m.

3.5.2.2 Comparison with optimum CH

The general performance of FEH at a certain frequency can be evaluated by comparing it with the performance of the optimum CH at the same frequency. The optimum CH which can give the maximum resonant amplification at a given frequency is that one with a tuned resonant frequency to the input frequency, null coulomb's friction (some CH designs may allow that), and the maximum possible Q-factor ($M\omega_n/C$) (minimum damping ratio). In fact, maximizing the Q-factor at a given frequency can be reached by minimizing the viscous damping and maximizing the oscillating mass. However, viscous damping cannot be decreased over a certain limit, and in some applications there is a restriction on the maximum oscillating mass. Since, the main advantage of FEH is having a high resonant amplification at low frequencies, it is expected to show better performance over a CH with Q-factor below a certain limit. Thus, the performance of FEH is compared here with the performance of CH (free of coulomb's friction) with different Q-factors and tuned to have a resonant frequency of 14 Hz (as an example). Different Q-factors are obtained by varying the total viscous damping coefficient (C), and tuning is done by altering the utilized spring stiffness, in which 232 Nm^{-1}, and 294 Nm^{-1} spring stiffnesses are used for CH and FEH respectively. The other simulation parameters are kept the same as listed in Tables 3-1, and 3-2 except coulomb's friction coefficient of CH is zero.

Figure 3-10 shows the relative amplitude ratio of CH with different Q-factors (different viscous damping – C) and FEH tuned at the same frequency. Higher relative amplitudes could be obtained by CH over FEH for Q-factors above 5.28 or viscous damping coefficients below 0.5 for the same oscillating mass. However, from this Q-factor and below FEH shows a better performance.

Table 3-3

Relative amplitude ratios at resonance of CH and FEH with the same resonant frequency of 14 Hz at different viscous damping coefficients.

Damping coefficient (C) (Nsm^{-1})	Damping ratio of CH ($\zeta = \frac{C}{2M\omega_n} = \frac{1}{2Q}$)	CH	FEH
0.1	0.019	26.05	8.18
0.2	0.038	13.13	7.7
0.4	0.076	6.57	6.41
0.5	0.095	5.28	5.74
0.6	0.114	4.38	5.11
0.8	0.152	3.30	4.06
1	0.189	2.64	3.3
1.5	0.284	1.76	2.23

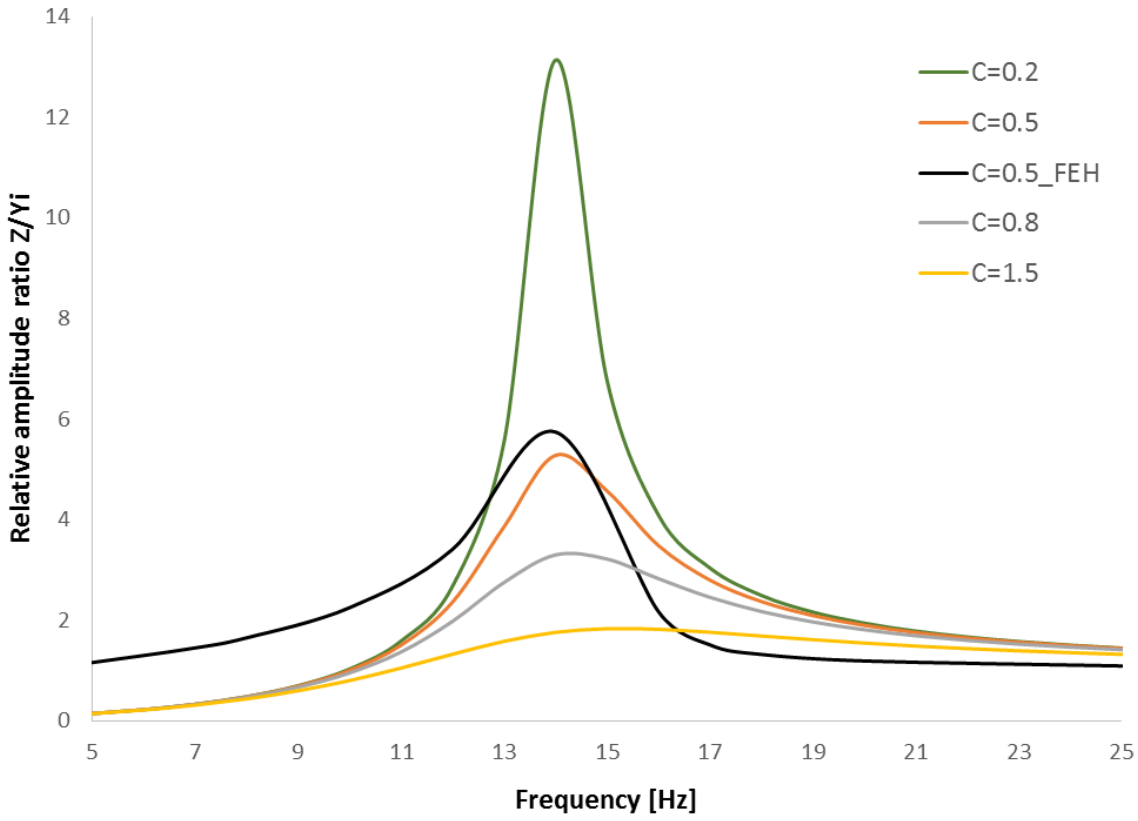

Fig. 3-10. Relative amplitude ratio (≅Q-factor) of CH with 0.03kg oscillating mass at different viscous damping coefficients over the range of input frequencies are shown with the relative amplitude ratio of FEH-0.015m stroke with the same mass and tuned at the same frequency of 14 Hz.

3.5.2.3 The effect of coulomb's friction

Coulomb's friction is another important parameter appears with the proposed design of FEH. The allowed free motion requires the mass to be supported by the frame to provide a guide for the mass motion and guarantee its right oscillation. Although the spring viscous damping is absent during the free motion, an additional sliding (coulomb) friction exists due to mass/frame support. In case of CH, the mass is always connected by the spring. If sufficient rigid mechanical springs are utilized, they can provide the mass support without the need for frame support. However, when matching low frequencies using compliant mechanical springs or when magnet springs are utilized, the frame support becomes necessary and coulomb's friction would exist. Hence, in this section the effect of coulomb's friction on the performance of FEH and CH is investigated. The relative amplitude of both FEH and CH are simulated and compared at different coulomb's friction coefficients. Simulation is carried out with the parameters listed in Tables 3-1, and 3-2 except the varied coulomb's friction coefficients.

Simulation of the relative amplitude of FEH and CH at different coulomb's friction coefficients are shown in Figs. 3-11 and 3-12 respectively. Increasing the involved coulomb's friction generally shows a decrease of the relative amplitude in both harvesters. In case of FEH, it prevents the impact – impact motion from starting at lower frequencies. In addition, it slightly shifts the corresponding frequency to the peak amplitude to lower frequency ranges. However, in case of CH increasing coulomb's friction has the same effect as increasing viscous damping (or damping ratio) on the resonant frequency. The peak amplitude appears at frequency higher than the harvester natural frequency ($f_n = \frac{1}{2\pi}\sqrt{K/M}$) by increasing either viscous damping (Fig. 2-2) or coulomb's friction (Fig. 3-12).

It is worth mentioning that, the effect of coulomb's friction is more significant when the oscillation is in the horizontal plane. However, when the oscillation or the harvester works in vertical plane, the effect of coulomb's friction could be neglected for both CH and FEH.

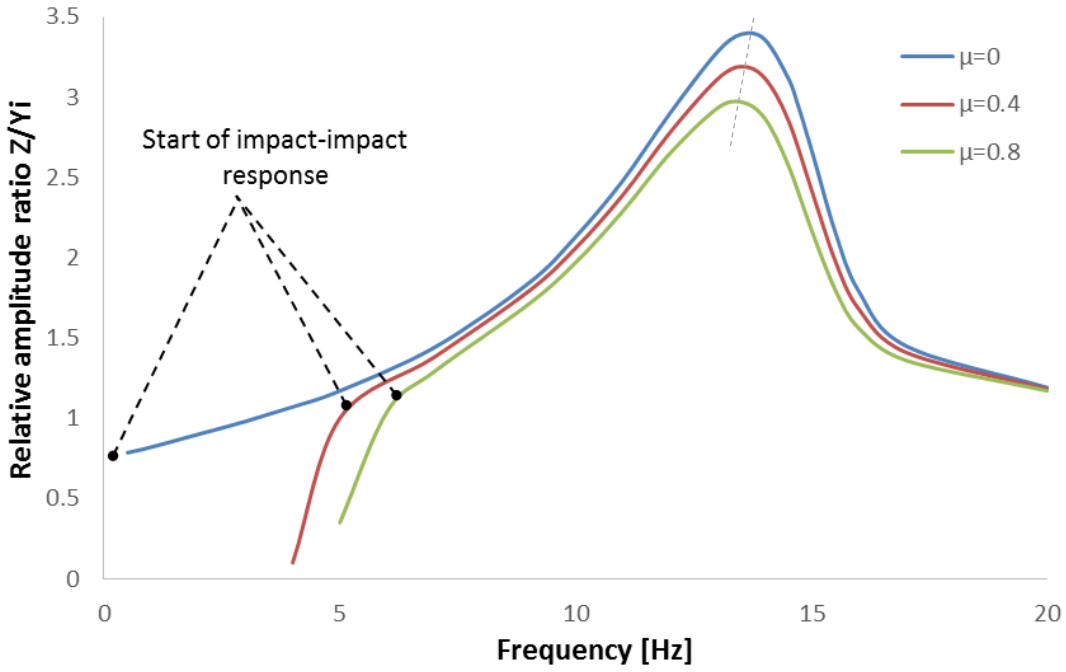

Fig. 3-11. Relative amplitude ratio of FEH with 0.015 m stroke and 294 Nm^{-1} spring stiffness at different coulomb's friction coefficients.

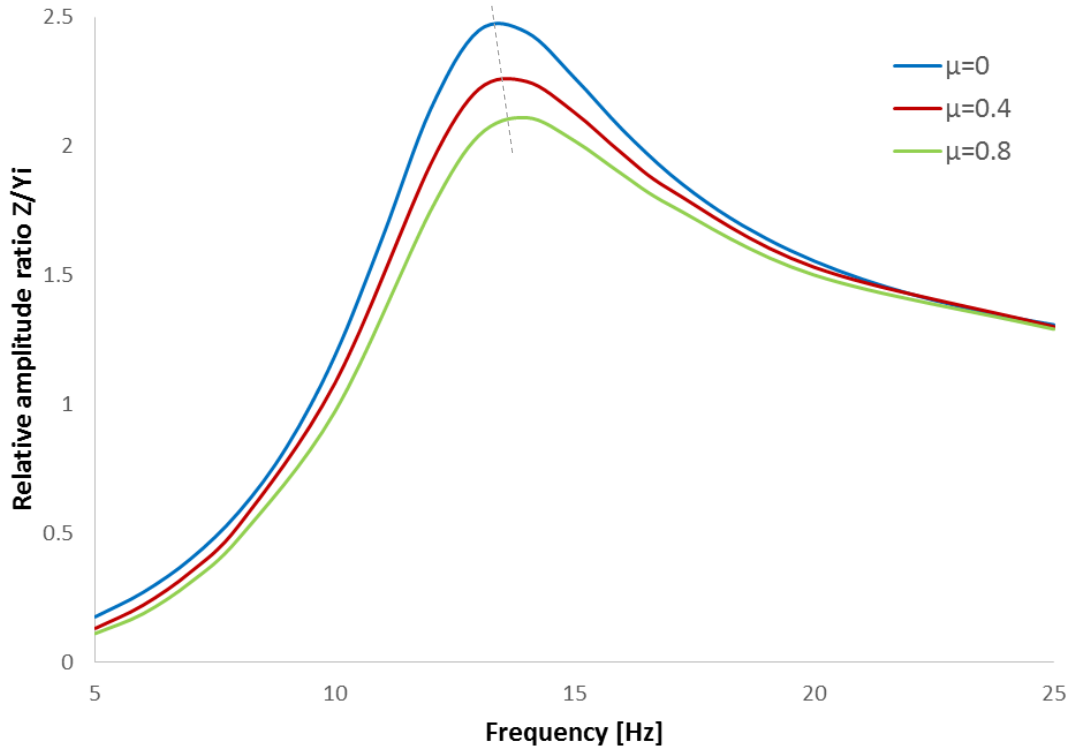

Fig. 3-12. Relative amplitude ratio of CH with 196 Nm^{-1} spring stiffness at different coulomb's friction coefficients ($f_n = 12.86\ Hz$).

3.5.3 Power harvesting

In general, the induced voltage and power generated by moving magnet inside a coil associated with electromagnetic energy harvesting depends on two main quantities, which are the average flux rate of change with respect to the magnet/coil relative displacement ($d\varphi/dz$), and the magnet/coil relative velocity (dz/dt) (Eq. 3-4). Higher flux rate of change means higher ability of mechanical to electrical energy conversion (Eq. 3-13), and higher relative velocity means higher kinetic energy available to be converted to electrical energy. The instantaneous flux rate of change increases with the magnet relative displacement inside the coil (Fig. 3-13). It takes its highest value near the coil ends and zero at the middle.

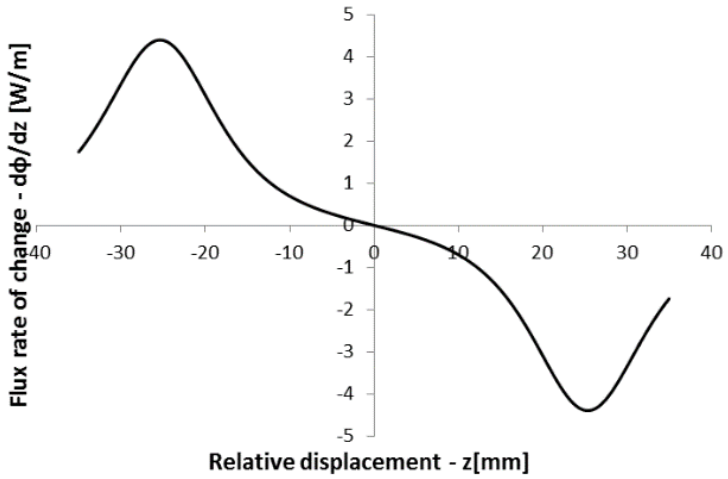

Fig. 3-13. Variation of the flux rate of change with respect to the relative displacement ($d\varphi/dz$) with magnet position within the coil for a coil length of 50 mm.

In case of CH, the relative velocity amplitude at resonance $(QY_i\omega_n)$ increases with higher resonant relative amplitude or with higher Q-factor. In the applications with a constraint on the maximum oscillating mass, matching low frequencies can be done using more compliant springs. Low spring stiffnesses are usually associated with a decline in the Q-factor, which will lead to a decrease in the induced voltage and generated power. However, in case of FEH the presence of mass – spring separation by stroke value allows matching lower frequencies with higher resonant relative amplitude. Hence, higher relative velocity can be obtained (Figs. 3-14, 3-15), and consequently more voltage and power could be generated (Fig. 3-16).

Therefore, FEH is preferred to be used and can beat CH under certain circumstances. Those circumstances are when there is a sufficient allowable internal mass displacement (for amplitude magnification) while there is a limit on increasing the Q-factor of CH at the operating frequency due to the application constraints. In fact, CH has a better performance in high Q-factor systems and the critical Q-factor below which FEH is preferred to be used depends on the design configuration. For instance, in the case of FEH Vs CH comparison (Fig. 3-10), FEH is preferred to be used over CH at a frequency of 14 Hz when the Q-factor of CH cannot be increased over 5.28. In such case FEH can give a higher resonant amplification and consequently better performance.

Figure 3-17 shows the power output of FEH and the optimum CH with Q=2.64 corresponding to C=1. More realistic value of viscous damping (C=1) is selected for the comparison based on a simple experiment carried on a free linear spring – mass system (M=0.036 Kg, K=240 $\mathrm{Nm^{-1}}$) oscillating in the open atmosphere. Detecting the viscous damping experimentally is done based on the logarithmic decrement method. An input vibration of amplitude of 0.01m is used. Both harvesters are tuned at the same frequency of 14 Hz. Tuning is done by selecting the appropriate spring stiffness for each harvester, in which $294\ \mathrm{Nm^{-1}}$ and $232\ \mathrm{Nm^{-1}}$ spring stiffnesses are selected for FEH and CH respectively, while other parameters are kept the same as listed in Tables 3-1and 3-2. The power generated at resonance by FEH appears more than three times that generated by CH (Q=2.64) with less compliant spring stiffness. In addition, the impact nonlinearity leads to a higher bandwidth as also concluded in [32, 36].

When we consider the comparison between FEH and optimum CH (Q=2.64) over a range of tuned frequencies, Table 3-4 shows the power generated and utilized stiffnesses by FEH and CH at different tuned frequencies. The power magnification of FEH over CH increases when matching lower frequencies. It can reach more than 7 times at frequency of 11 Hz. However, this power magnification decreases by matching higher frequencies where the performance of both harvesters approach each other (Fig. 3-18).

The power magnification of FEH over CH is higher at lower frequencies since the increase of internal displacement due to stroke value is quite large compare to the spring deflection. However, when matching higher frequencies the spring deflection overwhelms the internal displacement in FEH and consequently the performance of both

harvesters will approach each other.

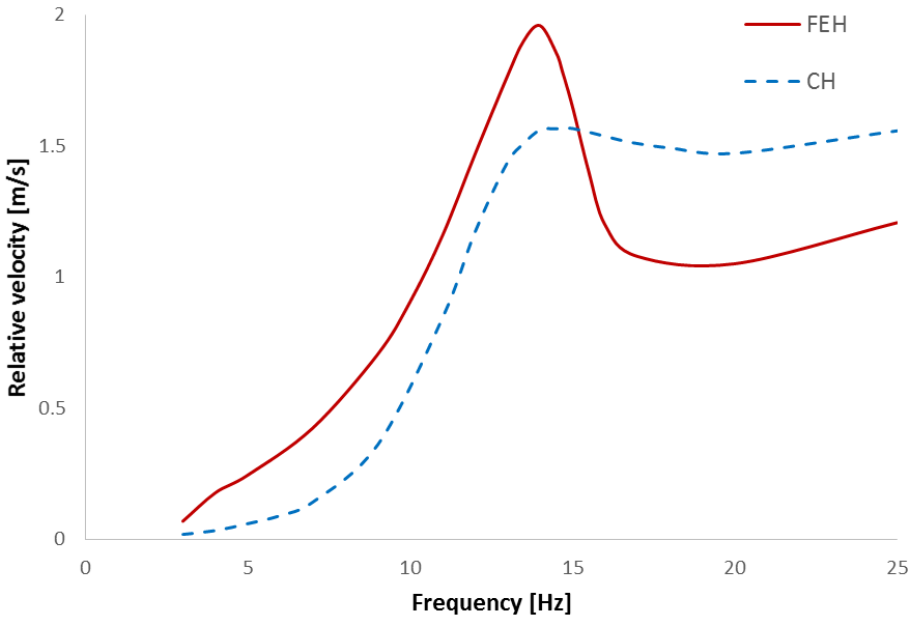

Fig. 3-14. RMS relative velocity of FEH with 0.015m stroke and CH (μ =0, Q=2.64), tuned to have a resonant frequency of 14 Hz using 294 Nm^{-1} and 232 Nm^{-1} spring stiffness respectively and input amplitude of 0.01 m.

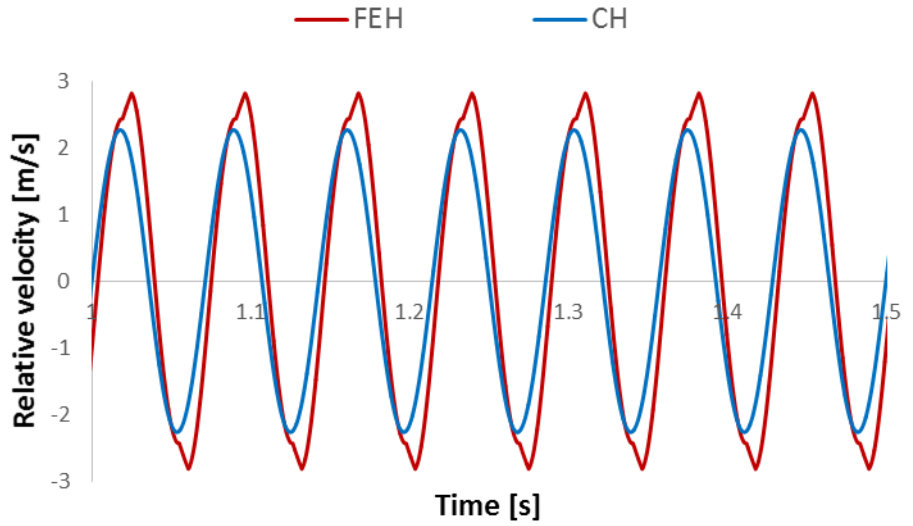

Fig. 3-15. Time variation of the relative velocity of FEH – 0.015 m stroke and CH (μ=0, Q=2.64) at their resonant frequency of 14 Hz and 0.01 m input vibration.

It is worth mentioning that, there is a minimum limit of the frequency that FEH can work with, which is determined by the input vibration acceleration and the internal sliding friction. If the input acceleration is less than the frictional acceleration (μg), no relative

motion would appear, and consequently no energy harvesting. However, the input frequency should be high enough so that the mean input acceleration becomes sufficiently higher than the internal friction acceleration, which allows sufficient relative motion to start (Fig. 3-11).

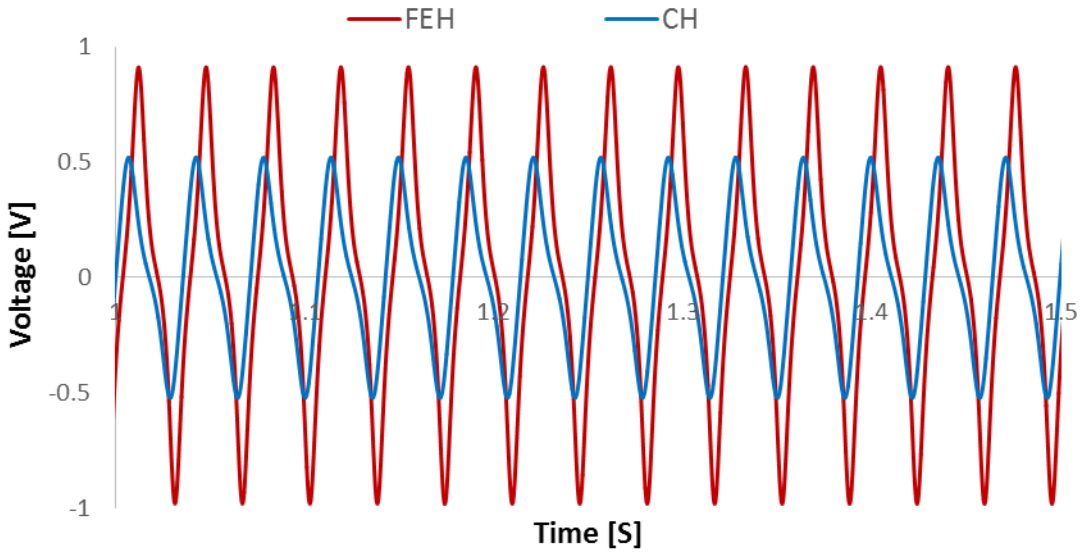

Fig. 3-16. Instantaneous *emf* generated by FEH – 0.015 m stroke and CH (μ=0, Q=2.64) at their resonant frequency of 14 Hz and 0.01 m input vibration.

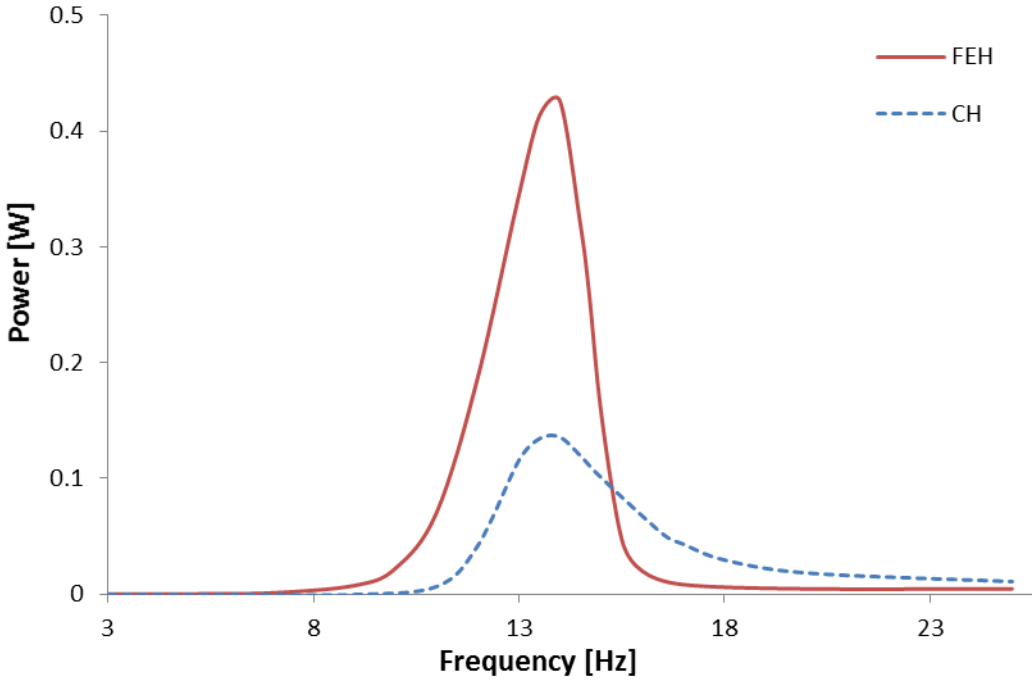

Fig. 3-17. RMS power generated by tuned FEH – 0.015m stroke and CH (μ=0, Q=2.64) at 14 Hz input vibration frequency and 0.01m input amplitude.

Table 3-4
RMS Power generated and utilized spring stiffness by tuned CH and FEH with 0.015 m stroke at different input frequencies and 0.01m input amplitude.

f (Hz)	k_{FEH} (N/m)	k_{CH} (N/m)	P_{FEH} (W)	P_{CH} (W)	PM P_{FEH}/P_{CH}
11	196	143	0.122	0.017	7.19
14	294	232	0.426	0.136	3.13
16	392	303	0.875	0.449	1.95
22	680	573	2.93	2.76	1.06

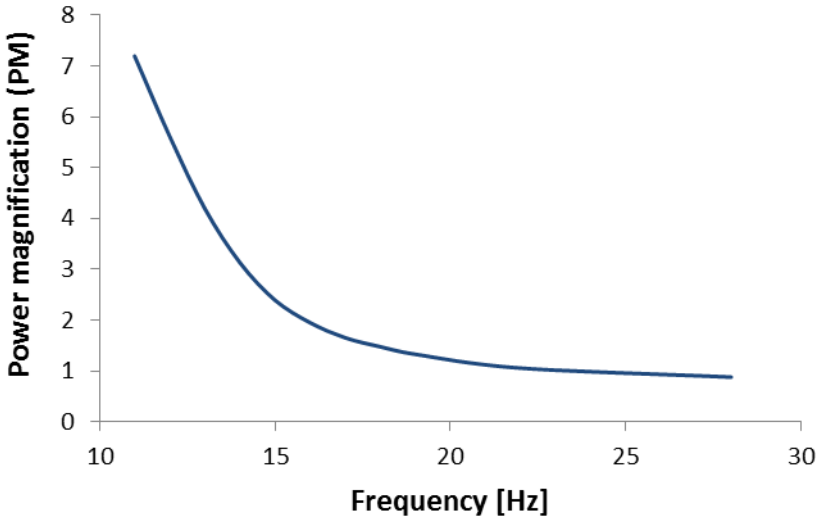

Fig. 3-18. Power magnification of FEH – 0.015m stroke over CH over the range of tuned frequencies with 0.01 m input amplitude.

One design advantage of FEH is that, the highest magnet relative velocity appears at the positions near stroke ends (just before impact) (Fig. 3-19). In the same time, the maximum instantaneous flux rate of change ($d\varphi/dz$) of a moving magnet inside a coil appears at the coil ends. Thus, improving the output voltage ($\frac{d\varphi}{dz} \times \frac{dz}{dt}$) by matching the region of high relative velocity with that with high instantaneous flux rate of change can be easily achieved using single coil with appropriate length.

However, in case of the linear spring-mass oscillator, the magnet relative velocity takes its highest value at the middle of the oscillating distance and decreases by moving towards the extreme positions. Hence, one way to improve the output voltage by matching the region of high relative velocity with that with high flux rate is to use two coils separated by a distance in the middle. This configuration was previously introduced [57], however,

additional harvester length is needed which may increase the total harvester size. If the same length is added to FEH, it will allow utilizing larger strokes which will boost the output power of FEH as well.

Since the instantaneous and RMS relative velocities of FEH are higher than that of CH (Figs. 3-14, and 3-15), the power generated by FEH would remain higher than that generated by CH, even if the flux/velocity matching issue is not considered and the average flux rate of change is considered the same from both harvesters.

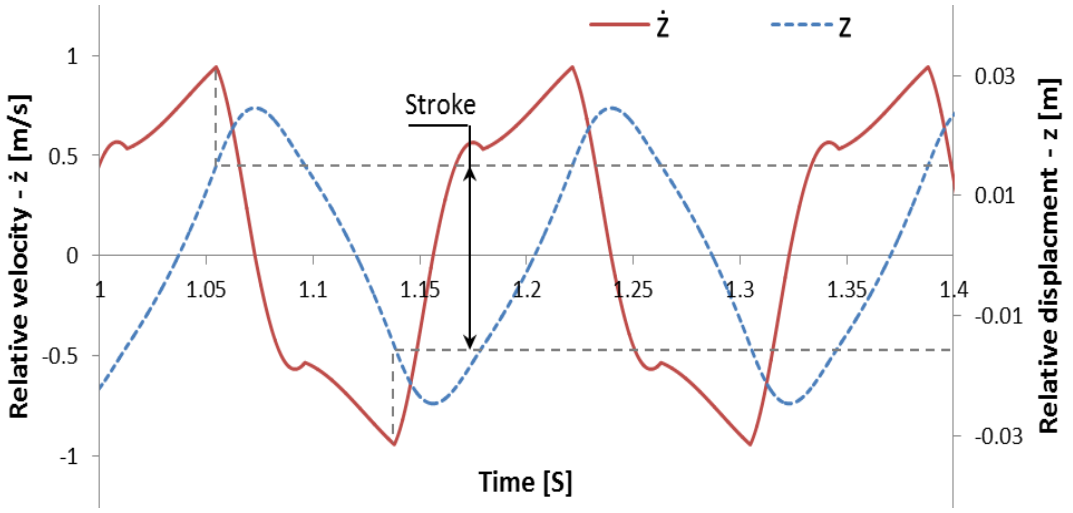

Fig. 3-19. Relative velocity and displacement of FEH with 0.03 m stroke for an input vibration of 0.01 m amplitude and 6 Hz frequency shows that the maximum relative velocity appear at stroke ends just before impact.

3.6 Experimental comparison

An experiment is carried out in this work to investigate the power magnification of FEH, however over the similar CH with the same mass and frictional parameters. A large size system of about 10 cm length is selected to facilitate fabrication and measurements. Both harvesters have the same coil, frame, and magnets (parameters are listed in Table 3-5) except the utilized spring. A helical spring of 128 Nm^{-1} stiffness is selected for CH while a shorter one with 240 Nm^{-1} stiffness is selected for FEH, so that both can give the peak power near the same frequency of about 10 Hz.

Table 3-5

Parameters of FEH and CH Used in the Experiment.

Fiction coefficient-μ	0.2	Total number of turns – N	88
Mass – M (kg)	0.036	Coil length (mm)	40
CH stiffness – k_{CH} (N/m)	128	Coil resistance – R (Ω)	1.19
Coil wire diameter (mm)	0.35	FEH stroke - S (mm)	26
Size – L (mm)	100	FEH stiffness – k_{FEH} (N/m)	240

The test input signal used in the experiment has amplitude of 0.01m and frequency ranged from 3 to 21 Hz. The vibration motion is provided by a screw powered linear guide actuated by AC servo motor. Closed loop control system consists of AC servo drive and incremental encoder included in the motor is used to ensure the accuracy of the input vibration. The energy harvester is attached to the linear guide slider through two vertical aluminum supports. The output electrical signals from both harvesters are measured using V/A meter source, which can detect voltage signal ranged from 1 μV to 211 V, and current signal from 10 pA to 1.055 A.

The energy harvester (Fig. 3-20) consists of a magnet mass vibrating within an electrical coil. The mass is composed of pieces of neodymium magnet rings arranged on an oil free bush to provide a low coefficient of friction. The mass slides over a smooth linear guide. The guide is assembled with four screw rods by two side flanges. The four rods are used as a support for enamelled copper wire, which is wounded over them to form the electrical coil.

The experimental results (Fig. 3-21) show that FEH has a significant improvement over CH when matching frequency of 10 Hz. The power generated by FEH can reach over 350 mW with a power magnification of about 10 times over similar CH. In addition, the impact nonlinearity increases the bandwidth of FEH over CH as shown in Fig. 3-22.

If we consider the effectiveness of FEH, according to the effectiveness formula presented by Mitcheson [58], the effectiveness of the experimental FEH is about 8.6 % based on an input vibration of 10mm amplitude and 10 Hz frequency.

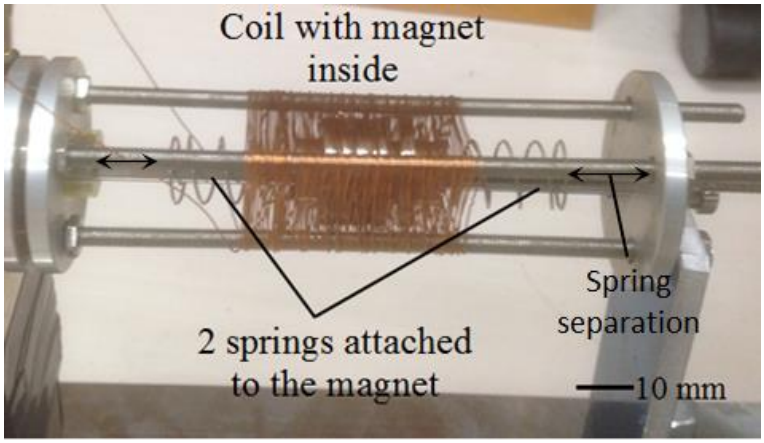

Fig. 3-20. Configuration of the energy harvester used in the experiment. The figure shows the set of FEH.

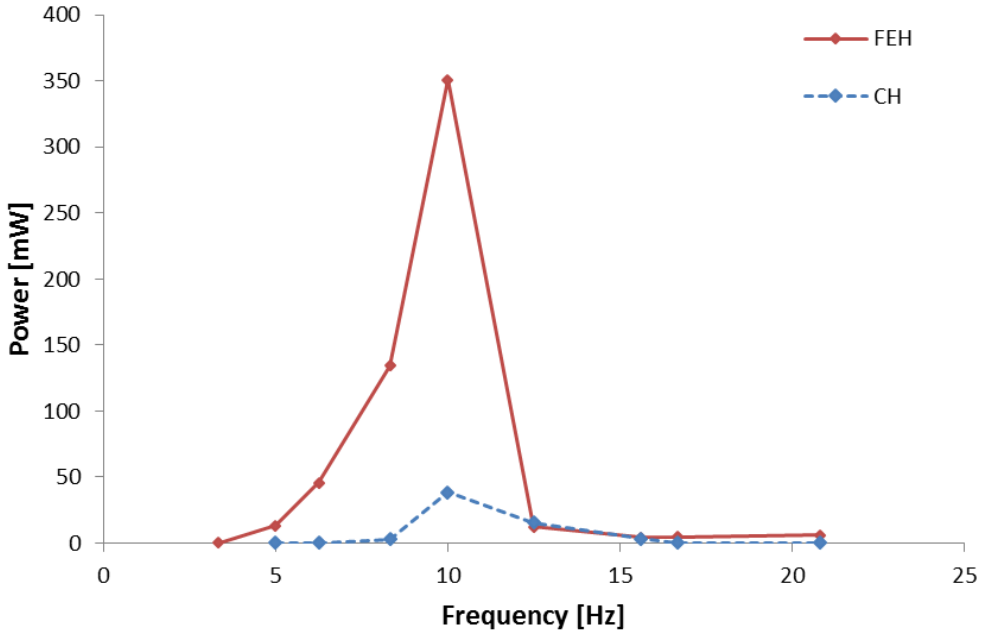

Fig. 3-21. Measured RMS power generated by both FEH and CH for input vibration amplitude of 0.01 m.

3.7 Summary

In this chapter, study of electromagnetic vibration energy harvesting based on free motion with elastic end stops impact is presented, which resulted in a harvester (FEH) that can work effectively at low frequencies. Unlike conventional energy harvester (CH), the mass in the proposed harvester is separated from the spring with a certain distance (stroke) which allows the mass to move freely inside the harvester frame and make impacts with spring end stops.

The presence of spring – mass separation with elastic end stops impact allows matching low frequencies with high resonant relative amplitude compared to similar linear spring-mass system (CH) with the same mass. As a result, higher relative velocity could be obtained and consequently higher power could be generated when matching low frequencies. Therefore, FEH is preferred to be used over CH under certain circumstances. Those circumstances are matching low frequencies with a sufficient allowable internal mass displacement while the Q-factor of CH cannot be increased over a certain limit due to the application constraints. In fact, CH has a better performance in high Q-factor systems and the critical Q-factor below which FEH is preferred to be used depends on the design configuration. A case study simulation of both FEH and CH with 0.03 Kg mass tuned at a frequency of 14 shows that FEH is preferred to be used when the Q-factor of CH cannot increase over 5.28.

FEH shows an uncommon dynamic behavior, in which the internal mass oscillation takes four different ways of response over the range of exciting frequencies. The relative amplitude is magnified within one response type over others, at which the magnet can make consecutive impacts with both stops periodically.

Simulation results show that FEH has a resonant frequency less than that of similar CH with the same mass and spring stiffness due to mass-spring separation. A derived mathematical relation of FEH's resonant frequency shows its dependency on stroke as well as the utilized mass and spring stiffness. Increasing the stroke relative to the input amplitude can shift the resonant frequency to lower ranges with an increases of the total internal mass displacement. Consequently, FEH can match lower frequencies with higher resonant relative amplitude which resulted in a significant power output at low frequencies.

The spring/mass impact exists in FEH can increase the frequency bandwidth due to impact nonlinearity. However, increasing stroke over twice the input vibration amplitude shows a decrease in the bandwidth which put a limit on the maximum stroke value that could be utilized. Simulation comparisons between FEH and optimum CH with Q=2.64 are carried out (more realistic Q is selected based on experimental value of viscous damping), in which the power magnification of FEH over CH can reach more than 3 and 7 times at a tuned frequency of 14Hz and 11Hz respectively (More realistic value of Q is

selected based on an experimental value of viscous damping). Experimental comparison also carried out with a similar CH in which a power magnification over 10 times can be obtained at 10 Hz tuned frequency. The power magnification generally increases by matching lower frequency, which emphasize the advantage of FEH for low frequency operations.

Chapter 4 Study of free / hard stops impact harvester (FHH)

4.1 Introduction

In this chapter, a study of electromagnetic vibration energy harvesting based on free motion with hard stops impact is presented. A proof magnet mass is allowed to move freely inside a tube-carrying electrical coil, and collide with two hard end stops when it reaches the extreme positions. Power harvesting is achieved from magnet/tube relative motion by electromagnetic induction. The free motion promotes power harvesting at low frequencies while combined free motion with hard stops impact leads to non-resonant dynamic behavior, in which the output power increases with both input amplitude and/or frequency. The spring – damper element model becomes inappropriate for modelling hard stops. Instead, the impact force is modelled according to Lankarani and Nikravesh [59], which considers the elastic and damping natural of the collided bodies. The obtained mathematical model is nonlinear which can be solved numerically. A case study of the free / hard stops impact harvester (FHH) with certain parameters is studied and analyzed using the derived model. Uncommon way of oscillation is observed in which four different ways of response of magnet/tube relative motion appear over the range of input amplitudes and frequencies. However, the last response type is different than the case of FEH. In addition, a continuous raise of the output power is observed with input amplitude and/or frequency.

Two different experiments are conducted. The first is carried out on four fabricated prototypes with identical sizes, however with different magnet shapes. This experiment shows the effect of different magnet shapes on the harvesting performance. The second is performed on two different size prototypes with the same magnets. Finally, comparison is made between some FHH prototypes presented in this work and some low frequency energy harvesters stated in literature. The comparison shows the advantageous of FHH for size minimization as well as its improved performance with large input amplitudes.

4.2 System configuration and fabrication

The schematic of the electromagnetic energy harvester based on free/ motion with hard stops impact (FHH) is shown in Fig. 4-1. It simply consists of a thin walled tube with a cylindrical permanent magnet inside and small gap in between (the magnet can also takes the shape of ball or double ball as shown in experimental section). The tube is closed at

both ends by two thin washers. Enamelled copper wire is wounded over the tube to form an electrical coil and secured in position by the tube flanges. The coil consists of multiple layer windings. Each coil layer has a number of horizontal turns, and the layers are arranged vertically one over another. By giving an input vibration to the tube (Fig. 4-1), the magnet can move freely, and collide with end washers which act as stops. The end washers are selected so that they allow air escaping from the tube during the magnet oscillation. The relative oscillation generates an electrical voltage in the coil by induction.

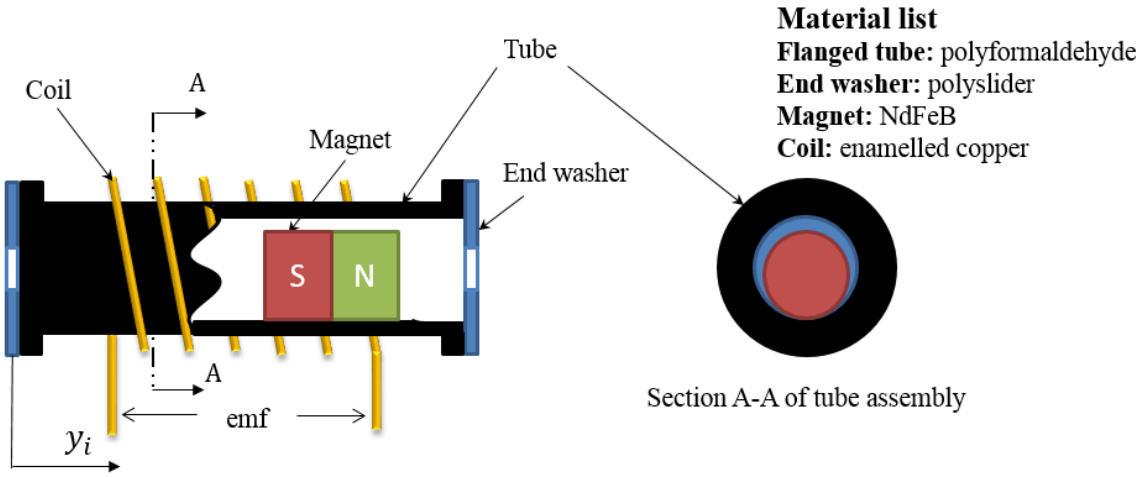

Fig. 4-1 Schematic of free / hard stops impact harvester (FHH)

The simple construction of FHH allows fabrication of a prototype of 10 mm in either total length or diameter, which can be conventionally assembled from commercially available components. The flanged tube is made from polyformaldehyde plastic with 4 mm inner diameter and 0.25mm thickness, glued at both ends with polyslider plastic thin washers to act as stoppers. Strong NdFeB magnets are utilized. These dimensions and configurations are taken for the modelled case study and all experimental prototypes. The electrical coil is wounded over the tube outer surface using manual coil winding machine.

4.3 Mathematical modelling

By giving an input vibration $y_i(t)$ to the tube, the equation of motion of the permanent magnet can be expressed as:

$$M\ddot{y} + C\dot{z} + \frac{z}{|z|}F_N + \frac{\dot{z}}{|\dot{z}|}\mu Mg = 0 \qquad (4-1)$$

where M is the magnet mass, y is the absolute magnet displacement, z is the magnet relative displacement ($z = y - y_i$), F_N is the impact force with stops, C is the total viscous damping coefficient which includes parasitic damping coefficient (C_a), and electrical damping coefficient (C_e) [60], μ is the coulomb's friction coefficient.

The contact between the cylindrical magnet and the flat end stop can be approximated to cylindrical/half-space contact. Hence, the impact force can be modelled according to Lankarani and Nikravesh [58], which is a modified hertz contact model that consider the elastic as well as the damping nature of the collided bodies as expressed by

$$F_N = \begin{cases} K\delta^n + D\dot{\delta} & \delta > 0 \\ 0 & \delta < 0 \end{cases} \qquad (4-2)$$

where $K\delta^n$ represents the elastic force and $D\dot{\delta}$ accounts for energy dissipation. K is the generalized stiffness parameters, D is the hysteresis damping coefficient, δ is the penetration in stopper ($\delta = |z| - \frac{S}{2}$), and $\dot{\delta}$ is the relative penetration velocity. The exponent n depends on the contact surfaces, which takes the value of (n =1) for cylinder/half-space contact [58], and S is the magnet stroke which is the full traveling distance by the magnet from one stopper to the other.

The generalized stiffness parameter K is given for cylindrical/half-space contact by [61]:

$$K = \frac{2a}{3(\sigma_m + \sigma_s)} \qquad (4-3)$$

where a is the magnet radius, σ_m and σ_s are material properties of magnet and stopper respectively which are given by

$$\sigma_h = \frac{1 - \nu_h^2}{E_h} \ (h = m, s) \qquad (4-4)$$

Where E_h and ν_h are Young's modulus and Poisson's ratio respectively.

The hysteresis damping coefficient D is given by

$$D = \frac{3K(1-e^2)}{4\dot{\delta}^-}\delta^n \qquad (4-5)$$

where e and $\dot{\delta}^-$ are the restitution coefficient and the penetration velocity just before impact.

Modelling of electromagnetic induction is the same as the model presented in chapter 3 for FEH, which is described by Eq. 3-7 to Eq. 3-13.

4.4 Simulation

The mathematical model of FHH is described by nonlinear equations, which can be solved by time domain simulation. The aim of simulation in this work is to study the behavior of the electromagnetic energy harvester based on free motion with hard stops impact, and investigate the energy harvesting performance over the range of input amplitudes and frequencies. Study of FHH's performance is carried out with steady harmonic input vibration. Although such vibration condition is not usually available in the real applications, analysis can be more understandable and more comparable to other harvesters' performances. Simulation of a case study with certain parameters listed in Tables 4-1 and 4-2 is obtained, followed by a detailed explanation and analysis of the obtained results. Those parameters are determined based on a harvester with cylindrical magnet of 3.5 mm diameter and 3 mm length including coulomb's and viscous friction coefficients which are determined experimentally.

Table 4-1

Mechanical system parameters

Young's modulus – E_m(Gpa)	160	Poisson's ratio– ν_m	0.24
Young's modulus – E_s (Gpa)	8	Poisson's ratio– ν_s	0.38
Magnet diameter – d_m (mm)	3.5	Restitution coeff – e	0.5
Magnet stroke – S (mm)	8	Magnet Mass – M (g)	0.214
Viscous COF – C_a(Ns/m)	0.002	Coulomb's COF -μ	0.25

Table 4-2

Magnetic and electrical circuit parameters

Coil mean diameter – D_c (mm)	5.4	Coil resistance – R (Ω)	2.92
Magnetic moment – m (A. m^2)	25e-3	Coil length – l (mm)	8
Total number of turns (N)	8×40	Number of layers(N_l)	8

4.4.1 Response types

Simulation of the relative displacement shows a unique behavior of FHH, in which four ways of response of tube/magnet relative motion appear. They can be nominated as "sticking motion" response, "free motion" response, "impact motion" response, and "multi-impact motion" response. The existence of one response type over another mainly depends on the input vibration acceleration (amplitude and frequency), and is also influenced by some system parameters.

"Sticking motion" appears at very low input acceleration, where the inertia force cannot overcome the tube/magnet friction force. During this response both tube and magnet move together. No relative motion appears and consequently no energy harvesting.

"Free motion" can start by increasing the input acceleration, so that the inertia force can overcome the friction force. Relative displacement appears during this response. However, the relative displacement amplitude is not large enough to allow the magnet to reach both stops periodically, and the magnet remains vibrate freely inside the tube (Fig. 4-2a). One side impacts may appear during this response type if the magnet tilts to vibrate near to one stop.

Increasing the input acceleration can increase the relative displacement amplitude. "Impact motion" appears when the magnet can reach both stops periodically. In this case, the magnet makes one impact with one stop followed by another impact with the other stop. The relative displacement takes an amplitude value of half the magnet stroke and frequency equals to the input vibration frequency (Fig. 4-2b).

The relative amplitude cannot be increased over half magnet stroke by further increase of the input acceleration (neglecting the stop deflection). However, the way of impact can be changed. The magnet can make few consecutive impacts with one stop followed by

another consecutive impacts with the other stop which is called the “multi-impact motion” response (Fig. 4-2c). In “multi-impact motion” two or more consecutive impacts or intermediate oscillations appear within the main vibration oscillation, and the number of those oscillations increases by further increase of the input acceleration (Fig. 4-2d).

Figure 4-3 shows the predicted output voltage at different motion responses. At the free motion, the output voltage is quite low and approaches zero at some instants where the instantaneous input acceleration is less than the frictional acceleration. Spikes appear in the output voltage during impact and multi-impact motion responses depending on the number of impacts per cycle.

Simulation of the instantaneous output voltage and corresponding relative velocity is illustrated by Fig. 4-4 and Fig.4-5 in case of the impact and multi-impact motion responses respectively. Four possible phases of magnet/tube relative motion appear, which can be nominated as “relative motion” phase, “impact motion” phase, “damping motion” phase, and “single body motion” phase (Fig. 4-4). During the relative motion phase the magnet can move freely relative to the tube and the instantaneous voltage increases by increasing the magnet/tube relative velocity. Impact appears when the magnet approaches the end stop, which occurs instantaneously and leads to a sudden change in the relative velocity and consequently the output voltage. The sudden velocity change is quickly damped through the damping phase and magnet/tube start to move together as one body (single body phase). The quick damping of the sudden velocity change can be done through one or few consecutive impacts which is the reason of the occurrence the multi-impact motion response.

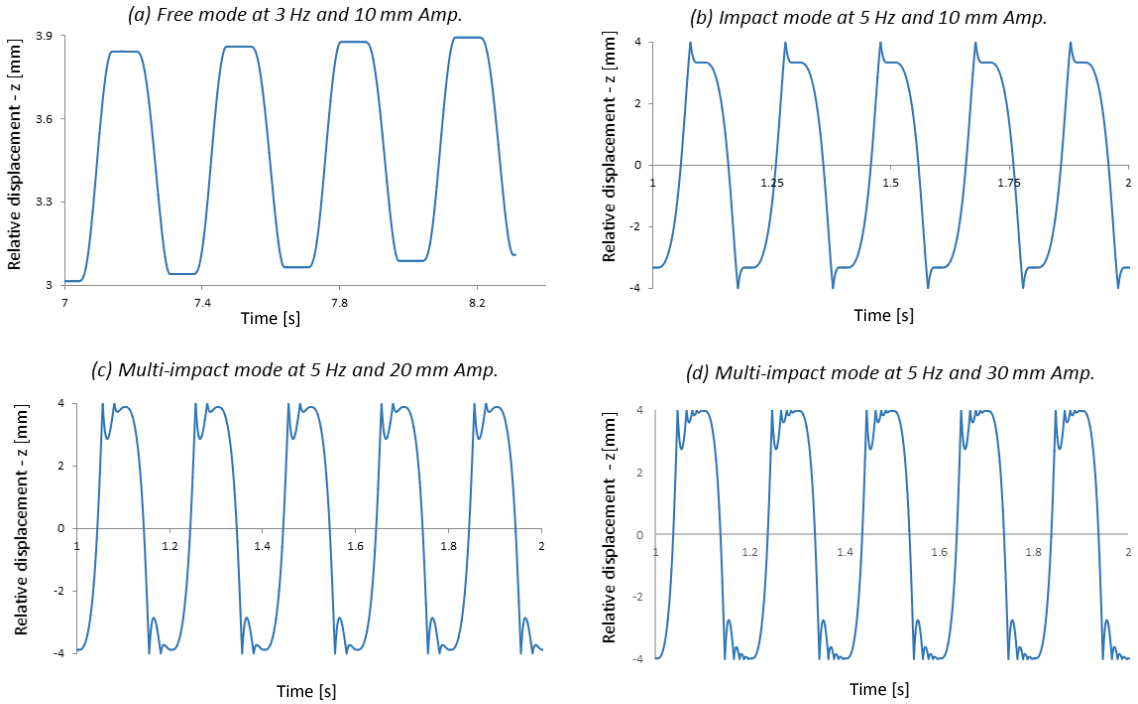

Fig. 4-2. Different response types are illustrated by the predicted relative displacement at different input amplitudes and frequencies

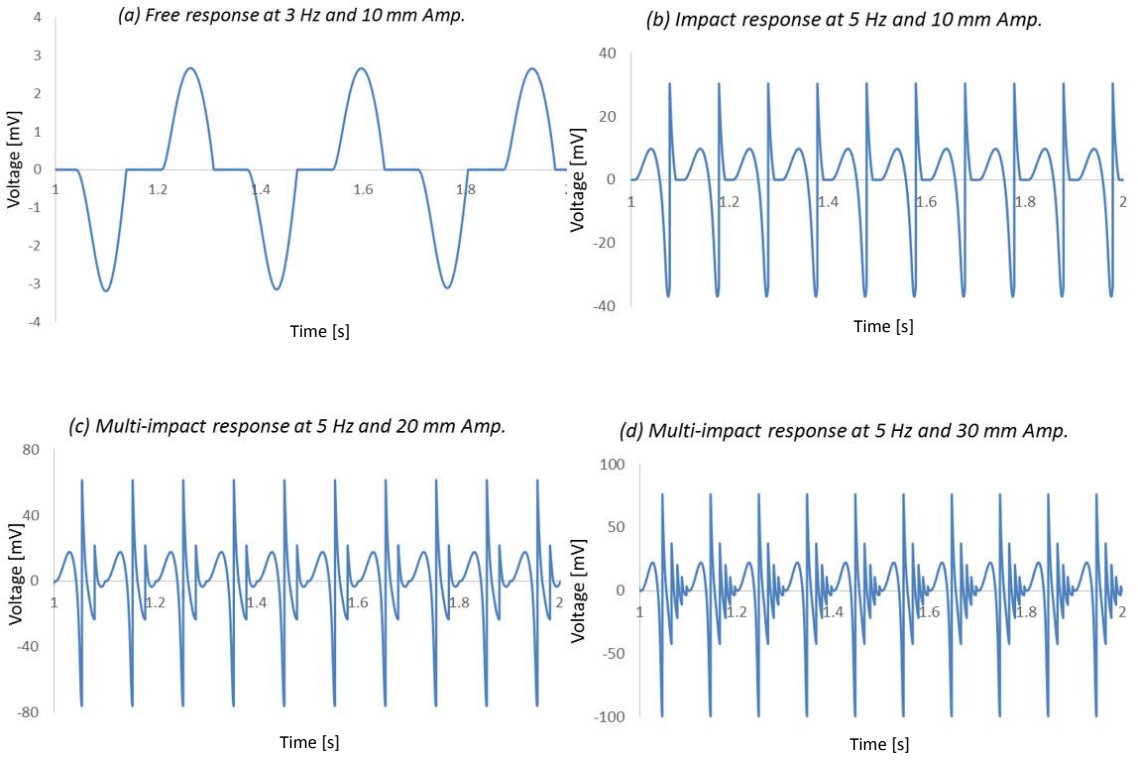

Fig. 4-3. Predicted output voltage versus time at different response types

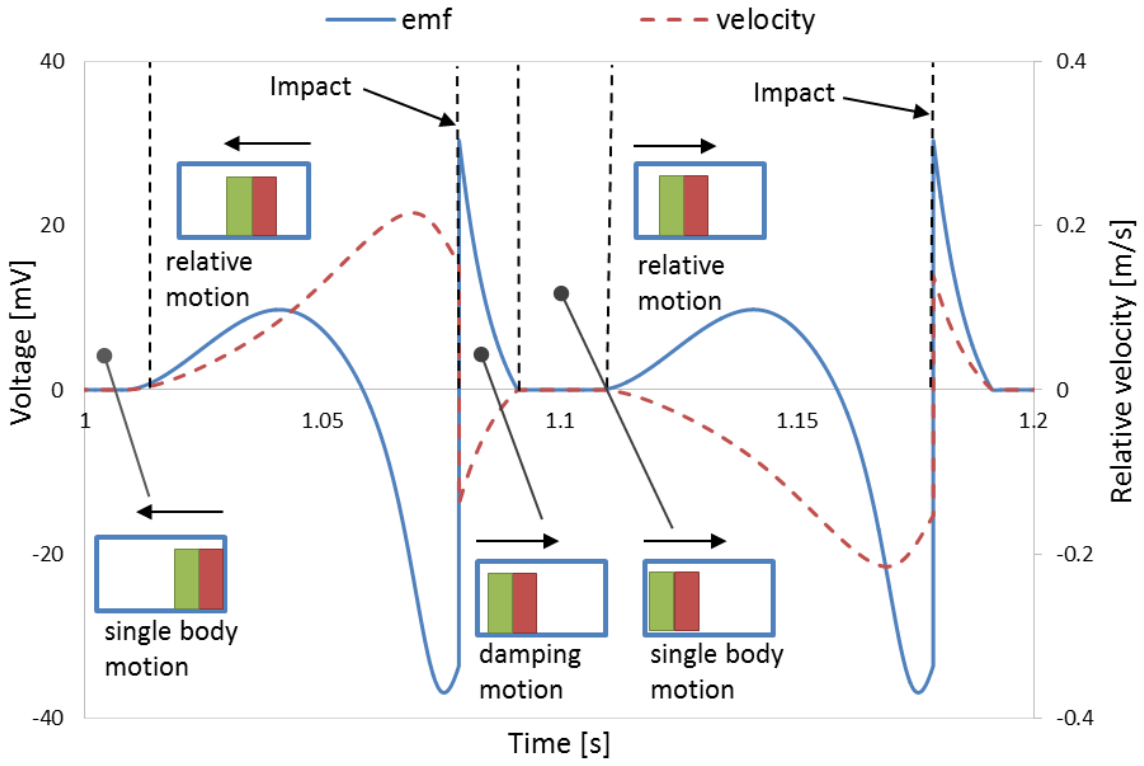

Fig. 4-4. The instantaneous *emf* and relative velocity during the impact motion response for one cycle of oscillation shows the different the magnet/tube relative motion phases

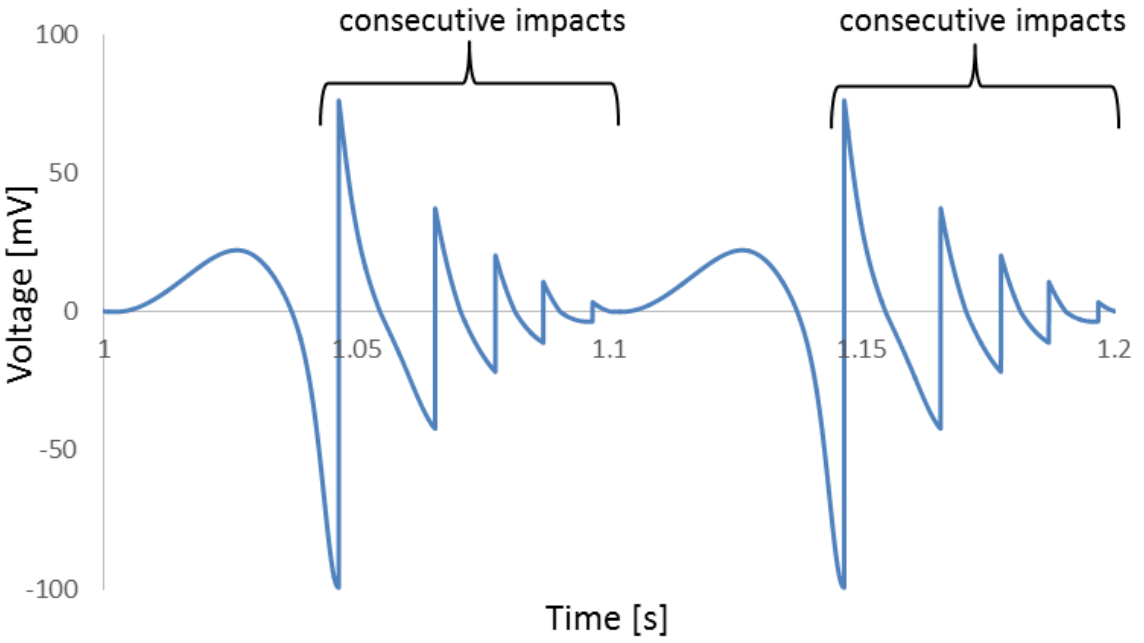

Fig. 4-5. The instantaneous *emf* during the multi-impact motion response for one cycle of oscillation shows the voltage peaks due to the consecutive impacts

The occurrence of one motion response over another is determined by the input vibration acceleration, which depends on the input frequency and amplitude. Two-dimensional graph that shows the existence region of each response type according to the input amplitude and frequency is illustrated in Fig. 4-6.

The response type existence is also affected by two main system parameters which are the magnet stroke in line with the frictional parameters. Controlling friction usually limited; however it should be reduced to the minimum limit for better energy harvesting especially at low input acceleration. Reducing magnet stroke allows the impact and multi-impact motion response to occur at lower input acceleration (Fig. 4-7), since the sufficient relative displacement of the magnet to reach the end stop becomes less. Hence, in the designing of FHH, the stroke value should be selected based on the input amplitude and frequency, so that the allowable internal mass displacement can be fully utilized for energy harvesting.

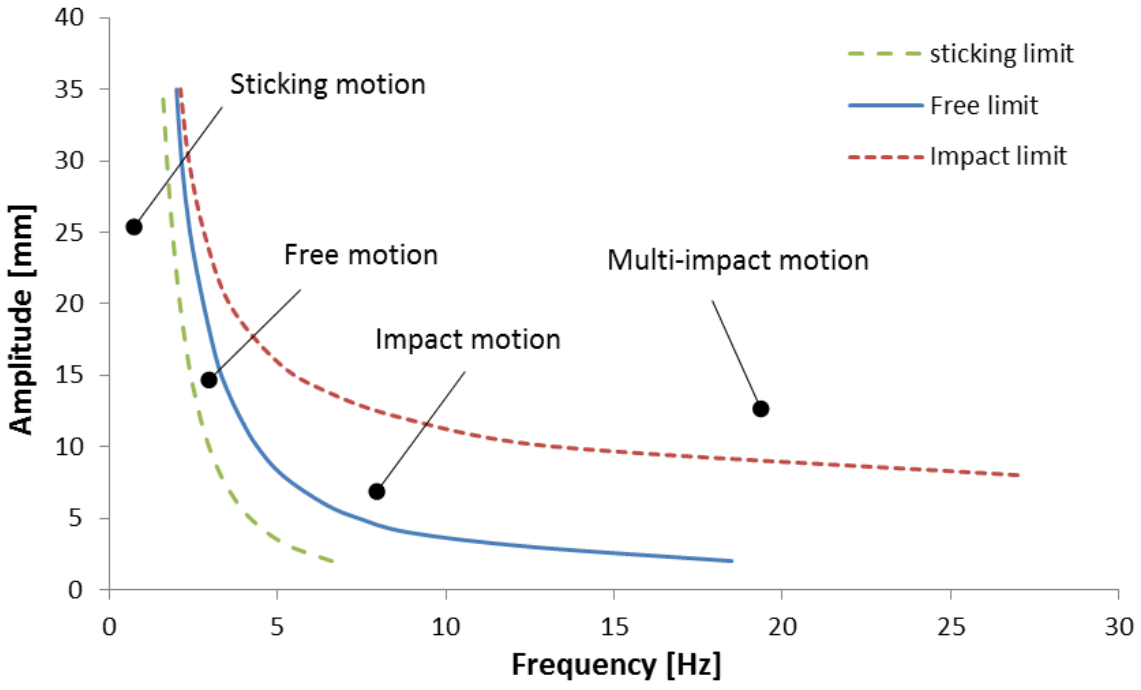

Fig. 4-6. Distribution of motion response existence regions over the range of input amplitudes and frequencies.

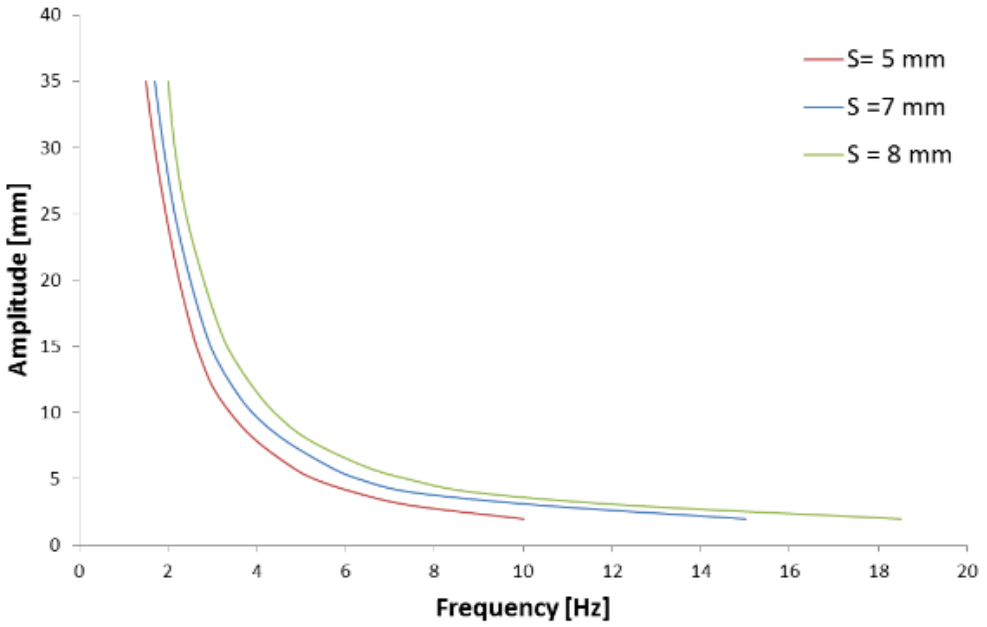

Fig. 4-7. Free limit line at different magnet strokes shows that the frequency and amplitude thresholds of "impact motion" decreases by decreasing the magnet stroke.

4.4.2 System performance

The performance of FHH can be investigated through the predicted output voltage and power over the range of input amplitudes and frequencies. Root mean square (RMS) is used as an indication for the average value of the predicted output voltage, power, and other variables that change instantaneously during the operation of the harvester.

The output voltage mainly depends on the magnet/tube relative velocity and the flux rate of change ($d\varphi/dz$). The instantaneous flux rate of change varies with the position of the magnet within the coil (Fig. 4-8 and Eq. 3-7). It takes its highest value at the position near the coil ends, when the magnet approaches the coil or completely leaving it, since the instantaneous flux rate of change through each turn ($d\varphi_t/dz$) and consequently the turns induced voltage are all positive or all negative.

Impact with hard end stops accompanies with the allowed free motion leads to a harvester with non-resonant behavior. The output voltage and power could be increased

by increasing the input amplitude and / or the input frequency. The effect of increasing the input amplitude and frequency on the relative velocity and consequently the output voltage and power are explained here in details with the aid of case study simulation.

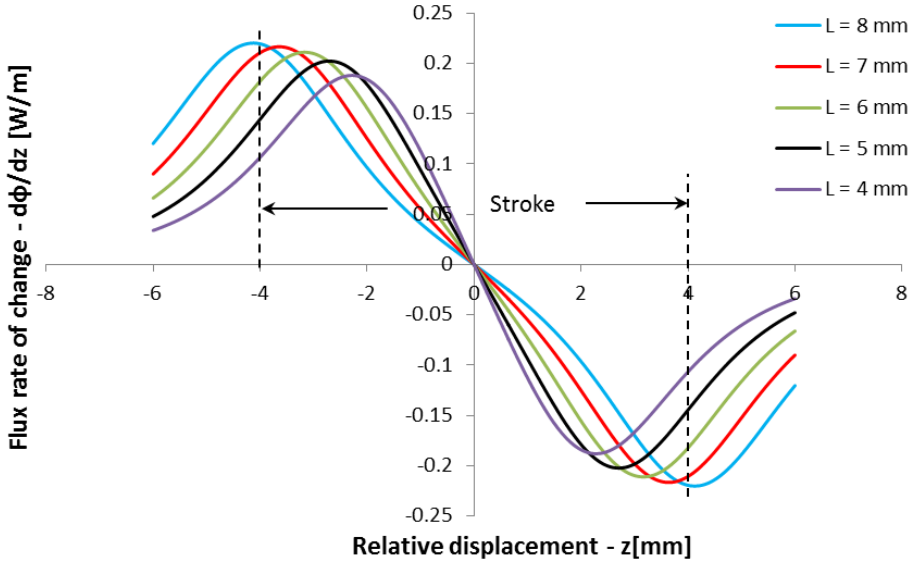

Fig. 4-8. Variation of the predicted flux rate of change with respect to the relative displacement ($d\varphi/dz$) with the magnet position within the coil (z) for different coil lengths (coil length of 8 mm is used in the model prediction of the case study).

4.4.2.1 The effect of input amplitude

Increasing the input amplitude at constant frequency after exceeding the free motion threshold increases the relative velocity (Fig. 4-9), as well as the relative displacement (tending to reach the impact motion). Hence, the induced voltage and power generated start to increase (Fig. 4-10). Upon reach the impact motion, the relative oscillation takes an amplitude of half magnet stroke and frequency equal to the input vibration frequency. Those values do not change by further increase of the input amplitude. However, the motion response starts to change from the impact motion to multi-impact motion. During the multi-impact motion, the main oscillation period is divided into two main periods, which are the impact period (t_i), and the traveling period (t_r) as shown in Fig. 4-11. The

impact period (t_i) is the time elapsed between just reach one stop and start leaving it. Within this time, the magnet makes number of consecutive impacts with the stop. Number of intermediate oscillations appears within the main oscillation. The traveling period (t_r) is the time taken by the magnet to travel from one stop to the other. Both time values are related to each other by a frequency depended relation as expressed by

$$t_i + t_r = \frac{1}{2f} \qquad (4-6)$$

where f is the main oscillation frequency.

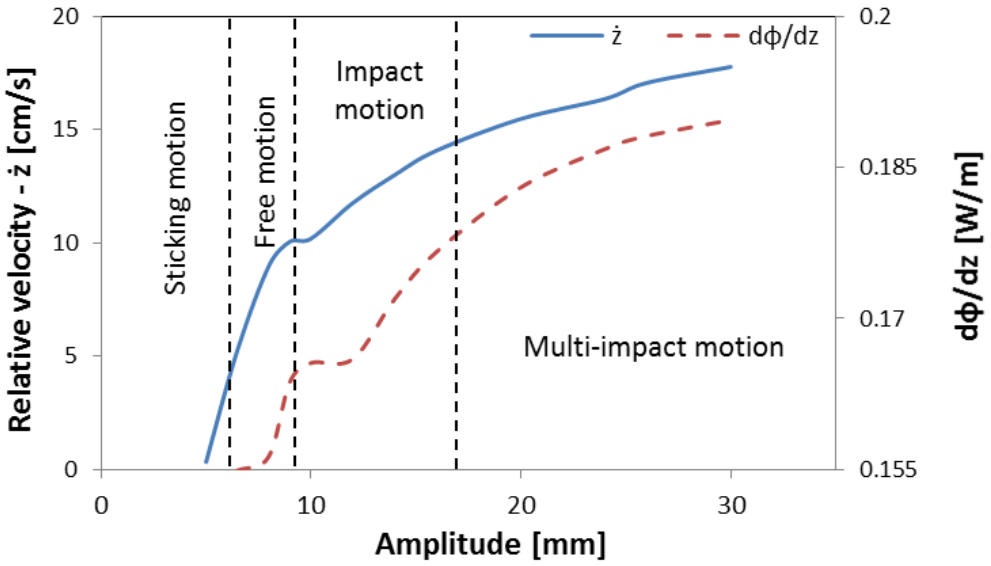

Fig. 4-9. RMS predicted magnet relative velocity and predicted flux rate of change ($d\varphi/dz$) with the input amplitude at 5 Hz.

Two actions happen simultaneously by increasing the input amplitude during the multi-impact motion. First, the impact time and the number of consecutive impacts increase (Fig. 4-11). The magnet spent more time oscillating at a position of high instantaneous flux rate of change. Consequently, the average flux rate of change increases (Fig. 4-9). Second, the traveling time decreases accordingly (the sum of impact and traveling times is constant for constant input frequency). Hence, the average relative velocity of the

magnet increases during its travel from one stop to the other. As a result of both actions, the induced voltage and power generated increase (Fig. 4-10).

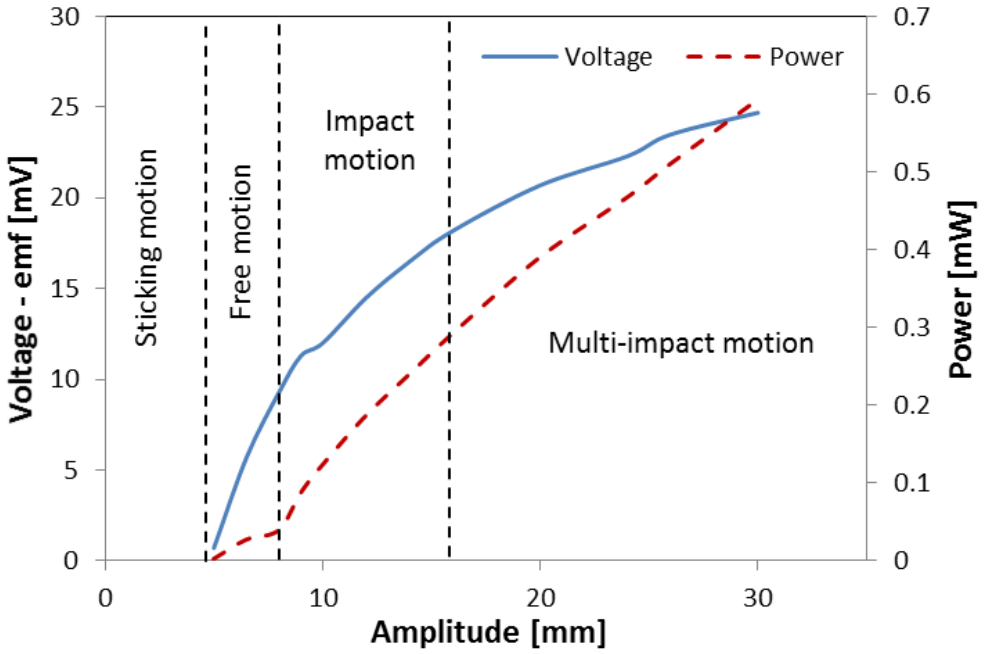

Fig. 4-10. RMS predicted output voltage and power with the input amplitude at 5 Hz input frequency.

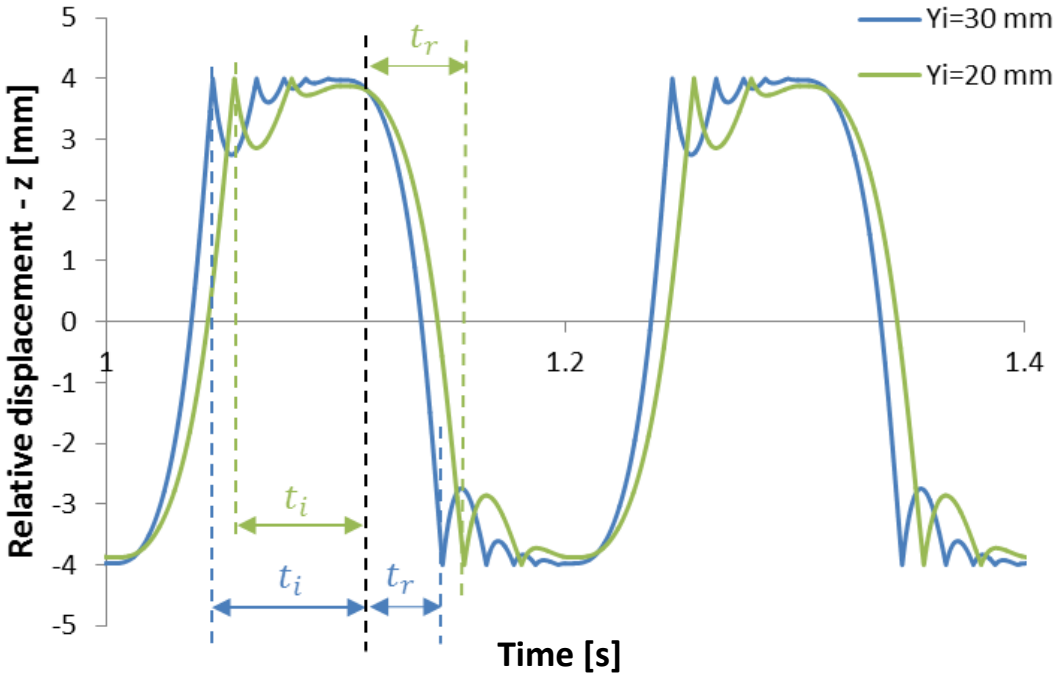

Fig. 4-11. Predicted relative displacement at two different input amplitudes show the impact and traveling times (t_i , and t_r) and how they are changed with the input amplitude.

4.4.2.2 The effect of input frequency

At very low input amplitude relative to the magnet stroke, increasing the input frequency can change from the sticking motion response to free motion response. However, the impact motion cannot be reached (Fig. 4-6), and the magnet remains vibrate freely within the tube. The relative oscillation frequency increases and accordingly the relative velocity however, with small increase in the induced voltage and power due to the low relative displacement amplitude.

At relatively large input amplitudes, increasing the input frequency increases the frequency of the main relative oscillation with a relative displacement amplitude of half magnet stroke after exceeding the threshold of the impact motion response. As a result, the relative velocity increases with significant voltage and power increase due to high relative amplitude (Fig. 4-12). The intermediate oscillations start to appear upon reach the mutli-impact motion response which participate in increasing the output power by further increasing the input frequency.

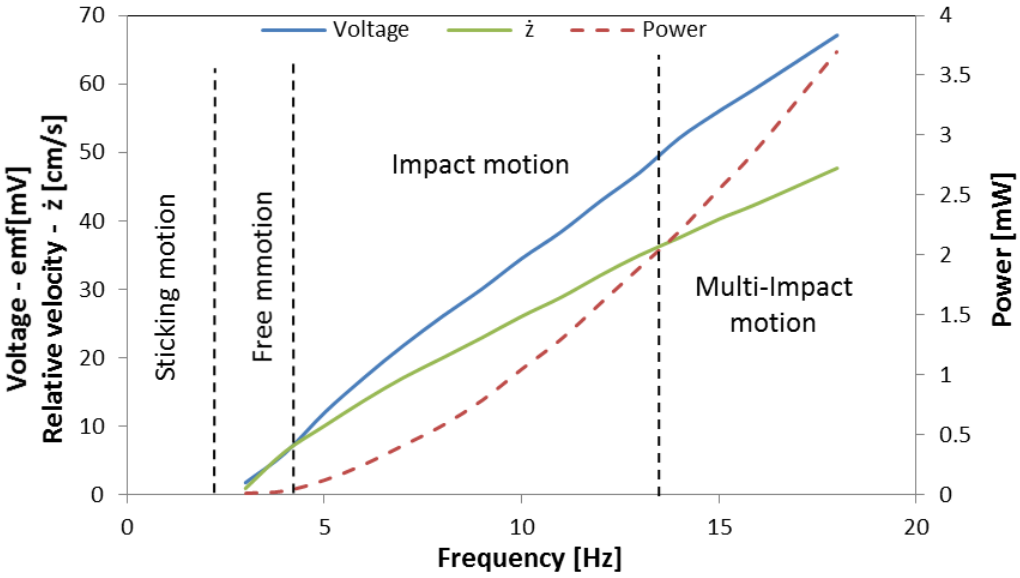

Fig. 4-12. RMS predicted relative velocity, induced voltage, and power generated by FHH at 10 mm input amplitude over the range of input frequencies.

4.4.3 Practical considerations and limitations

Simulation results show the non-resonant behavior of FHH. The output power increases with both input amplitude and frequency. However, no significant power increase can be obtained with input frequency at very low input amplitudes. In such case, resonant harvesters are suitable at high frequencies. The resonant amplification is needed to increase the internal displacement over the input amplitude and boost the output power. Usually resonant harvesters are suitable for single high frequency-vibration sources (over 100 Hz) with small amplitudes. This condition can be found in some engines and machine vibrations. However, some vibration sources such as human induced vibration is unstable with a very low frequency, usually ranged from 1 to 5 Hz [62], which is difficult to be matched by resonant harvesters with small sizes. In addition, the amplitude is relatively large which cannot be covered with allowable internal displacement especially in the presence of resonance amplification. In such vibration condition, FHH can be suitable. Free motion promotes power harvesting at low frequencies. Non-resonant behavior is appropriate for amplitude/frequency variations. Besides, the free motion with hard stops impact can benefit from large amplitudes due to the intermediate oscillations. Moreover, the simple design of FHH enhances small size fabrication (as also seen in experimental section), which makes it more suitable for human – powered devices.

The impact force exerted on the stops is another important limitation. Neither the input amplitude nor frequency can be increased over a certain limit that the stops can withstand the resulted impact force or the whole device can withstand the shaking force due to impact. Nevertheless, this problem becomes uncritical in the design of micro-size harvesters due to lower impact force especially for low frequency applications (Fig. 4-13).

Analysis and testing of FHH in this work is done with horizontal vibrations. In vertical plane, the input acceleration should exceed the gravitational acceleration for the relative motion to start. However, similar behavior can be achieved in vertical plane, by balancing the gravitational force, for example by adding a calibrated magnet behind the stop at a proper distance. The resulted configuration would be similar to some fabricated electromagnetic harvesters utilized magnetic levitation [57, 63]. In such case, complete balancing cannot be achieved; however the behavior may become closer to horizontal plane behavior to some extent at relatively high input accelerations.

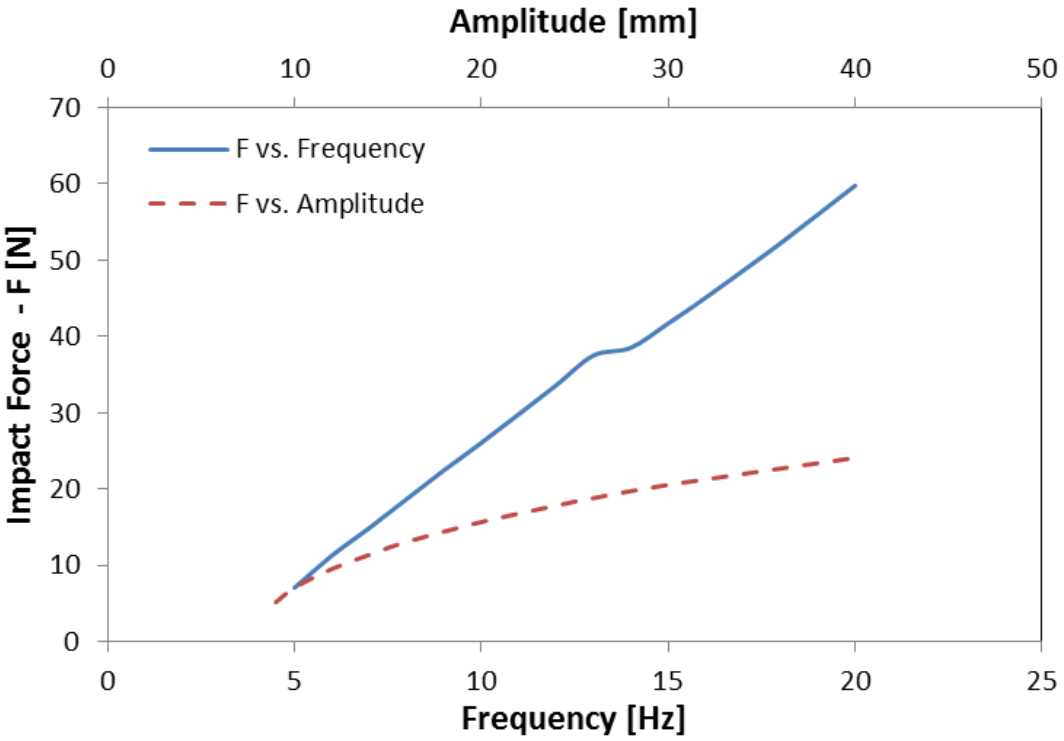

Fig. 4-13. Variation of predicted maximum impact force exerted on the stops with the input amplitude at 5Hz, and input frequency at 10 mm amplitude

4.5 Experimentation

Two experiments are conducted in chapter. The first is carried out on four fabricated prototypes having identical sizes and coils, but different magnet shapes. The second is performed on two different size prototypes with different number of coil turns and the same magnets. The aim of the first experiment is to examine the effect of magnet shape on the harvesting performance, which is difficult and less effective to be analyzed by modelling and simulation, as well as verifying the presented theoretical model. However, the second is to investigate the power and power density of FHH with different number of coil turns at variable large amplitude – low frequency vibrations, and evaluates the overall system performance with small size devices.

4.5.1 Experimentation on different magnet prototypes

The magnet shape shows a significant effect on the performance of FHH for the same allowable tube space. Each shape gives different friction, and magnetic characteristics. Four Neodymium magnets (same magnetic material) with different shapes are experimentally tested with FHH, which are a ball magnet of 3.5 mm diameter (B3.5), cylindrical magnet of 3.5 mm diameter and 3 mm length (C3.5×3), cylindrical magnet of 3mm diameter and 3.5 mm length (C3×3.5), and double-ball magnet which consists of two 3.5 mm diameter ball magnets attached to each other by the magnetic force (DB3.5) and vibrates in the direction of their common center line. An electrical coil of 300 turns, 0.2 mm wire diameter, and 8 mm length is taken for each prototype. The total dimensions of each prototype are about 9 mm diameter and 12 mm length except the double-ball magnet prototype. It has 16 mm length in order to have the same stroke of 8 mm. The prototypes are tested by 10 mm amplitude vibration over a range of exciting frequency. The RMS voltage and power generated in each case is shown in Figs. 4-15 and 4-16 respectively.

Each magnet shows different frictional and magnetic characteristics which affect the voltage and power generation at high and low frequencies. The oscillation of ball magnet involves rolling motion, thus it can give a low coulomb's friction. Free and impact motion responses are expected to start at lower frequencies (acceleration), and consequently higher relative amplitude and power could be obtained from the ball magnet prototype at

low frequencies (Table 4-3). However, the involved rolling motion itself causes orientation change of the magnet dipole during oscillation. The magnetic flux component normal to the area bounded by the coil turns highly decreases during oscillation due to the rolling motion. That is why a performance degradation of B3.5-magnet prototype is observed over other prototypes at higher frequencies where no rolling is involved (Figs. 4-15, and 4-16).

The double-ball magnet has the largest size and consequently can give the highest magnetic strength (highest magnetic moment (Eq. 3-7)). Hence, the highest power is expected from DB3.5-magnet prototype at high frequencies (Fig. 4-15, and 4-16). In addition, it has a point contact with the tube surface, which can give a lower coulomb's friction than cylindrical magnets with line contact. However, DB3.5-magnet prototype must be larger in length to have the same magnet stroke which affects the power density of the harvester.

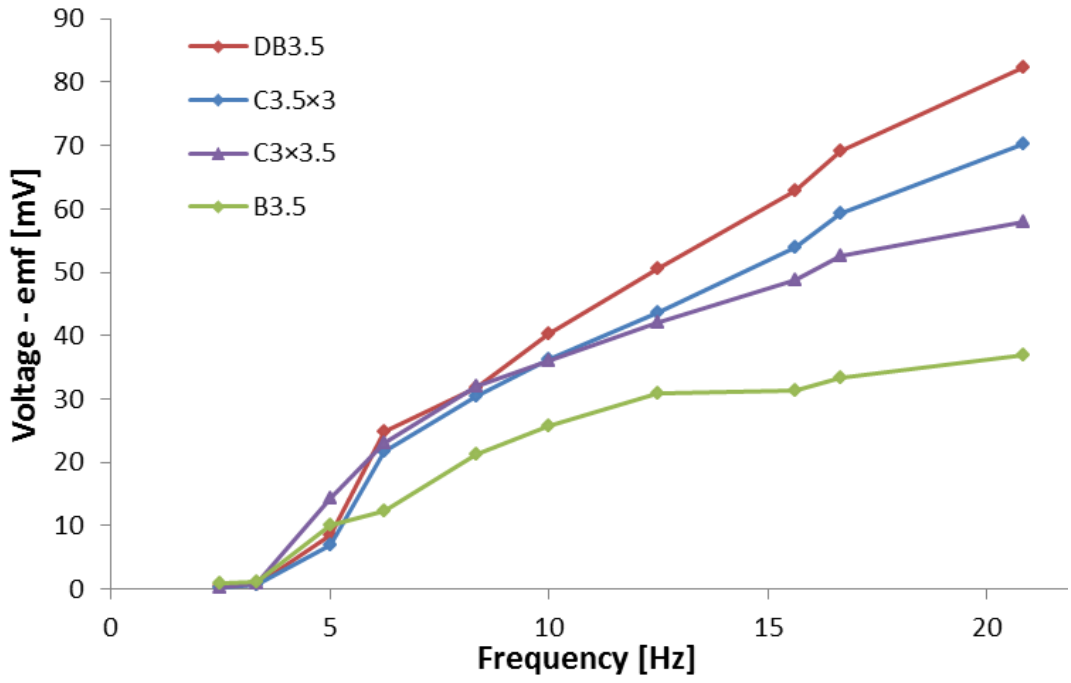

Fig. 4-15. RMS Measured output voltage produced by the four magnet prototypes over the range of exciting frequencies.

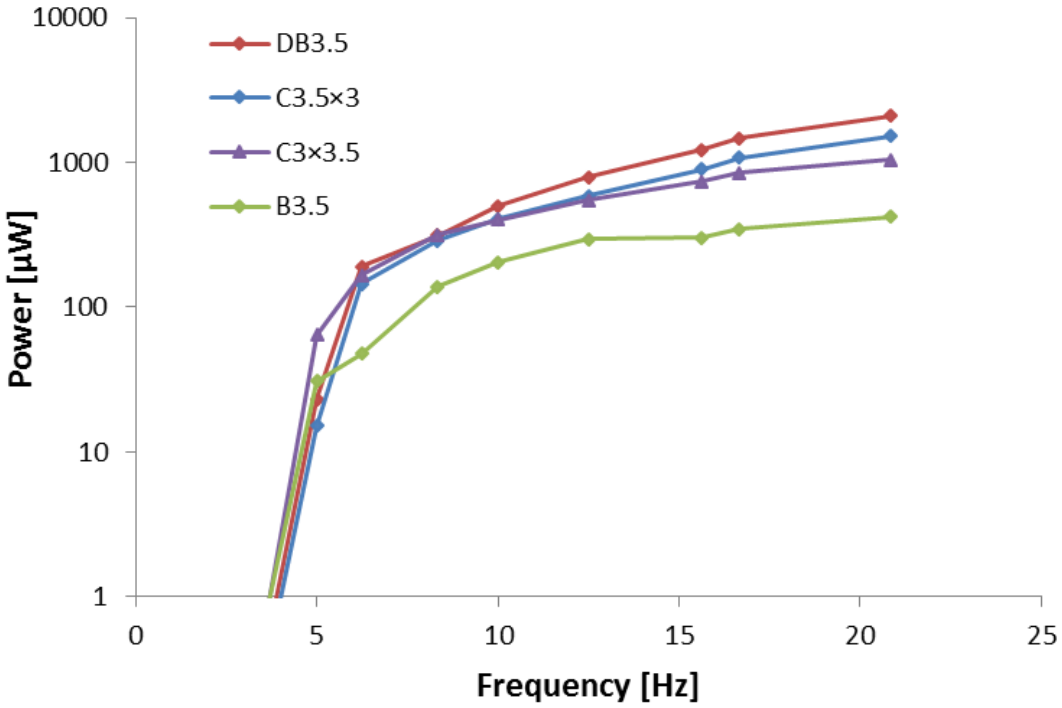

Fig. 4-16. RMS measured power generated by the four magnet prototypes over the range of exciting frequencies.

C3×3.5-magnet has a smaller diameter, which can give a lower viscous friction. This can allow a rapid transfer from free motion response to impact motion response by small increase of frequency increment. Hence, C3×3.5-magnet prototype can give a high power output at low frequency range once the magnet/tube sticky contact is broken (Table 4-3). C3.5×3-magnet is larger in size, thus can give higher magnetic strength than C3×3.5 magnet. Therefore, C3.5×3-magnet prototype generates a higher power at high frequencies (Fig. 4-16).

Comparison between different magnet prototypes shows that friction whether coulomb's or viscous one are very crucial matter for energy harvesting at low input acceleration. Thus, if size minimization is needed, a way of reducing friction should be considered, for example by improving the surface quality as much as possible, using ball magnets if low acceleration vibration is the predominate. A way introducing vacuum inside the harvester tube is also possible. However, if a large acceleration vibration is the predominant; more attention should be given to improve magnetic strength.

The theoretical model presented in this work could be verified by comparing the

predicted output voltage of the case study with the measured output voltage of C3.5×3-magnet prototype as shown in Fig. 4-17

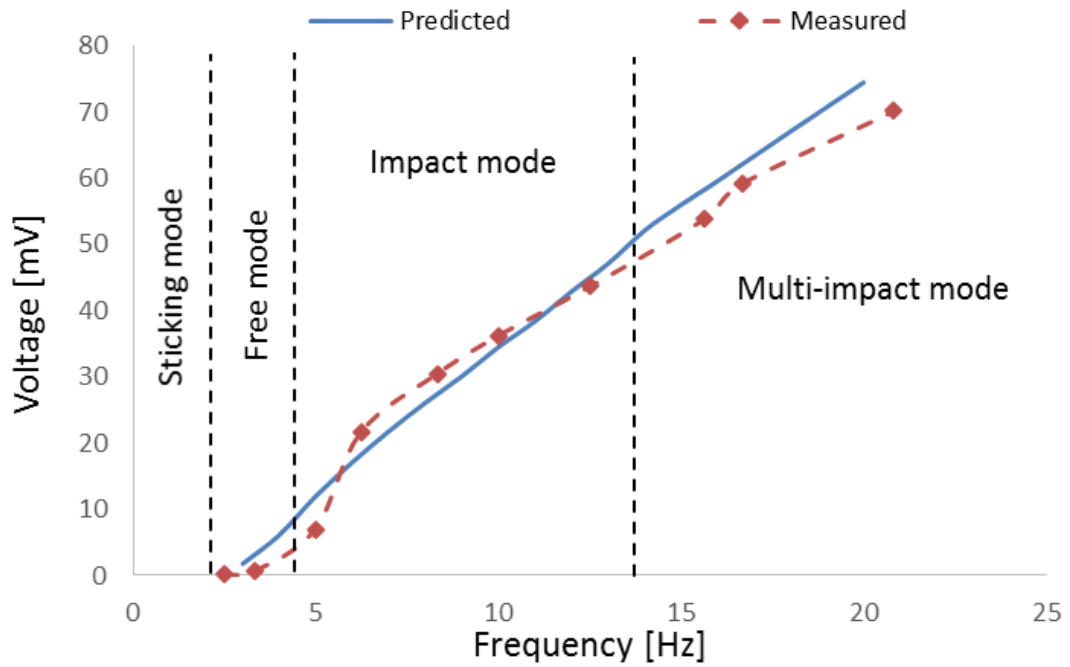

Fig. 4-17. Measured and predicted output voltage of C3.5×3-magnet prototype over the range of exciting frequencies

Table 4-3

RMS measured power (μW) generated by the four magnet prototypes at 10 mm input amplitude

Type/F(Hz)	2.5	3.33	5	6.25	10	15.63	20.8
B3.5	0.319	0.357	30.95	47.81	205.6	304.1	421
DB3.5	0.043	0.198	23.05	191.2	500.8	1227.5	2102
C3.5×3	0.008	0.1499	15.18	145.7	407.1	897.7	1526
C3×3.5	0.01	0.291	64.05	165.9	401.5	740.3	1042

4.5.2 Experimentation on different size prototypes

Two size prototypes with the cylindrical magnet (C3×3.5) are fabricated and tested at 2.5 Hz and 3.33 Hz frequencies over a range of large amplitudes (from 10 to 40 mm). The simple design of FHH allows fabrication of small size prototypes of $D9 \times L12$ mm, and $D7 \times L12$ mm, with 300 and 200 total number of turns respectively (Fig. 4-18). Parameters of each prototype are listed in Table 4-4. The RMS power generated and power densities of each are shown in Fig. 4-19.

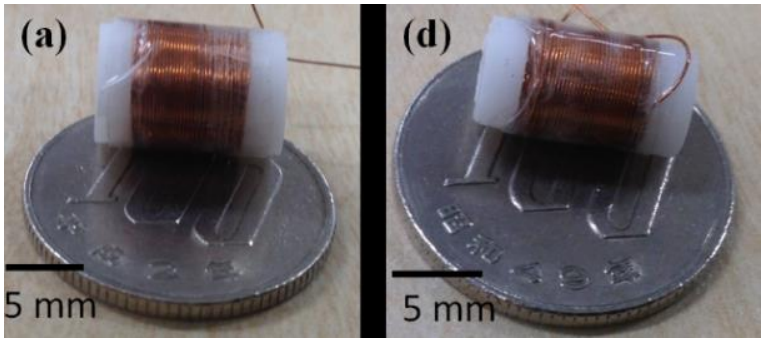

Fig. 4-18. Photographs of (a) D9L12 size prototype with 300 turns and (b) D7L12 size prototype with 200 turns, both are shown with 100 yen coin (22.6 mm diameter).

Table 4-4

Parameters of the two harvester prototypes

Type	D9L12	D7L12
Total dimensions ($D \times L$) in mm	9×12	7×12
Magnet dimensions ($d \times l$) in mm	3×3.5	3×3.5
Magnet mass (g)	0.186	0.186
No. of Coil turns (N)	300	200
Coil length (mm)	8	8
Wire diameter (mm)	0.2	0.2
Coil resistance (Ω)	3.23	1.8
Stroke (mm)	8	8

The output power of each prototype increases with the input amplitude and frequency. One prototype has a larger number of coil turns, so it is expected to generate higher power than the other. For instance, D9L12 prototype can generate 71.8μW and 91.3μW, while D7L12 prototype can generate 28.4 μW and 42.2 μW both at 2.5Hz input frequency, and 5.2 and 9.87 ms^{-2} average acceleration respectively. However, at 3.33 Hz, D9L12 prototype can generate 81.9 μW, while D7L12 prototype can generate 65.2 μW both at 9.29 ms^{-2} average acceleration. Higher power density could be obtained from D7L12 prototype than D9L12 prototype (Fig. 4-19), which shows the minimization effectiveness of FHH under some operating condition. The power measurements presented here are considered as the ideal powers generated by FHH, which are expected to be reduced by

integrating the harvester with an application depending on the application load resistance.

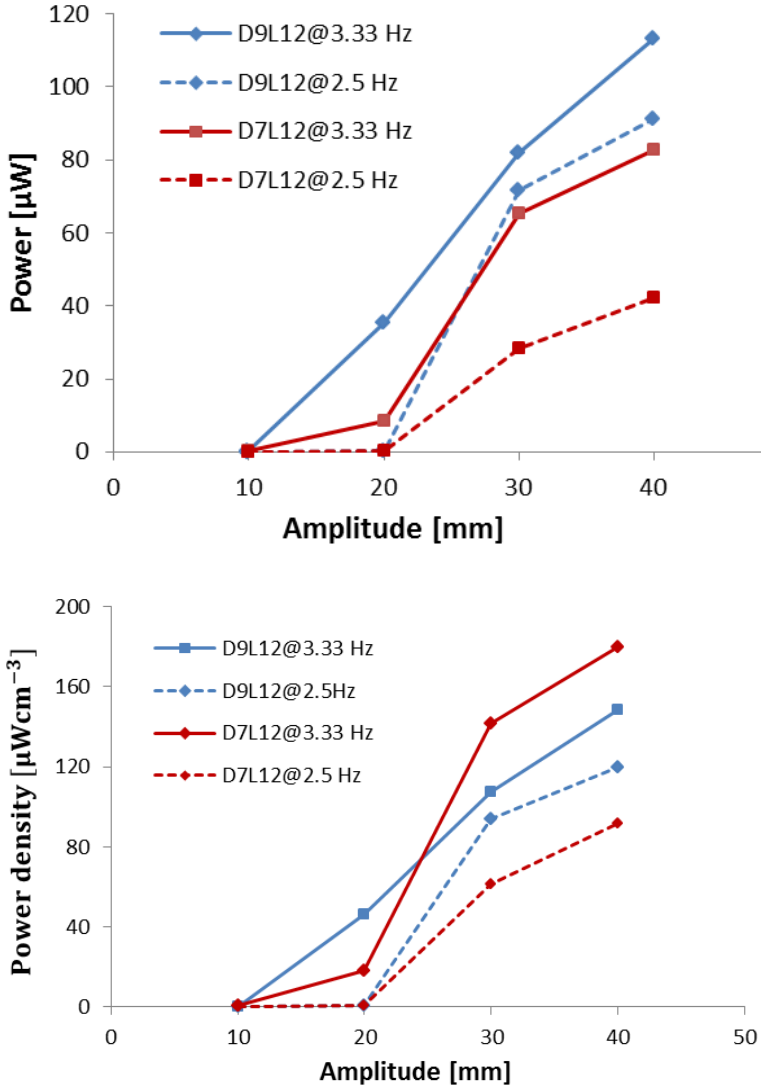

Fig. 4-19. RMS measured power and power density of each size prototype with C3×3.5-magnet at input frequency of 2.5, and 3.33Hz over the range of input amplitudes.

4.6 Comparison and evaluation

One important application of FHH is the powering of human body associated devices. The criterion of evaluating vibration energy harvester for human-powered applications is the ability to match variable low frequency – large amplitude vibrations with large power output and a small size system. The best evaluation of FHH can be done by comparing

the power generated by it with the power generated by other low frequency energy harvesters with the same size and input vibration. However, data published in previous works diverse extensively (different harvester sizes tested by different input vibrations). Thus, some cases presented in this work are compared with other previously fabricated low-frequency harvesters tested by periodic vibrations (Table 4-5).

Table 4-5

Comparison between some previously fabricated low frequency energy harvesters and FHH prototypes

Reference	P (μW)	F (Hz)	A (ms^{-2})	V (cm^3)	PD (μWcm^{-3})	Details
Pillatsch 2014 [29] Imperial college of London	43	2	20	5	8.6	PZT
Lee 2013 [27] University of Ulsan	65.3(max.)	8	1.96	21	3.1	EM
Naruse 2009 [31] SANYO Electric Japan	40	2	3.92	20×45 mm	----	ES
Jo 2012 [32] Yonsei University, Seoul	430	8	---	10	43	EM
Galchez 2011 [28] University of Michigan	2.3	2	0.54	70.23	0.0327	EM
Moss 2012 [64] Defence Sci. &Tech.	121	9.8	0.6	~26	4.65	EM
D9L12-C3×3.5	**71.8**	**2.5**	**5.2**	**0.763**	**94.1**	**EM**
D9L12-C3×3.5	**91.3**	**2.5**	**6.97**	**0.763**	**119.66**	**EM**
D7L12-C3×3.5	**28.4**	**2.5**	**5.2**	**0.461**	**61.6**	**EM**
D7L12-C3×3.5	**82.9**	**3.33**	**12.38**	**0.461**	**179.82**	**EM**
D9L12- C3×3.5	**113.3**	**3.33**	**12.38**	**0.763**	**148.49**	**EM**
D9L12-C3×3.5	**64.05**	**5**	**6.97**	**0.763**	**83.94**	**EM**

Previous work shows many trials to match low frequency vibrations by using different techniques and transaction mechanisms. Two important features appear from FHHs. The first is the small size device compare to other harvesters. The fabricated FHHs in this work are of 0.461 and 0.763 cm^3 size, even smaller sizes are possible. The reason of this

minimization ability is the simple construction of FHH which can be fabricated from only small hollow tube carrying an electrical coil with a magnet inside. This minimization allowance makes the harvester more compatible with implantable and wearable devices. The second is the significant increase of the output power with the input amplitude not only the input frequency. The presence of intermediate oscillations or consecutive impacts within the main oscillation by increasing the input amplitude boost the output power, which can benefit from larger amplitude human body motion.

Another measure that can be used to evaluate the performance of FHH is the harvesting efficiency or effectiveness. For example, according to the formula presented by Mitcheson [57], the effectiveness of D7L12-C3×3.5 is 5.25 %, at an input amplitude and frequency of 40 mm and 3.33 Hz. The effectiveness of D9L12 - C3×3.5 is 7.34 % at an input amplitude and frequency of 30 mm and 2.5 Hz.

4.7 Summary

In this chapter, study of electromagnetic vibration energy harvesting based on free motion with hard stops impact is presented. Free relative motion is allowed between tube-carrying an electrical coil directly connected to the vibration source and a permanent magnet inside. Impacts appear between the magnet and two hard end stops. Free motion enhances power harvesting at low frequencies, while the combined free motion with hard stops impact resulted in non-resonant behavior, in which the output power increases with input amplitude and/or frequency. In addition, the harvester has a simple construction which allows fabrication with small sizes. Hence, the harvester based on free motion with hard stops impact (FHH) becomes suitable for the small size applications encountered variable large amplitude – low frequency vibrations such as human-powered devices. In fact, linear spring-mass harvesters are inappropriate for such kind of applications. They

could hardly match low frequencies with small size devices. In addition, the harvester resonant behavior cannot efficiently deal with random vibrations.

A nonlinear mathematical model of FHH is derived and used for a case study simulation. The magnet/tube relative motion shows a unique style, in which four different motion response appear over the range of exciting frequencies and amplitudes. Detailed analysis of motion responses is carried out followed by study of the system performance Different prototypes are fabricated and undergo two different experimental testing. The first is used to verify the theoretical model, and investigate the effect of the magnet shape on power harvesting. The ball magnet shows a superior performance at low frequencies due to low associated coulomb's friction, while the cylindrical and double-ball magnets show better performance at higher frequencies due to the high magnetic flux component normal to the area bounded by the coil turns during oscillation. The second experiment shows the output power and power density of two small size prototypes with different number of coil turns with large amplitude – low frequency vibrations. A prototype of D9×L12 mm cylindrical total size and 300 coil turns can generate RMS power of 71.8μW at (2.5 Hz and 5.2 ms^{-2}), and 113.3μW at (3.33 Hz, and 12.38 ms^{-2}). Another of D7×L12 mm total size and 200 coil turns can generate RMS power of 28.4 μW at (2.5 Hz and 5.2 ms^{-2}), and 82.9 μW at (3.33 Hz, and 12.38 ms^{-2}). This experiment shows that increasing the number of turns can improve the output power. However, in some cases increasing the number of turns may decrease the power density due to the increase of the harvester size without a corresponding significant increase in the output power.

A comparison is made between FHH and previously fabricated low frequency energy harvesters, where two distinguish features of FHH appear. The first is the ability of FHH design for size minimization, which makes it appropriate for implantable and wearable

devices. The second is the significant power increase with the input amplitude which enhances the output power with large amplitude vibrations.

Chapter 5 Investigation of energy harvesting by FHH from human induced vibration

5.1 Introduction

The electromagnetic vibration energy harvester based on free motion with hard stops impact has been studied, analyzed and tested with horizontal harmonic vibrations in chapter 4. It shows an effective performance with low frequency – large amplitude vibrations. The output power increases with input amplitude and/or frequency. FHH also has a simple design which promotes fabrication with small sizes. Therefore, it can be well suited for human body applications. In fact, there is an argument for the convenience of FHH and its effective performance with these important applications, since human body motion during daily activities are away from harmonic, unsteady, and multidirectional. Such complicated dynamics could have different effects on the harvester performance or another issues may arise when applied with human-powered devices. Thus, the performance of FHH cannot be guaranteed with human body – associated devices unless it is tested with the actual human body motion. Besides, human powered devices usually deem small size harvesters, which puts a constraint in the utilized harvester size. Hence, design of FHH for human body application with size constraint is needed to be discussed.

In this chapter the performance of FHH is investigated with human body motion. Energy harvesting from three body locations which are the ankle, wrist, and pocket place (upper leg) are investigated during three different activates, which are walking with speed of 75 m/min, fast walking with 108 m/min, and jogging with 150 m/min. Two harvester prototypes are tested. One is fabricated with a ball magnet and another with cylindrical magnet. Voltage waveforms produced by each prototype during the three activities are measured and recorded. The harvester performance is investigated through the experimental results and the input vibration provided by the body motion. The experimental results generally show an effective performance of FHH with human body

motion.

FHH involves some design parameters such as number of coil layers, wire diameter, magnet diameter, etc. An optimization procedure or selection guidelines for the harvester parameters are discussed. Parameters selection procedure is based on a constrained size harvester related to the application and the body location where the harvester is intended to be attached

5.2 Harvester design

The harvester tested in this chapter is similar to that presented in the experimental section of chapter 4. It has a cylindrical total size of D9×L12 as shown in Fig. 5-1. Two prototypes are considered. The first is fabricated with 3.5 mm diameter ball magnet and the second with D3×L3.5 mm cylindrical magnet.

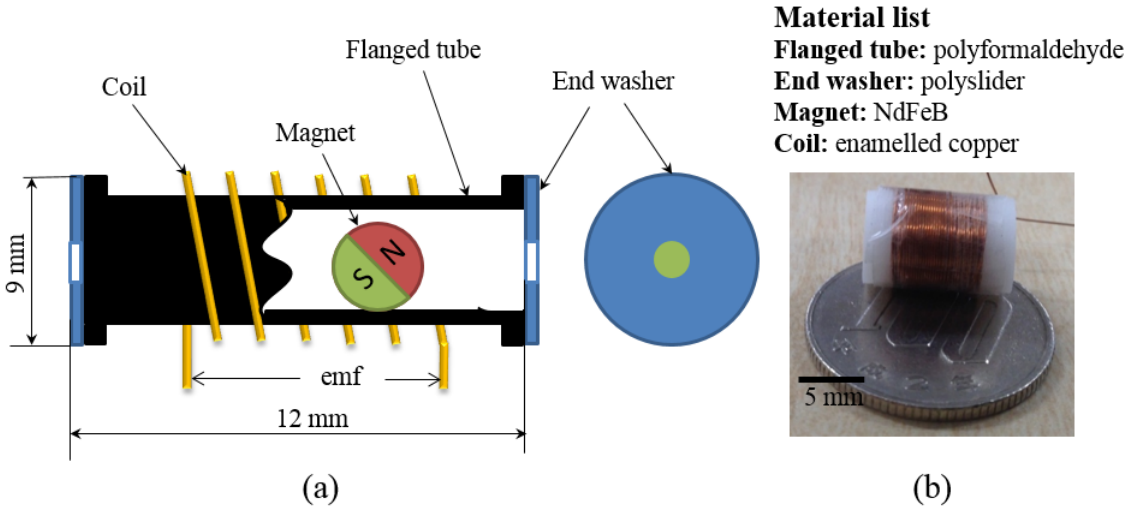

Fig. 5-1 (a) Schematic of electromagnetic energy harvester based on free motion with hard stops impact (FHH) (b) photograph of FHH shown with 100 yen coin (22.6 mm diameter).

5.3 Human body input vibration

The performance of FHH mainly depends on the input vibration. The output power increases with the input amplitude and/or frequency. However, the input vibration provided by the human body are not purely harmonic, multidirectional, and complicated in nature, which could have a different effect on the magnet/tube relative oscillation and consequently the overall harvester performance. Thus, the convenient way for evaluating the harvester performance with human body applications is to test it directly with the physical body motion.

Energy harvesting during three common natural gaits are investigated, which are walking with a speed of 75 m/min, fast walking with 108 m/min and jogging with 150 m/min. During each, the body parts and limbs have certain movement patterns which affect the input vibration at the different body locations.

Energy harvesting is tested at three body locations, which are the human wrist, ankle and pocket place (upper-leg). Those specific locations are selected for three reasons. First, some human body-related devices and portable electronics such as mobile phones, music players, and wrist watches are associated with those locations. Second, more motion or vibrations are expected from those locations [65]. The last is that passively energy harvesting could be obtained without making discomfort in the human daily activates [52]. The harvester is attached to the body at each location by keeping the harvester tube axis initially coincident with the body moving direction while the body is in the correct standing posture as shown in Fig. 5-2. This orientation generally can guarantee that most of the input vibrations to the harvester are in the direction of the harvester tube axis.

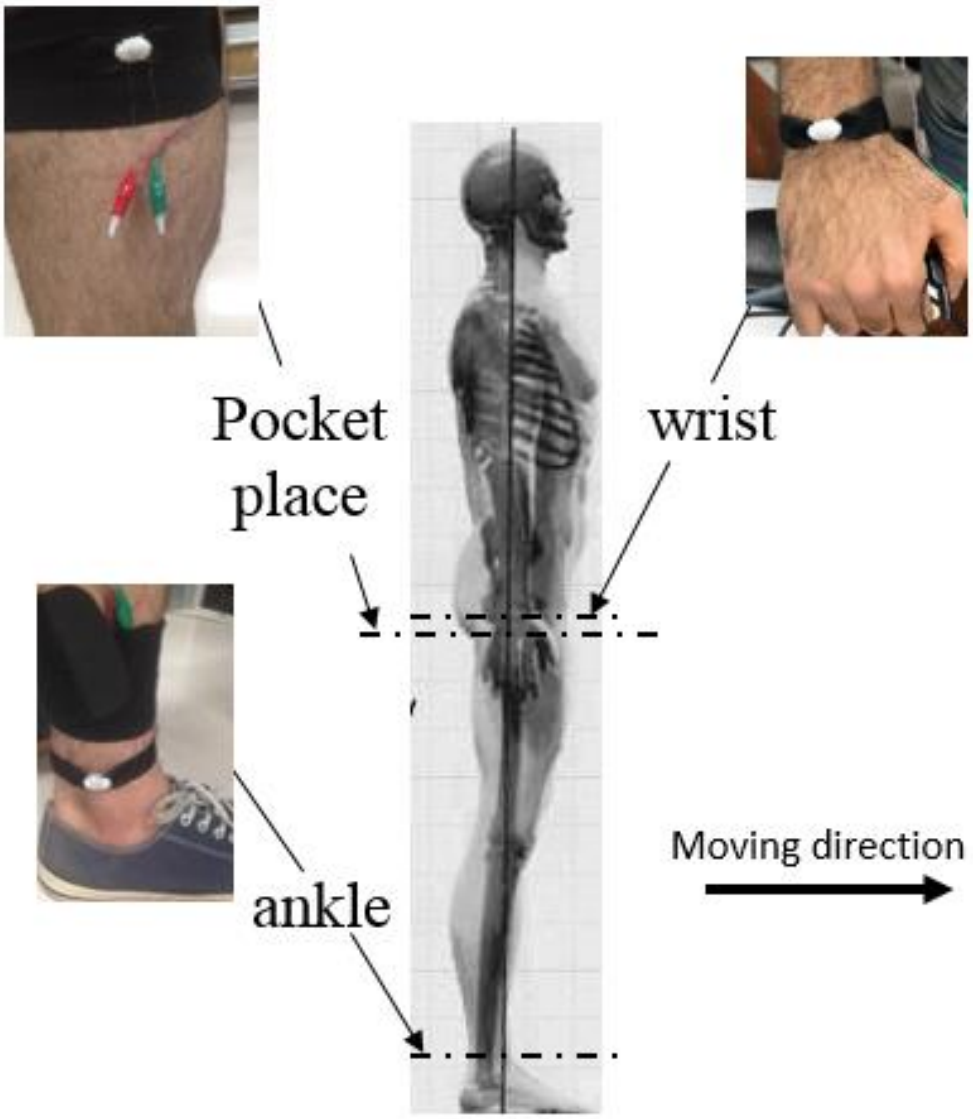

Fig. 5-2 shows the different body parts where the harvester is attached

5.3.1 Input vibration during walking

Human moving speed during walking mainly depends on stride rate or frequency and stride length [66, 67]. Stride frequency relates to the leg movement rate while stride length relates to how much distance covered by stride. The input frequency and amplitude to the harvester while attached to the leg (ex: at the ankle or pocket place) could be increased by increasing the stride frequency and stride length respectively. Since, the walking speed increases by increasing the stride frequency and/or stride length. We can expect an increase in the output power of a harvester placed at the ankle or pocket place by increasing the walking speed.

Regarding wrist energy harvesting during walking, the input vibration to the harvester mainly appears through arm swing. The frequency ratio between the arm and leg movement at a walking speed less than 0.8 m/s is 2:1, while it is 1:1 and the arm moves in-phase with the leg at a speed higher than 0.8m/s [68, 69]. The amplitude of the arm swing increases with the walking speed [70]. Hence, increasing the walking speed can increase both the input amplitude and frequency to the harvester at the wrist which in turns increase the output power.

In addition to large amplitude – low frequency movement of the body limbs during walking, there is some degree of impact on the heel of the foot at each step. This impact is transmitted from the foot to the whole body and quickly damped through by the body joints [71]. Hence, this impact is expect to significantly affect the harvester at the ankle over any other location.

5.3.2 Input vibration during jogging

The main difference between jogging and walking is that both feet could leave the ground at one step during jogging however, at least one foot should be kept in contact with the ground all the time during walking [72]. Accordingly, the leg has a different movement pattern during jogging. Foot impact with the ground is more significant. In addition, the lower arm has much bent over the upper arm. Thus, the gravitational force may has more effect on the magnet/tube relative motion of the wrist-attached harvester

5.4 Experimental results

In this experiment, voltage waveforms produced by each harvester prototype while attached to the body limbs are measured and recorded during the three activities. Hence, nine waveforms are obtained for each prototype as indicated by Figs. 5-3 to 5-5 for cylindrical-magnet prototype and Figs. 5-6 to 5-8 for ball-magnet prototype. The experiment is carried out on a male of 70 Kg weight, 176 cm height, and 27 years age.

The results show that signficant power could be harvested by FHH from the motion of the body limbs. The amount of harvested power depends on the body location where the harvester is attached, and the human activity. During the three activities, the highest power is obtained from ankle, then pocket place, and the lowest from wrist (Figs. 5-9 to 5-11), which could be a result of high input acceleration to the harvester at the ankle

[69].RMS power of about 445 µW is harvested from ankle by the ball-magnet prototype during jogging, while 221 µW and 174 µW are harvested from the pocket place and the wrist respectively (Fig. 5-9). Also, the cylindrical-magnet prototype generates an RMS power of about 175 µW from ankle, while it generates 126 µW, and 86 µW from pocket place, and wrist respectively during jogging (Fig. 5-9).

Increasing the body moving speed increases the output power as expected before, which is a result of increasing the input amplitude and/or frequency to the harvester at different body locations. RMS powers of 160 µW, 189 µW, and 221 µW are generated during walking, fast walking, and jogging from pocket place by ball-magnet protoype respectively. However, there is one case of the obtained results that the output power obtained from the ankle during jogging is less than that obtained during fast walking. This case appears in the cylindrical-magnet prototype results (Fig. 5-5). The power generated during jogging is about 175 µW, while that generated during fast walking is about 187 µW. This difference could be a result of the high impact force on the ankle during jogging. The impact force component normal to the harvester tube axis with high coloumb's friction involved in the cylindrical-magnet prototype can affect the magnet/tube relative oscillation and consequently the genertated voltage by induction. This effect does not signficantly appear in the ball-magnet prototype which has a lower frictional charractristics (Fig. 5-8).

The ball-magnet prototype generally can generate higher power than cylindrical-magnet one from different body locations during different actvities, which is a result of low coloumb's friction associated with the ball magnet. Lower friction resulted in higher magnet/tube relative motion from such low frequency motion and consequently higher induced voltage. In case of very low input vibration acceleration provided by the body motion such as that appears at the wrist during walking, the high coloumb's friction involved in the cylindrical-magnet prototype does not allow sensable magnet/tube relative motion to exist. Consequently, no or neglegable power could be generated in that case (Fig. 5-3a, Fig. 5-11).

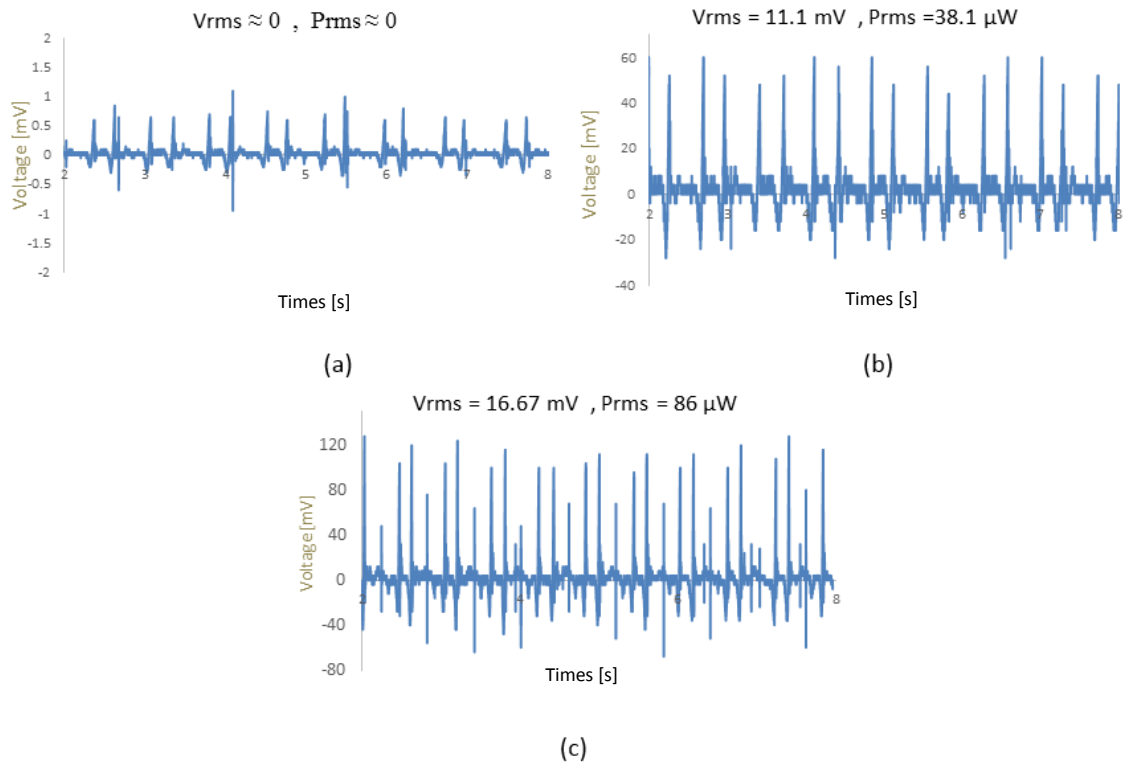

Fig.5-3. Measured voltage waveform of the cylindrical-magnet prototype while attached to the wrist (a) during walking (b) fast walking (c) during jogging.

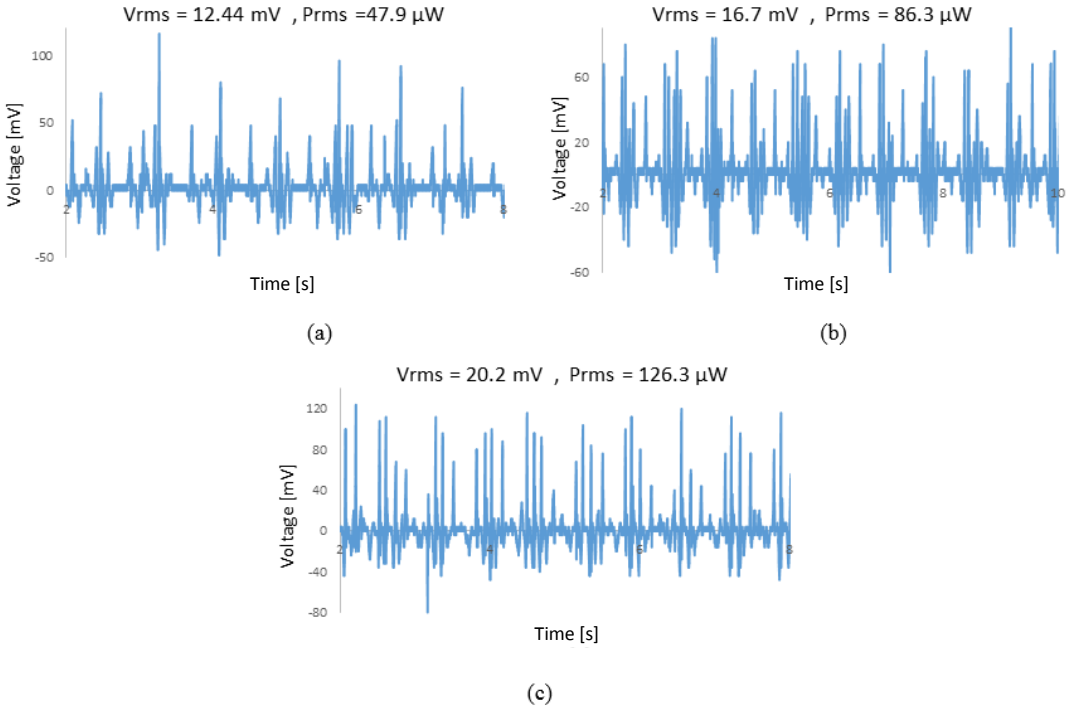

Fig.5-4. Measured voltage waveform of the cylindrical-magnet prototype while attached to the pocket (a) during walking (b) during fast walking (c) during jogging.

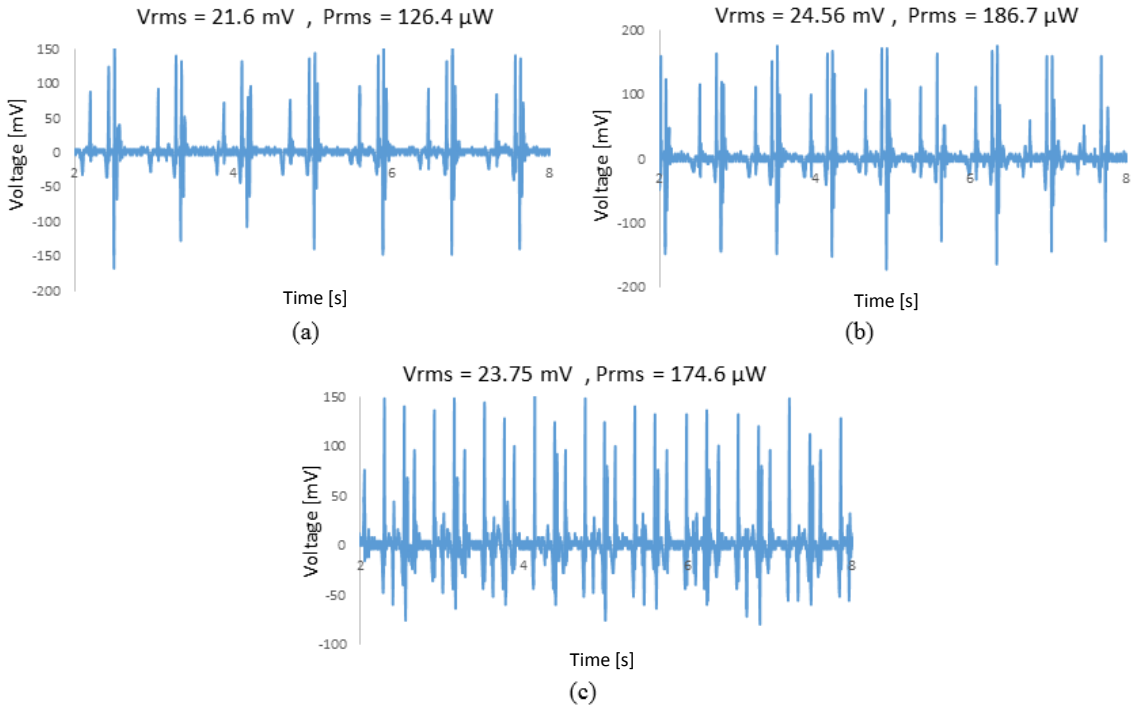

Fig.5-5. Measured voltage waveform of the cylindrical-magnet prototype while attached to the ankle (a) during walking (b) during fast walking (c) during jogging.

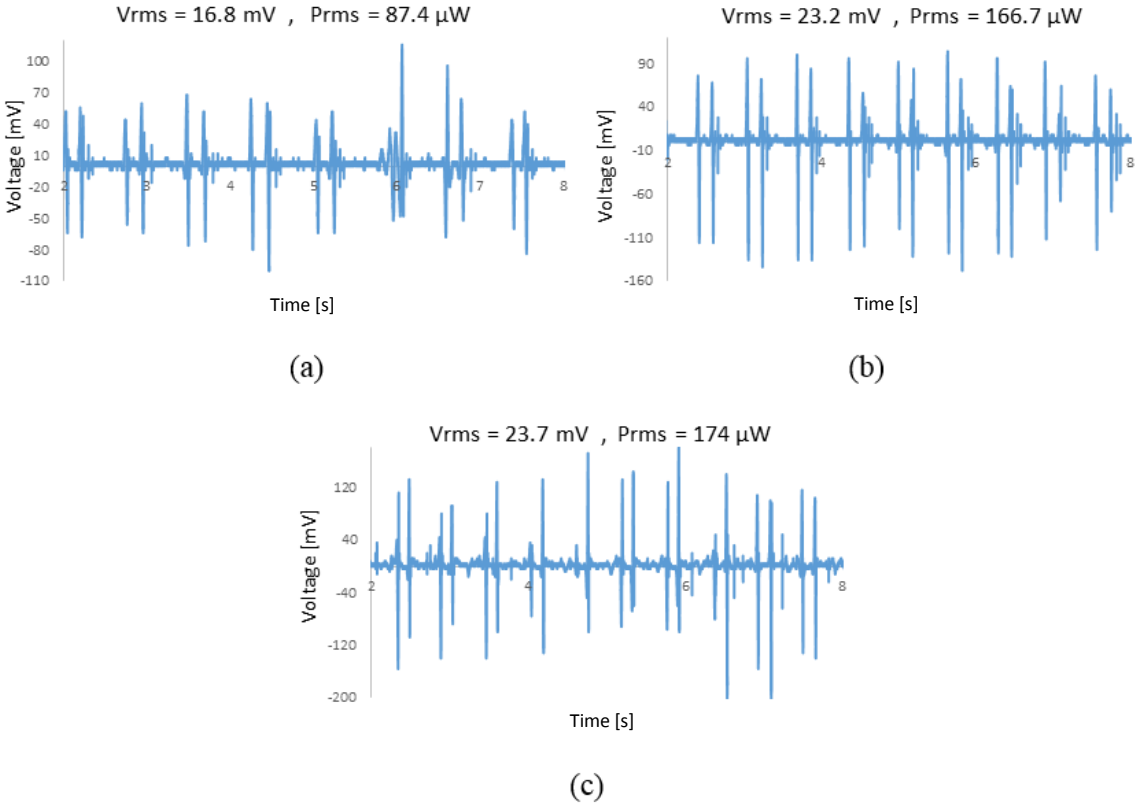

Fig.5-6. Measured voltage waveform of the ball-magnet prototype while attached to the wrist (a) during walking (b) during fast walking (c) during jogging.

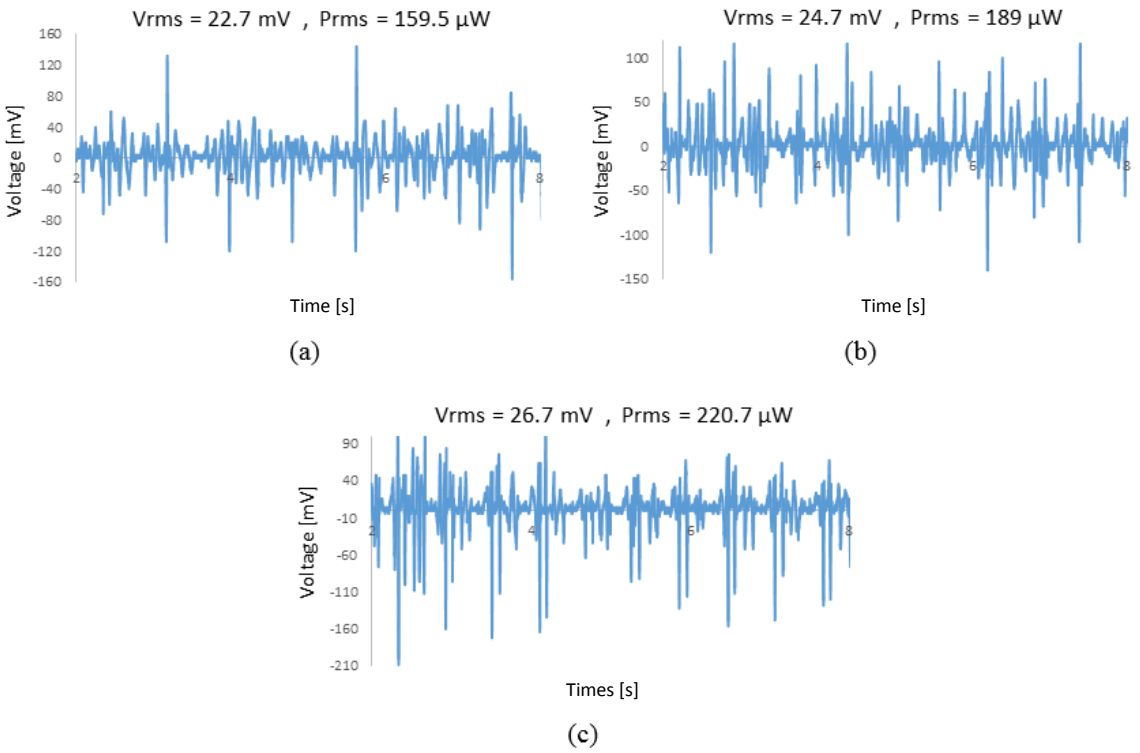

Fig.5-7. Measured voltage waveform of the ball-magnet prototype while attached to the pocket (a) during walking (b) during fast walking (c) during jogging.

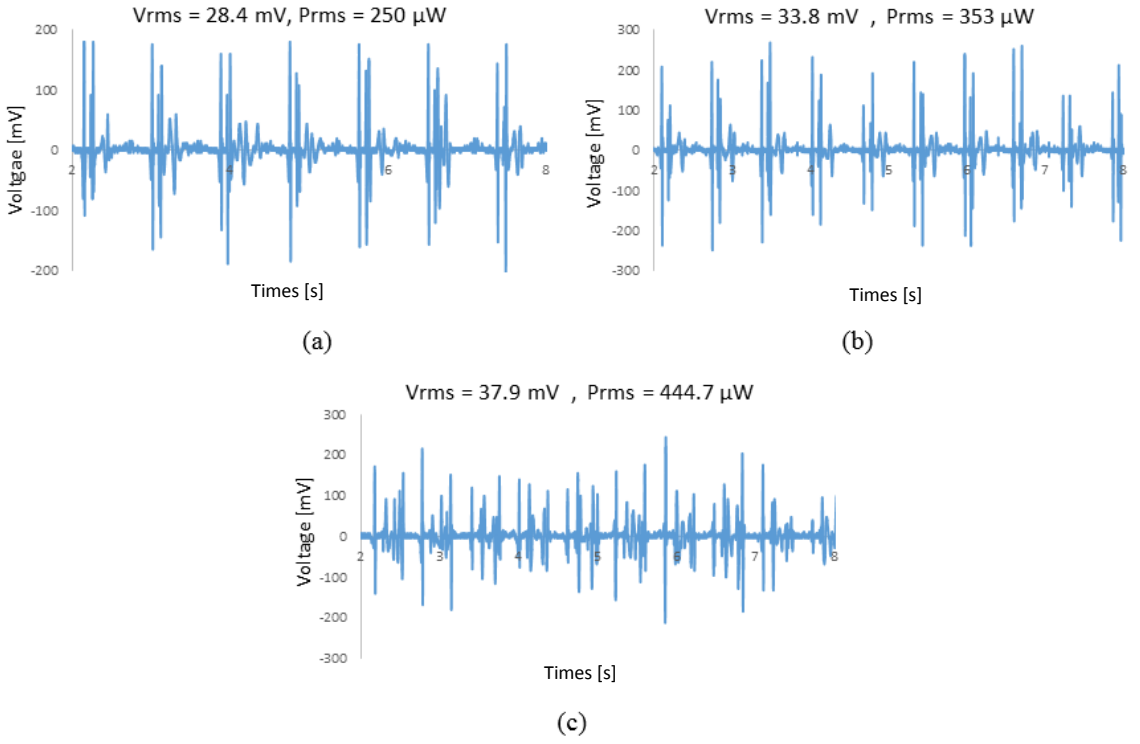

Fig.5-8. Measured voltage waveform of the ball-magnet prototype while attached to the ankle (a) during walking (b) during fast walking (c) during jogging.

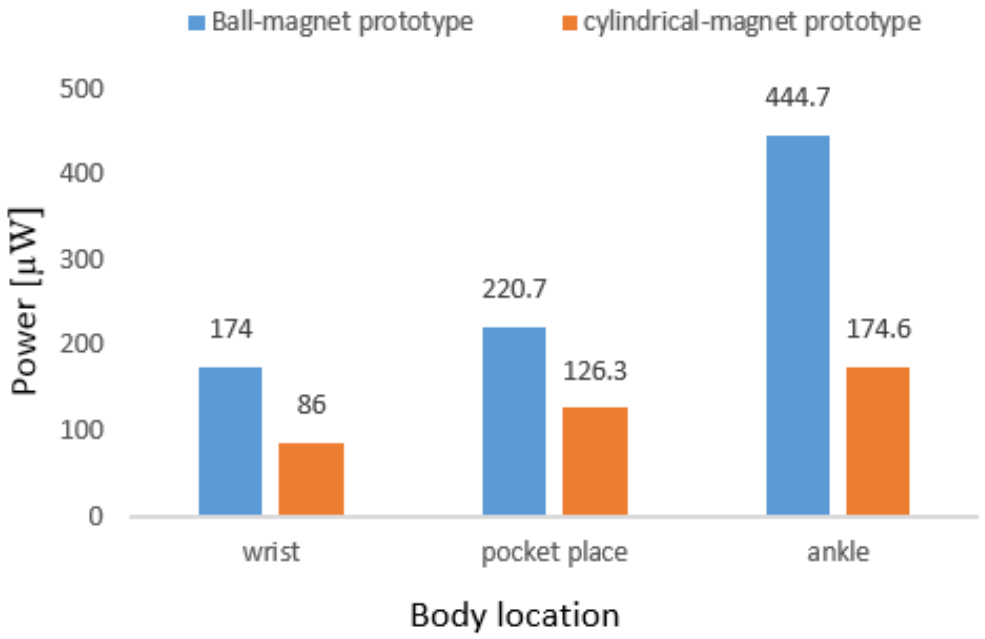

Fig. 5-9. RMS power generated by each prototype at different body locations during jogging with 150 m/min

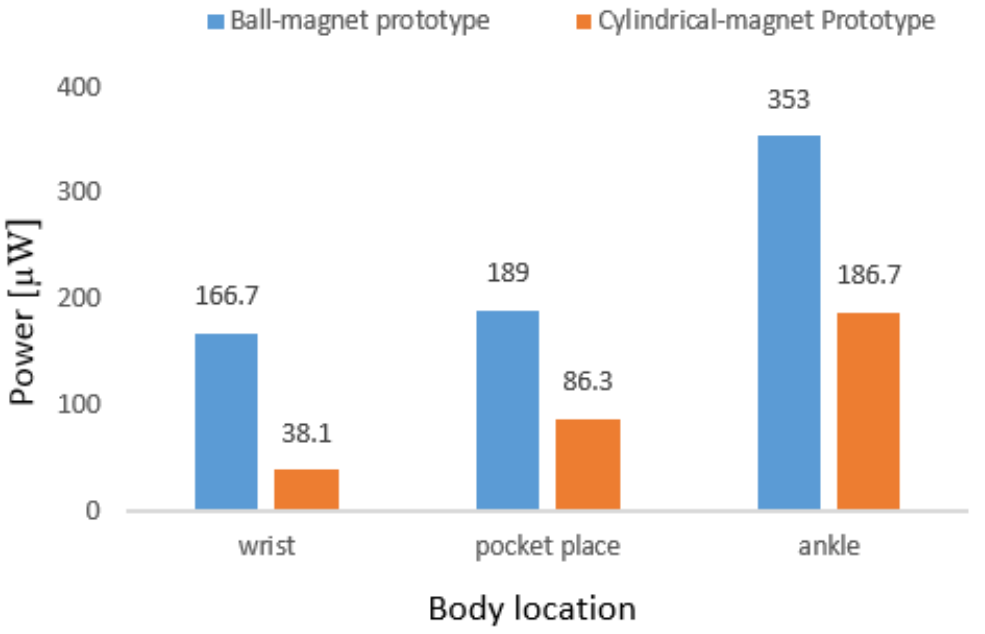

Fig. 5-10. RMS power generated by each prototype at different body locations during fast walking with 108 m/min

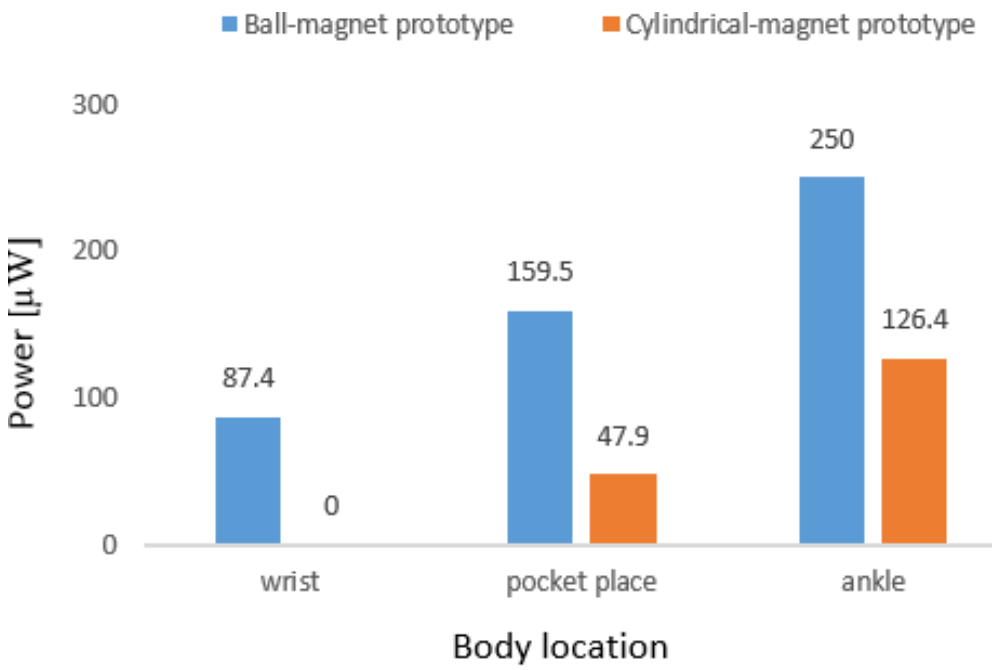

Fig. 5-11. RMS power generated by each prototype at different body locations during walking with 75 m/min

5.5 Comments on parameters selection

Design of FHH for human body energy harvesting depends on selecting the appropriate values of the harvester parameters. Many parameters are involved such as number of coil layers, wire diameter, coil length, effective tube length, magnet shape and size, etc. The optimum parameters are those which enable delivering the maximum amount of energy under the application constraints and working vibration condition.

Due to the variety of coupled and uncoupled parameters that need to be optimized as well as the random natural of human body motion which largely changes depending on the body activity, gait configuration, body features, etc., we present in this chapter an approximate selection procedure or selection guideline for the appropriate parameters of FHH that is going to be used for human body energy harvesting from a specified body location.

Usually human body associated devices are seeking for small size harvesters. Thus, size constraint become the main application constraint on the design of FHH. The application size constraint which includes the maximum allowable total harvester length and diameter or the maximum total size puts a limit on the selected harvester parameters, which can be

considered as a frame boundary of the design process.

5.5.1 Harvester length

Two harvester parameters are constrained by the harvester total length which can be nominated as length parameters. Those parameters are the effective tube length and the coil length.

- ***Effective tube length***

The effective tube length is the length that the magnet is allowed to move inside the tube, which equals to magnet stroke plus magnet length or diameter. The maximum stroke value of FHH as mentioned in chapter 4 should be selected according to the input vibration amplitude and frequency so that the whole allowable internal mass displacement could be utilized for energy harvesting and at least the impact motion is guarantee as the exist motion response during harvesting operation. However, the input amplitude by the movement of the body limbs is quite large which can cover larger strokes for energy harvesting. Thus, effective tube length can generally be selected according to the harvester length constraint, which enables utilizing the allowable harvester length for energy harvesting as much as possible.

- ***Coil length***

The flux rate of change ($d\varphi/dz$) is affected by the coil length. The optimum coil length for a certain magnet stroke can be that one which can give the maximum average flux rate of change by moving the magnet inside the coil. For example, Fig.5-6 shows the variation of the flux rate change of the magnet within the coil at different coil lengths for a harvester of 8 mm stroke. The maximum calculated average flux rate of change in this case is obtained at 6 mm coil length. Thus, a coil length of 6 mm is recommended to be used in that case.

5.5.2 Harvester diameter

Ball magnet shows a better performance with low frequency human body motion due the associated low coulomb's friction. Thus, it is recommended to be used with FHH for energy harvesting from human body motion during different activities.

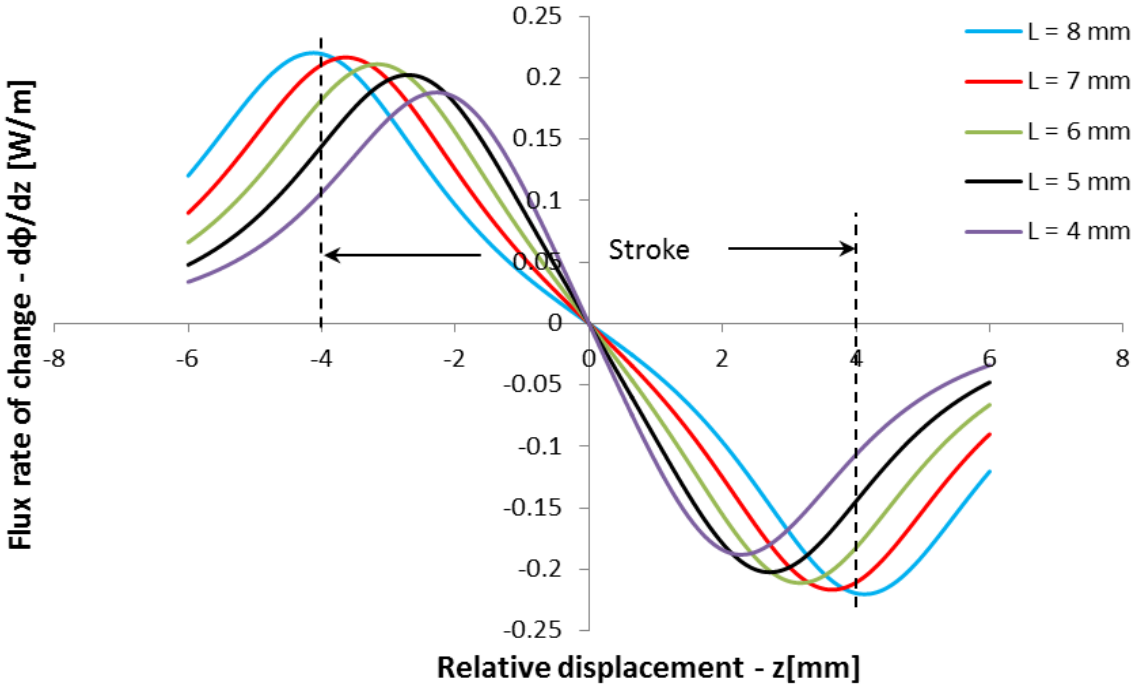

Fig. 5-6 shows the variation of flux rate of change with the magnet position within the coil for different coil lengths, and stroke of 8 mm.

The harvester total diameter is formed by the magnet diameter, magnet/tube clearance, wire diameter and number of coil layers which can be nominated as diameter parameters. Changing one of those parameters for a constant harvester diameter will affect the other, as well as affecting the harvesting performance. For instance, increasing the magnet diameter increases the magnetic strength, increasing the tube/magnet clearance reduce the friction and improve power harvesting. One the other hand, reducing wire diameter increase the coil resistance, and reducing the number of coil layers reduces the average flux rate of change and in the same time reduces the coil resistance.

Therefore, it could be difficult to optimize those four parameters analytically. In addition, making experimental optimization may involve an infinite number of iterations or experiments. However, we propose in this chapter a way of parameter selection and iterative experiments that can enable determining appropriate values of the diameter parameters for an effective harvesting performance as follows:

- **Magnet diameter**

First, select an appropriate magnet diameter. For example, it could be one third of the total harvester diameter.

- **Tube/magnet clearance**

Based on the selected magnet diameter, the clearance value could be selected, so that a sufficient magnet travel through the whole stroke could be guaranteed under the input vibration condition. This can be done by testing the magnet with different tube diameters by the input body motion where the harvester is intended to be attached during a certain common activity.

- **Wire diameter**

Second, select an appropriate wire diameter. For example, it could be one twentieth of the total diameter or according to the commercially available enameled copper wires.

- **Number of coil layers**

Number of coil layers could then be selected based on the total harvester diameter and other selected diameters.

5.5.3 Iterative selections

After the first selection of the harvester parameters, it should be tested experimentally with the body motion at the location where the harvester is intended to be attached. The selection procedure should be repeated few times with different magnet diameters and constant wire diameter until approximately reaches the magnet diameter of the higher output power, then with different wire diameters and constant magnet diameter until reach the wire of the higher output power.

The final parameter values would be the appropriate values of FHH’s parameters that is going to be used at a specific body location during a common daily activity. Fig. 5-7 also shows a summary the selection procedure steps.

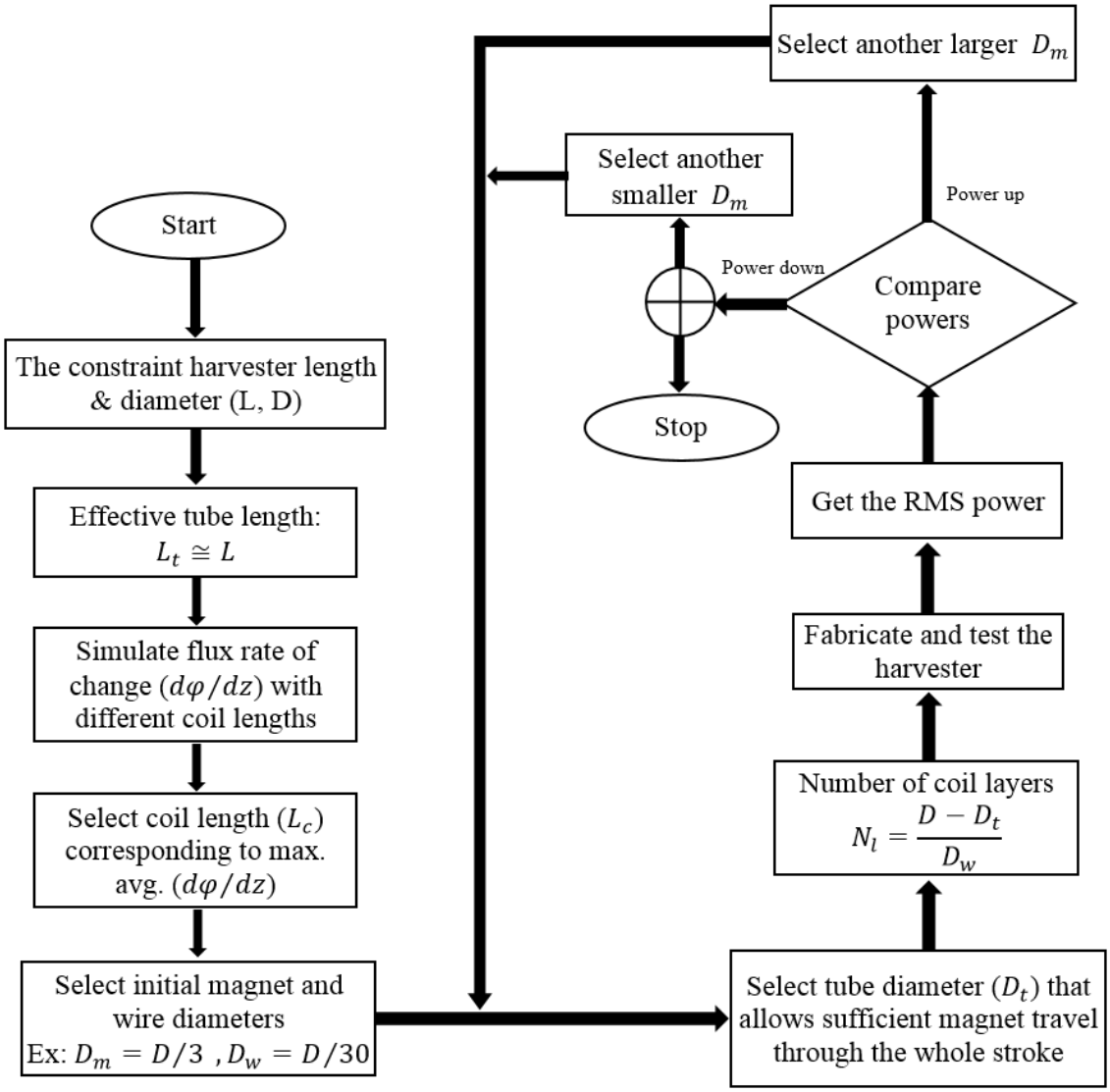

Fig. 5-7. Chat shows the parameter selection steps of FHH for energy harvesting from human body motion at a specific body location during a common body activity

5.6 Summary

In this chapter, the electromagnetic vibration energy harvester based on free motion with hard stops impact (FHH) is tested with human body motion. Two harvester prototypes of total cylindrical size of D9×L12 mm are considered; one is fabricated with 3.5 mm diameter ball magnet, while the other is fabricated with D3×L3.5 mm cylindrical magnet. Both prototypes are attached to three different body locations which are the wrist, ankle, and pocket place (upper-leg), and tested during three different moving activities which are walking with 75 m/min speed, fast walking with 108 m/min, and jogging with 150 m/min. Voltage waveforms produced by each prototype are measured and recorded during each activity which show the harvester ability to generate significant amount of power from the motion of body limbs. The power can reach 445 μW RMS, with an average power density of about 0.6 mW/cm³. The ball-magnet prototype shows a better performance over cylindrical-magnet one at different body locations during different activities, owing to low coulomb's friction associated with the ball magnet oscillation. For instance, the ball-magnet prototype can generate an RMS power of 445 μW from the ankle during jogging, 167 μW from pocket place during walking and 160 μW from wrist during fast walking. However, the cylindrical-magnet prototype generates an RMS power of about 175 μW from the ankle during fast jogging, 48 μW from pocket place during walking, and 38 μW from wrist during fast walking.

The maximum power harvesting during the three activates appears at the human ankle, due to the high input acceleration to the harvester at this location. Increasing the body moving speed generally boosts the power harvesting from different body locations. The power generated during jogging is higher than that generated during fast walking which is higher than that generated during walking in most cases. One case of cylindrical-

magnet prototype results that the power generated during fast walking is higher than that generated during jogging. The prototype at the ankle generates an RMS power of 186.7 μW during fast walking, while it generates 174.6 μW during jogging. This difference can be a result of the high impact force exerted on the ankle during jogging.

An optimization procedure or parameters selecting guidelines of FHH are presented. Selection is based on determining a certain harvester size according to the application size constraint, and the body location where energy harvesting is deemed.

Chapter 6 Conclusions

6.1 Conclusions

This work presents study of a vibrating system or oscillator based on generating combined free / impact motion with electromagnetic vibration energy harvesting. The proposed oscillator can work effectively at low frequencies. It consists of a permanent magnet mass allowed to move freely inside a frame – carrying an electrical coil which is directly connected to the vibration source. The magnet/frame relative oscillations are converted into electrical energy by induction.

The way of magnet /frame impact has a significant effect on the oscillator dynamic behavior and consequently the harvesting performance. Hence, in this work two kinds of oscillators or energy harvesting architectures based on two different ways of magnet/frame impact are studied. The first includes impact with elastic end stops (FEH) and the second includes impact with hard end stops (FHH). Theoretical modeling on the non-linear behavior and numerical simulation of both architectures are vigorously conducted with some experiments results.

Unlike linear spring – mass harvester, FEH can give an increase in the resonant relative amplitude when matching lower frequencies using larger allowed free motion distance (Stroke). Higher resonant relative amplitude gives higher relative velocity and consequently higher voltage and power output. Thus, it would be preferred for low frequency applications that are seeking for resonant amplification. However, FHH shows a non-resonant behavior in which the output power increases with both input amplitude and/or frequency. In addition, it has a simple construction that allow fabrication with small size, which can makes it suitable for important kinds of applications such as human powered devices. The detailed conclusions are obtained below.

(1) Free / elastic end stops impact harvester (FEH).

In the free / elastic end stops impact harvester (FEH), the magnet is allowed to freely move within a certain distance inside the frame and makes impacts with two spring end stops. The presence of spring mass separation with elastic end stops impact allows matching low frequencies with high resonant relative amplitude compare to similar linear spring-mass system (CH) with the same mass. As a result, higher relative velocity could be obtained and consequently higher power could be generated when matching low frequencies. Therefore, FEH is preferred to be used over CH in some cases; when matching low frequencies with a sufficient allowable internal mass displacement while there is a restriction on the maximum utilized Q-factor. In fact, CH has a better performance in high Q-factor systems and the critical Q-factor below which FEH is preferred to be used depends on the design configuration. For example, simulation case study shows that FEH is preferred to be used over CH with 0.03 Kg oscillation mass at 14 Hz when the Q-factor cannot increase over 5.28.

FEH shows an uncommon resonant dynamic behavior, in which the magnet/frame relative oscillation can take four different ways of response over the range of input frequencies. Unlike the linear spring – mass system, the resonant frequency of FEH can be shifted to lower frequency ranges using larger strokes without a decrease in the resonant relative amplitude. Simulation comparisons between FEH and optimum linear spring – mass harvester with zero coulomb's friction and Q=2.64 (Q is determined based on experimental value of C) at the same resonant frequency are carried out as well as an experimental comparison with similar CH. Simulation results show FEH's power magnification of more than 3 and 7 times at a frequency of 14 Hz and 11 Hz respectively. The power magnification generally increases by matching lower frequencies. The

effectiveness of an experimental prototype can reach 8.6% at 10 Hz and 10mm input amplitude.

Due to the resonant natural of FEH as well as the significant resonant magnification at low frequencies, it could be well suited for quite steady-low frequency applications that are seeking for resonant amplification. This vibration condition could be observed in some machine mediums or associated with some engine vibrations.

(2) Free / hard stops impact harvester (FHH).

The free / hard stops impact harvester simply consists of a permanent magnet mass allowed to move freely inside a frame – carrying an electrical coil and make impacts with two hard end stops. Simulation of a case study shows a unique behavior of FHH, in which four different ways of response appear over the range input amplitudes and frequencies. FHH shows a non-resonant behavior. The output power increases with input amplitude and / or frequency. The allowed free motion enables efficient harvesting at low frequencies. In addition, FHH has a simple construction which allows harvester fabrication with small sizes. Therefore, FHH could be well suited for the application that deem small size harvesters and involved unsteady large amplitude – low frequency vibrations such as human body associated devices.

Two different experiments are conducted. The first is to show the effect of magnet shape on the system performance, and the second is to investigate the power and power density of different size prototypes with the input amplitude. The first experiment shows the superior performance of a ball magnet prototype at low input frequencies due to low associated coulomb's friction. It can generate 30.95 μW at an input vibration of (5 Hz and 10 mm Amp.), while cylindrical and double-ball magnets can generate 15.18 μW and

23.05 µW respectively at the same input vibration. However, cylindrical magnet and double-ball magnet prototypes have better performance at higher frequencies due to the large magnetic flux component normal to the area bounded by the coil turns during oscillation. They can generate 500 µW and 407 µW respectively at an input vibration of (10 Hz and10 mm Amp.) while ball magnet can generate only 205.6 µW at the same input vibration. The second experiment shows that the output power can be increased with the number of coil turns. For example, a prototype of D9×L12 mm cylindrical total size and 300 coil turns can generate RMS power of 71.8 µW at (2.5 Hz and 5.2 ms^{-2}), and 113.3µW at (3.33 Hz, and 12.38 ms^{-2}). Another of D7×L12 mm total size and 200 coil turns can generate RMS power of 28.4 µW at (2.5 Hz and 5.2 ms^{-2}), and 82.9 µW at (3.33 Hz, and 12.38 ms^{-2}). However, the power density in some cases decreases with the number of coil turns due to the increase of the harvester size without a corresponding significant increase in the output power. The effectiveness of D9L12 prototype can reach 7.34% at 2.5 Hz and 30 mm input amplitude.

The advantages of FHH can make it more suitable for an important kind of applications, which are the human body associated devices. However, in order to correctly evaluate the performance of FHH with such important applications, FHH has been tested with actual human body motion. FHH is selected to be tested at three body locations which are ankle, pocket place (upper leg), and wrist during three natural gaits which are walking with 76 m/min, walking with 105 m/min, and jogging with 150 m/min. Two similar prototype of different magnet shapes (ball and cylindrical) are tested. FHH generally shows an effective performance with human induce vibration, in which the RMS output power could reach 445 µW. Ball magnet prototype shows a better performance over cylindrical magnet one. The output power of FHH generally increases with the body moving speed

as well as the power harvesting from ankle is higher that from pocket place than that from wrist. Finally, a way of parameters selection of FHH for a certain body application with a size constraint is discussed.

6.2 Future work

This dissertation is focusing on study, analysis and testing of two mechanical oscillators that can work effectively with low frequency vibration energy harvesting. Each of them is suitable for certain kinds of applications depending on the input vibration conditions and application constraints. However, the research in there utilization with vibration energy harvesting is still open. In this section we are mentioning to some research ideas and future prospective of employing the proposed harvesting architectures (FEH and FHH) with vibration energy harvesting.

(1) FEH is a resonant harvester with high resonant amplification that can works effectively at low frequencies. Thus, it is suitable for low frequency steady vibrations. However, some low frequency applications that are seeking for resonant amplification associate with variable input frequency. In that case, the power generated by FEH would drop sometimes during operation. Autonomous tuning of FEH is a possible solution to this problem. Tuning can be done by controlling FEH's stroke through adjusent stroke mechanism actuated by a control system based on FHH (Fig. 6-1)

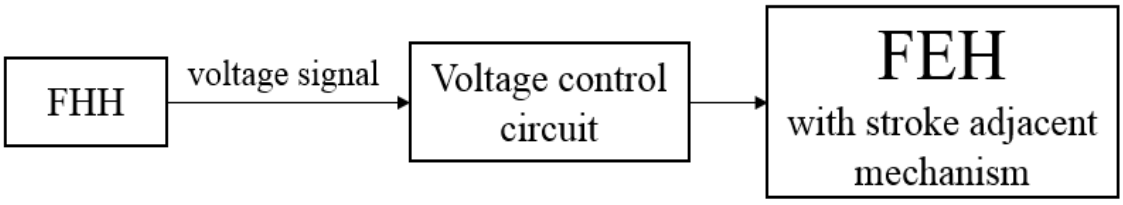

Fig. 6-1 Autonomous tuning of FEH using FHH transducer

FHH acts as a non-resonant electromagnetic transducer with an output voltage proportional to the input frequency. The output voltage from FHH can be used as an actuation signal to the stroke adjacent mechanism through a voltage control circuit.

(2) Fabrication of FHH in this work is done by the assembly of commercially available components with manual coil winding for a harvester size of around 10 mm. However, small sizes are possible (e.g. few millimeters in total). Micro fabricated multi-layer planner coil could be utilized in that case. Some design or configuration changes may be involved, as well as anti-friction measures should be considered especially in case of low input acceleration.

(3) Energy harvesting by FHH mainly depends on electromagnetic transduction. Increasing the internal relative velocity by increasing the input amplitude or frequency increases the induced voltage. However, impact with hard end stops could also be used as a slave transduction. Piezoelectric end stops could be used instead of solid hard end stops (Fig. 6-2). In that case impact energy could be converted to useful electrical energy that can increase the total output power of the system.

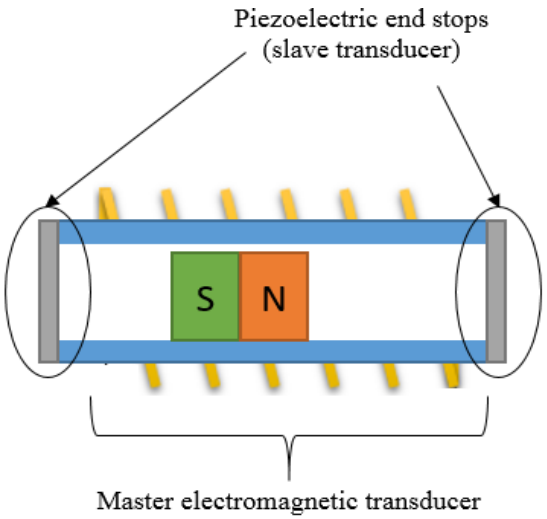

Fig. 6-2 FHH with piezoelectric slave transducer

(4) Coulomb force parametric generator (CFPG) presented by Mitcheson et al [47, 48, 49] is one of the earlier electrostatic non-resonant harvesters that could work effectively with human – powered devices. In the optimized CFPG, the relative displacement is allowed only at the maximum input acceleration. This can be achieved by adjusting a holding electrostatic force to an optimum value, which is slightly below the maximum inertia force. Exciting CFPG with a high acceleration allow a higher holding force to be adjusted and consequently higher power harvesting. In fact, holding force can be easily adjusted by setting the prime voltage to an optimal value for a given source of acceleration. However, for a variable acceleration source such as human body motion, optimization should be carried out dynamically, which requires an optimization module.

FHH as a system that produces voltage proportional to the input acceleration (amplitude and frequency) can provide prime voltage signal to CFPG (Fig. 6-3). The voltage signal generated by FHH is supplied to a voltage control circuit that can generate a prime voltage to dynamically optimize CFPG.

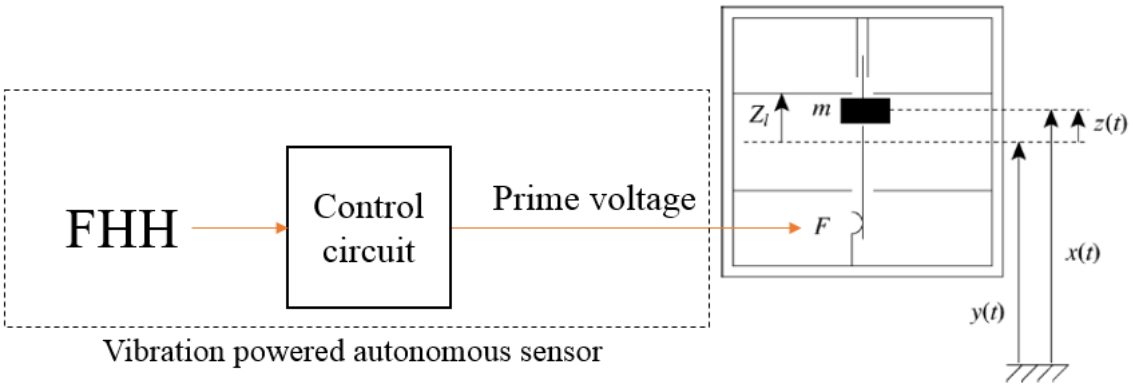

Fig. 6-3 FHH is used with CFPG [47] to provide online optimization

Acknowledgement

Foremost, I would like to express my sincere gratitude to my dear advisor Prof. Shin'ichi Warisawa for the continuous support of my PhD study and research, for his patience, motivation, and enthusiasm. His guidance helped me in all the time of research, writing of the thesis and related publications. He was always encouraging and supporting me in my experiments, and in my whole research. I want to thank him deeply for his general advises, and kindness.

Besides my advisor, I would like to thank Prof. Ichiro Yamada for his advises and useful comments on my research, as well as for his continuous support to my research

I want to thank all Yamada-Warisawa laboratory members for their comments and suggestions on my research. I want to thank Mr. Matsuki for helping me to learn some micro fabrication techniques. I want to thank Mr. Matsuki again, Mr. Kouyama, Mr. Ishizuka, and Mr Bano for helping me in my life in Japan, and helping with Japanese language.

I would like to thank the committee members, Prof. Yuji Suzuki, Prof. Kiyoshi Matsumoto, Prof. Kimihiko Nakano, and Prof. Takeshi Morita for accepting the invitation to be referees to my dissertation, and for their comments to improve my dissertation.

Finally I want to express my dear thanks to my family; my father, my mother and my sister, who always encourage and support me in my work, research, and whole my life.

References

[1] T.von Buren, G.Troster, “Design and optimization of a linear vibration driven electromagnetic micro-power generator”. *Sensors and Actuators: A 135 (2007) 765 – 775.*

[2] S.P.Beeby, R.N.Torah, M.J.Tudor, P.Glynne-Jones, T.O'Donnell, C.R.Saha, S.Roy, “A micro electromagnetic generator for vibration energy harvesting”. *Journal of Micromechanics and Microengineering 17 (2007) 1257-1265.*

[3] P.Wang, W.Li, L.Che, “Design and fabrication of a micro electromagnetic vibration energy harvester”. *Journal of Semiconductors 10 (2012) 104009.*

[4] E.O.Torres, Gabriel A.Rincon-Mora, “Electrostatic energy harvester and li-ion charger circuit for Micro-scale applications”. *Proceeding of 49th IEEE International Midwest Symposium on Circuits and Systems, San Juan, 2006, vol 1, pp. 65 – 69.*

[5] Paul D.Mitcheson, Tim C.Green, “Maximum Effectiveness of Electrostatic Energy Harvesters When Coupled to Interface Circuits”. *IEEE Transaction on Circuits and Systems 59 (2012) 3098-3111*

[6] M.E.Kiziroglou, C.He, E.M.Yeatman, “Electrostatic Energy Harvester with External Proof Mass”. *Proceeding of PowerMEMS 2007, Freiburg- Germany, pp.117-120.*

[7] M.Marzencki, S.Basrour, B.Charlot, S.Spirkovich, M.Colin, “A MEMS piezoelectric vibration energy harvesting device”. *Proceeding of. PowerMEMS 2005, Tokyo, pp 45-8.*

[8] D.Isarakorn, D.Briand, P.Janphuang, A.Sambri, S.Gariglio, J.M.Triscone, F.Guy, J.W.Reiner, C.H.Ahn, “N.F.de Rooij, Energy harvesting MEMS device based on an epitaxial PZT thin film: Fabrication and characterization”. *Power MEMS Tech. Dig., 2010, pp.203 -206*

[9] P. Muralt, et al., “Vibration Energy Harvesting with PZT Thin Film Micro Device”, *PowerMEMS 2009, Washington DC, USA.*

[10] Tang L., Yang Y., Soh C. K., “Toward broadband vibration-based energy harvesting. *Journal of intelligent material systems and structures”, 21(18) 1867- 1897 (2010).*

[11] Arman Hajati, and Sang-Gook Kim, “Ultra-wide bandwidth piezoelectric energy harvesting”, *Applied physics letters 99, 083105 (2011).*

[12] Lihua Tang, and Yaowen Yang, “A nonlinear piezoelectric energy harvester with magnetic oscillator”, *Applied Physics Letters 101 094102 (2012)*

[13] M. Ferrari, V. Ferrari, M. Guizzetti, B. Andò, S. Baglio, C. Trigona, “Improved energy harvesting from wideband vibrations by nonlinear piezoelectric converters”, *Sensors and Actuators A 162 (2010) 425-431*

[14] Francesco Cottone, Philippe Basset, Helios Vocca, Luca Gammaitoni, and Tarik Bourouina, “Bistable electromagnetic generator based on buckled beams for vibration energy harvesting” *Journal of intelligent material systems and structures 25(12) 1484-1495(2013)*

[15] Rencheng Zheng, Kimihiko Nakano, Honggang Hu, Dongxu Su, and Matthew P. Cartmell, “An application of stochastic resonance for energy harvesting in a bistable vibrating system” *Journal of sound and vibration 33(12) 2568-2587 (2014)*

[16] Vinod R. Challa, M.G.Prasad, Frank T. Fisher, “Towards an autonomous self-tuning vibration energy harvesting device for wireless sensor network applications”. *Smart Materials and Structure 20 (2011) 025004.*

[17] C.Eichhorn, F.Goldschmidtboeing, P.Woias, “Bidirectional frequency tuning of a piezoelectric energy converter based on a cantilever beam”. *Journal of. Micromechanics and Microengineering 19 (2009) 094006 (6pp).*

[18] Lei Guand, and Carol Livermore, “Compact passively self-tuning energy harvesting for rotating applications”, *Smart material and structure 21(1)015002 (2012)*

[19] Scott Moss, Alex Barry, Ian Powlesland, Steve Galea, Gregory P. Carman, “A low profile vibro-impacting energy harvester with symmetrical stops”. *Applied physics letters 97 (2010) 234101(4pp)*

[20] C. L. Zhang, J. S. Yang, W. Q. Chen, “Harvesting magnetic energy using extensional vibration of laminated magnetoelectric plates”, *Applied physics letters 95 (2009) 013511 (4pp).*

[21] Xianzhi Dai, Yumei Wen, Ping Li, Jin Yang, Ming Li “Energy harvesting from mechanical vibrations using multiple magnetostrictive/piezoelectric composite transducers”, *Sensors and Actuators A 166 (2011) 94–101*

[22] Jin Yang, Yumei Wen, Ping Li, Xihai Yue, Qiangmo Yu, and Xiaoling Bai, "A two-dimensional broadband vibration energy harvester using magnetoelectric transducer", *Applied physics letters, 103 (2013) 243903*

[23] Jin Yang, Xihai Yue, Yumei Wen, Ping Li, Qiangmo Yu, Xiaoling Bai, "Design and analysis of a 2D broadband vibration energy harvester for wireless sensors", *Sensors and Actuators A 205 (2014) 47–52* .

[24] Xiaoling Bai, Yumei Wen, Ping Li, Jin Yang, Xiao Peng, Xihai Yue, "Multi-modal vibration energy harvesting utilizing spiral cantilever with magnetic coupling", *Sensors and Actuators A 209 (2014) 78–86*

[25] Yating Hu, Yong Xua, "A wideband vibration energy harvester based on a folded asymmetric gapped cantilever", *Applied Physics Letters 104, 053902 (2014)*

[26] Haluk Kulah, Khalil Najafi, "Energy scavenging from low-frequency vibrations by using frequency up-conversion for wireless sensor applications". *IEEE Sensors 8 (2008) 261-268.*

[27] D.Lee, G.Carman, D.Murphy, C.Schulenburg, "Novel micro vibration energy harvesting device using frequency up conversion", *Proceeding of 14th International Conference on Solid-State Sensors, Actuators and Microsystems, Lyon, 2007, pp.871–874.*

[28] T.V.Galchev, J.McCullagh, R.L.Peterson., K.Najaf, "Harvesting traffic-induced vibrations for structural health monitoring of bridges", *Journal of Micromechanics and Microengineering 21 (2011) 104005 (13pp).*

[29] Pit Pillatsch, Eric M. Yeatman, Andrew S. Holmes, "A piezoelectric frequency up-converting energy harvester with rotating proof mass for human body applications" *Sensors and Actuators: A 206 (2014) 178– 185.*

[30] Lei Gu, Carol Livermore, "Impact-driven, frequency up-converting coupled vibration energy harvesting device for low frequency operation". *Smart Materials and Structure 20 (2011) 045004 (10pp).*

[31] Y Naruse, N Matsubara, K Mabuchi, M Izumi and S Suzuki, "Electrostatic micro power generation from low-frequency vibration such as human motion", *J. Micromech. Microeng. 19 (2009) 094002 (5pp).*

[32] S.E. Jo, M.S. Kim and Y.J. Kim, "Electromagnetic human vibration energy harvester comprising planar coils", *Electronics Letters 48 (14) (2012) (2pp).*

[33] M.S.M.Soliman, E.M.Abdel-Rahman, E.F.El-Saadany, "A wideband vibration-based energy harvester", *Journal of. Micromechanics and Microengineering. 18 (2008) 115021 (11pp).*

[34] Lars-Cyril, Julin Blystad, Einar Halvorsen, "Piezoelectric MEMS energy harvesting systems driven by harmonic and random vibrations". *IEEE Transactions on Ultrasonics, Ferroelectrics, and Frequency Control 57(4) (2010) 908-919.*

[35] Lars-Cyril Julin Blystad, Einar Halvorsen, "A piezoelectric energy harvester with a mechanical end stop on one side". *Microsystem Technology 17(4) (2011) 505-511.*

[36] Cuong Phu Le, Einar Halvorsen, "MEMS electrostatic energy harvesters with end-stop effects". *Journal of Micromechanics and Microengineering 22 (2012) 074013 (12pp).*

[37] Cuong Phu Le, Einar Halvorsen, Oddvar Sorasen, Eric M. Yeatman, "Microscale electrostatic energy harvester using internal impacts". *Journal of Intelligent Material Systems and Structures 23(13) (2012) 1409–1421.*

[38] Mikio Umeda, Kentaro Nakamura, Sadayuki Ueha, "Analysis of the Transformation of mechanical impact energy to electrical energy piezoelectric vibrator", *Japanese Journal of Applied Physics 35(1) (1996) 3267-3273.*

[39] Michael Renaud, Paolo Fiorini, Chris van Hoof, "Optimization of piezoelectric unimorph for shock and impact energy harvesting", *Smart Materials and Structure 16 (2007) 1125-1135. doi:10.1088/0964-1726/16/4/022*

[40] E.Jacquelin, S Adhikari, M.I.Friswell, "A piezoelectric device for impact energy harvesting". *Smart Materials and Structure 20 (2011) 105008 (12pp).*

[41] Lei Gu, Carol Livermore, Impact-driven, frequency up-converting coupled vibration energy harvesting device for low frequency operation. Smart Materials and Structure 20 (2011) 045004 (10pp).

[42] M.Renaud, P.Fiorini, R.van Schaijk, C.van Hoof, "Harvesting energy from the motion of human limbs: the design and analysis of an impact-based piezoelectric generator". *Smart Materials and Structure 18 (2009) 03500.*

[43] S Moss, A Barry, I Powlesland, S Galea, G P Carman, “A broadband vibro-impacting power harvester with symmetrical piezoelectric bimorph-stops”, *Smart Mater. Struct. 20 (2011) 045013 (12pp).*

[44] Scott Moss, Alex Barry, Ian Powlesland, Steve Galea, and Gregory P. Carman, “A low profile vibro-impacting energy harvester with symmetrical stops”, *Applied physics letters 97 (2010) 234101 (3pp).*

[45] Scott D. Moss, Genevieve A. Hart, Stephen K. Burke, Steve C. Galea, Gregory P. Carman, “Vibration energy harvesting using a spherical permanent-magnet”, *Proc. of SPIE Vol. 9057, Active and Passive Smart Structures and Integrated Systems 2014.*

[46] L A Vandewater, S D Moss, “Probability-of-existence of vibro-impact regimes in a nonlinear vibration energy harvester”, *Smart Mater. Struct. 22 (2013) 094025 (9pp)*

[47] Mitcheson PD, Green TC, Yeatman EM, Holmes AS “Architectures for vibration-driven micro-power generators”, *IEEE/ASME J Microelectromech Syst 13 (2004) 429–440.*

[48] Mitcheson PD, Miao P, Stark BH, Yeatman EM, Holmes AS, Green TC “MEMS electrostatic micro-power generator for low frequency operation”. *Sensors and Actuators A 115 (2004) 523–529.*

[49] P. Miao, P. D. Mitcheson, A. S. Holmes, E. M. Yeatman, T. C. Green, and B. H. Stark. “Mems inertial power generators for biomedical applications” *Microsyst. Technol. 12 (2006) 1079–1083.*

[50] T. von Büren, P. D. Mitcheson, T. C. Green, E. M. Yeatman, A. S. Holmes, and G. Tröster, “Optimization of Inertial Micropower Generators for Human Walking Motion”, *IEEE Sensors 6 (2006) 28–38.*

[51] Benjamin J Bowers and David P Arnold, “Spherical, rolling magnet generators for passive energy harvesting from human motion”, *J. Micromech. Microeng. 19 (2009) 094008 (7pp).*

[52] Yuan Rao, Shuo Cheng, David P Arnold, “An energy harvesting system for passively generating power from human activities” *J. Micromech. Microeng. 23 (2013) 114012 (9pp).*

[53] Byung-Chul Lee, and Gwiy-Sang Chung, “Design and fabrication of low frequency driven energy harvester using Electromagnetic conversion”, *Transactions on Electrical and Electronic Materials 14 (3) (2013) 143–147.*

[54] S. Graham Kelly, “Mechanical vibration: theory and applications”. *SI Global Engineering Christopher M. Shortt, ISBN-13: 978-1-4390-6214-2, 2012*

[55] Chow, Tai L., “Introduction to electromagnetic theory: a modern perspective”. *Jones & Bartlett Learning. ISBN978-0-7637-3827-3, 2006, pp.146–1*

[56] Shad Roundy, Eli S. Leland, Jessy Baker et al, “Improving power output for vibration-based energy scavengers” *IEEE CS and IEEE ComSoc* 5 (2005) 1536 – 1268

[57] B.P. Mann, N.D. Sims, “Energy harvesting from the nonlinear oscillations of magnetic levitation”, *Journal of sound and vibration 319 (2009) 515-530.*

[58] Paul D. Mitcheson, “Vibration energy harvesting basics”, *NIPS workshop 2014*

[59] Lankrani, H. M., and Nikravesh, P. E., “A Contact force model with hysteresis damping for impact analysis of multibody Systems,” *J. Mech. Des. 112 (1990) 396–376*

[60] S P Beeby, M J Tudor, N M White, “Energy harvesting vibration sources for microsystems applications”, *Measurement Science and Technology 17 (2006) 175–195.*

[61] Sneddon, I. N., “The relation between load and penetration in the axisymmetric boussinesq problem for a punch of arbitrary profile”.*Int. J. Eng. Sci. 3 (1965) 47–57*

[62] EPSRC (2011), the energy harvesting network, “Energy harvesting from human power: A roadmap to new research challenges”, *1st workshop on human power, London, UK, 2011*

[63] Y. Zhu, J.W. Zu, “A megnetoelectric generator for energy harvesting from the vibration of magnetic levitation” *IEEE Trans. Magn. 48 (2012) 3344-3347*

[64] Scott D. Moss, Joshua E. McLeod, Ian G. Powlesl, Steve C. Galea, “A bi-axial magnetoelectric vibration energy harvester”, *Sensors and Actuators A 175 (2012) 165–168.*

[65] Elvin N G and Elvin A A, “Vibrational energy harvesting from human gait” *IEEE/ASME Trans. Mechatronics, 18 (2012) 6 37–44*

[66] Aki I.T. Salo, Ian N. Bezodis, Alan M. Batterham, and David G. Kerwin, “Elite Sprinting: Are Athletes Individually Step-Frequency or Step-Length Reliant?”. *Medicine & Science in Sports & Exercise 43(6) (2011) 1055-1062*

[67] Yasushi Enomoto, Hirosuke Kadono, Yuta Suzuki, Tetsu Chiba, Keiji Koyama, “Biomechanical analysis of the medalists in the10,000 metres at the 2007 World Championships in Athletics”. *IAAF 23(3) (2008) 61-66.*

[68] Wagenaar RC, van Emmerik REA. “Resonant frequencies of arms and legs identify different walking patterns”. *J Biomech 33 (2000) 853–61.*

[69] Donker SF, Beek PJ, Wageenar RC, Mulder T. “Coordination between arm and leg movements during locomotion”. *J Mot Behav 33 (2001) 86–102.*

[70] S. F. Donker, Th. Mulder, B. Nienhuis, J. Duysens. “Adaptations in arm movements for added mass to wrist or ankle during walking”. *Experimental Brain Research, 146(1) (2002) 26–31.*

[71] Stephen Beeby, Neil White, “Energy harvesting for autonomous systems”. *1st ed., Artech House, England, 2010.*

[72] G. Cappellini, Y. P. Ivanenko, R. E. Poppele, and F. Lacquaniti, “Motor Patterns in Human Walking and Running”. *J Neurophysiol 95(2006) 3426 –3437.*

Achievements

Journal papers

1. Haroun A., Yamada I., Warisawa S., “Study of electromagnetic vibration energy harvesting with free / impact motion for low frequency operation”, *Journal of sound and vibration 349 (2015) 389-402*
2. Haroun A., Yamada I., Warisawa S., “Micro Electromagnetic Vibration Energy Harvester Based on Free/Impact Motion for Low Frequency - Large Amplitude Operation”, *Sensors and Actuators A 224 (2015) 87-98*